IntechOpen

Multidimensional Flow Cytometry Techniques for Novel Highly Informative Assays

Edited by Marica Gemei

MULTIDIMENSIONAL FLOW CYTOMETRY TECHNIQUES FOR NOVEL HIGHLY INFORMATIVE ASSAYS

Edited by **Marica Gemei**

Multidimensional Flow Cytometry Techniques for Novel Highly Informative Assays
http://dx.doi.org/10.5772/intechopen.68879
Edited by Marica Gemei

Contributors

Toshiyuki Takahashi, Iuri Marinov, Andrea Illingworth, D. Robert Sutherland, Katarzyna Piwocka, Catherine Bardelle, David Murray, Vincent Sauzeau, Gervaise Loirand, Mark Carter, Zhaoping Liu, Ina Laura Pieper, Catherine Thornton, Gemma Radley

Notice

First published in London, United Kingdom, 2018 by IntechOpen
eBook (PDF) Published by IntechOpen, 2019
IntechOpen is the global imprint of INTECHOPEN LIMITED, registered in England and Wales, registration number: 11086078, The Shard, 25th floor, 32 London Bridge Street
London, SE19SG – United Kingdom
Printed in Croatia

British Library Cataloguing-in-Publication Data
A catalogue record for this book is available from the British Library

Additional hard and PDF copies can be obtained from orders@intechopen.com

Multidimensional Flow Cytometry Techniques for Novel Highly Informative Assays
Edited by Marica Gemei

p. cm.

Print ISBN 978-1-78923-344-5

Online ISBN 978-1-78923-345-2

eBook (PDF) ISBN 978-1-83881-361-1

Meet the editor

Marica Gemei started her career in the field of flow cytometry within her PhD experience at CEINGE in Naples, where she worked for six years in a flow cytometry facility equipped with the most advanced of instruments; this allowed her to exploit the potential of flow cytometry to its utmost. Her work in the field of flow cytometry was successful and gained tens of collaborations and valuable publications. She further exploited her experience, propensity for innovation and open mind by growing up in the variegate world of flow cytometry and the industrial drug discovery and development field and moving to the pharmaceutical industry in 2014, first as a researcher and then as a manager. Now she is an appreciated consultant and project manager for preclinical and clinical drug development programs in different biotech and pharmaceutical companies such as Dompé Farmaceutici SpA with which she has a long-lasting and profitable collaboration.

Contents

Preface

In spite of flow cytometry being the gold standard in hematologic and oncohematologic research and diagnosis, its use in industrial drug discovery and research has been minimal for many years. Additionally, it has been used for simple and low content analysis, from cell cycle evaluation to transfection level control, often on homogeneous cell populations. This is because for many years it has not been a widespread technique in research laboratories and its use requires in-depth training and experience to gain reproducible and sound results. More recently, instruments have evolved that are now both stable and easy to use, and analysis software has become user friendly and affordable, even for beginners. Industrial research has implemented flow cytometry in routinely used techniques because of its validation as a simple and cost-effective substitute for many assays, because of its radioligand bindings, and because of the strong automation achievable. Recently, various high-throughput flow cytometry screening applications have been reported in formats up to 1536. In addition to cell-based applications, there has also been an increase in performing high-throughput flow cytometry using bead-based immunoassays to screen for cytokines and other proteins in a multiplexed format.

Flow cytometry has been incorporated in research programs as a flexible and multipurpose technique to evaluate many biological responses and readouts with a single instrument. Flow cytometers allow high-speed analysis of particles (up to thousands of single cells per second) and measure multiparameters (up to 18) on single cells simultaneously. Because of its characteristics, flow cytometry can be used to perform high-throughput analysis but also high content screening. Complex tissues can be homogenized and treated as mixtures of cell lineages in a single run, while composing cell populations can be isolated later during the analysis allowing the visualization of an entire tissue and of the cell interactions and changes in different physiopathological conditions. Using cell barcoding techniques, different samples, treated in different ways or deriving from different tissues or experimental conditions, can be mixed and directly compared in a single run, further increasing the multiparametric potential of flow cytometry.

Recently, the introduction of imaging flow cytometry has filled the gap between flow cytometry and imaging allowing the precise evaluation of visual parameters as a speckled distribution of mutant proteins inside the cells, which is impossible to evaluate in conventional cytometry. Flow cytometry can be further exploited than it is today using the full potential of new instruments and new reagents and kits available for multiparameter and high content analysis.

This book collects some examples of how different parameters can be combined and analyzed to obtain a valuable analysis in different contexts. Some chapters describe applications

in the diagnostic and prognostic field as common CD4 T-cell enumeration or more advanced analysis as PNH clone identification and cell-cell interaction analysis in the leukemia microenvironment. Other chapters treat the less widespread analysis of microalgae quality assessment, an emerging industrial need, or the use of flow cytometry in the testing of blood handling medical devices, thus showing that flow cytometry is not only applicable to research and clinical analyses. Finally, practical examples of how academically developed assays can be optimized and standardized for industrial purposes have prompted all of us to support flow cytometry development and its widespread use.

The contributors to the book include flow cytometry users from both academia and industry with different needs and visions; the high diversity of flow cytometer applications is resumed by the presented diverse mix of expertise, a hallmark of the flow cytometry community in which innovation is a driver. I wish to sincerely thank all the contributors for their expertise, personal vision and effort in the writing of this book. Thanks also to IntechOpen for approaching me about a project I really care about. Finally, thanks to Luigi Del Vecchio for introducing me to flow cytometry without the barrier of a formal education and training, leaving me free to explore all the potential and to try something new every day.

Dr. Marica Gemei
Chelonia SA, Switzerland

Chapter 1

Accurate and High Sensitivity Identification of PNH Clones by Flow Cytometry

Iuri Marinov, Andrea Illingworth and
D. Robert Sutherland

Additional information is available at the end of the chapter

http://dx.doi.org/10.5772/intechopen.71286

Abstract

Flow cytometry performs a key role in the diagnosis of paroxysmal nocturnal hemoglobinuria (PNH). Careful selection and validation of antibody conjugates have allowed the development of reagent cocktails suitable for the high sensitivity detection of PNH red blood cells (RBCs) and white blood cells (WBCs) in PNH and related diseases such as aplastic anemia (AA) and some subsets of myelodysplastic syndromes (MDS). A CD235a-FITC/CD59-PE assay was developed capable of detecting Type III PNH RBCs at a limit of quantification (LOQ) of 0.01% or better. While separate 4-color Fluorescent Aerolysin (FLAER), CD24, CD15 and CD45-based neutrophil and FLAER, CD14, CD64 and CD45-based monocyte assays were developed to detect PNH WBC phenotypes, 5-, 6- and 7-color assays have subsequently been developed for more modern cytometers equipped with five or more fluorescence detectors. For instrumentation with five detectors, a single tube 5-color FLAER, CD157, CD15, CD64 and CD45-based assay to simultaneously detect PNH neutrophils and monocytes has been developed. For instruments with six or more detectors and multiple lasers, a variety of 5-, 6- and 7-color assays have been developed using combinations of FLAER, CD24, CD14 and CD157. All WBC assays have a limit of quantification (LOQ) of 0.1% or better. Using these standardized approaches, results have demonstrated good intra- and inter-laboratory performance characteristics even in laboratories with little prior experience performing PNH testing.

Keywords: PNH, flow cytometry, high sensitivity assay, validation, standardization

1. Introduction

Paroxysmal nocturnal hemoglobinuria is a rare, life-threatening acquired hematopoietic stem cell disorder resulting from the somatic mutation of the X-linked phosphatidylinositol glycan

complementation Class A (PIG-A) gene [1]. PIG-A normally encodes an enzyme involved in the first stage of glycosylphosphatidylinositol (GPI) biosynthesis but in PNH, as a result of the mutation(s) in this gene, there is a partial or absolute inability to make GPI-anchored proteins, including complement defense structures such as CD55 and CD59 on red blood cells (RBCs) and white blood cells (WBCs) [2, 3]. Absence of CD59 in particular [4] and CD55 on RBCs is responsible for intravascular hemolysis associated with clinical PNH. Clonal expansion of the PNH population frequently occurs in patients with aplastic anemia in which normal hematopoiesis has failed, and with modern, high sensitivity assays, up to 70% of AA patients have detectable PNH clones [5]. Small populations of GPI-deficient PNH phenotypes have been reported in patients with early stage myelodysplastic syndrome (MDS) [6, 7]. Patients present with a wide range of clinical features, including intravascular hemolysis (that leads to hemoglobinuria), bone marrow failure and thrombosis, with the latter being a major cause of morbidity and mortality [5, 8]. As PNH is an acquired stem cell disease, it is important to demonstrate the loss of GPI-linked cell surface structures in at least two hematopoietic cell lineages, traditionally RBCs and neutrophils, although as more data have recently accumulated, monocytes should also be assessed as monocytes often exhibit a higher 'clone size' than is present in neutrophils. For true high-sensitivity assay design, it is critical to include carefully validated lineage-specific gating reagents such as CD235a (Glycophorin A) for RBC identification, CD15 for neutrophil identification and CD64 for monocyte identification. Examination of RBCs in the non-transfused PNH patient provides the most accurate assessment of the distribution of Type III PNH RBCs (complete CD59 deficiency), Type II PNH RBCs (partial CD59 deficiency) and normal Type I RBCs (normal CD59 expression). The distributions of these populations show a wide variation from patient to patient and delineation between the various types is not always clear-cut [9]. RBC analysis is important in PNH, as accurate determination of the distribution of Type II and III cells; patients with greater than 20% Type III RBCs almost always show clinical evidence of hemolysis [5]. While the loss of GPI-linked CD55 and CD59 was traditionally used to detect PNH RBCs [10, 11], 'routine' CD55 and/or CD59-based approaches are neither accurate nor sensitive below the 1–2% clone size, rendering them inadequate to detect small PNH clones typically found in PNH+ AA and MDS cases [5] or even in some heavily transfused PNH cases.

2. Pre-analytical phase

2.1. Red blood cells

2.1.1. Sample and reagent requirements

Freshly drawn EDTA (preferred) or heparin anti-coagulated whole peripheral blood is used for analysis. If samples are shipped or need to be stored prior to analysis, the blood sample should be kept at 4°C and should generally be used within 48 hours of sample draw. For high-sensitivity RBC analysis, the International Clinical Cytometry Society (ICCS) Guidelines recommended the use of CD235a (for RBC gating) and CD59 (to detect GPI-deficient cells) [12]. In the follow-up 'Practical Guidelines' [13], a large number of clones/conjugates to CD235a-FITC and CD59-PE were tested but only a few were found to have acceptable performance

Target	Antibody Conjugates	Purpose	Clone and Vendor
RBC	CD235a-FITC	Gating on RBC	10F7MN (eBio) YTH 89.1 (Cedarlane) KC16 (BC) JC159 (DAKO)
	CD59-PE	GPI-linked for RBC	OV9A2 (eBio) MEM-43 (Invitrogen) MEM-43 (EXBIO/Cedarlane)

Table 1. Recommended CD235a-FITC and CD59-PE conjugates for high-sensitivity PNH RBC assay.

characteristics and further validated for a variety of instrument platforms (**Table 1**). Of note, even selected conjugates required extensive titration on an individual basis to minimize aggregation prior to premixing or 'cocktailing' for this assay. Only by performing extensive titrations, we were able to identify conjugates with the best performance characteristics for this specific assay. Premixing of reagents once adequately titrated is critically important in PNH assays as both RBC and WBC assays are designed to detect GPI-deficient phenotypes, i.e., cells unstained by the GPI-specific reagents. Given the very small volumes of reagents used for the RBC assay in particular, it is usually necessary to make a dilution of the RBC cocktail such that accurately pipettable volumes of reagent can be employed.

2.1.2. Staining procedure

Blood samples are diluted 1:100 with fresh clean PBS and 100 μL is carefully pipetted using reverse pipetting techniques directly into the bottom of the staining tube taking care to avoid aerosols and blood trails on the inside of the tube. The appropriate volume of diluted CD235aFITC/CD59PE is then pipetted directly into the bottom of the tube and admixed with the diluted sample by gently up-and-down pipetting. After careful removal of the tip, the sample can be gently 'swirled' on a vortex set at a very low speed to avoid aerosol generation. After 20 minutes, the sample must be washed twice with clean phosphate buffered saline (PBS), resuspended in 1 ml of PBS and then 'racked' immediately before data acquisition to disrupt any RBC aggregates generated during the staining process [13].

2.2. White blood cells

2.2.1. Sample and reagent requirements

For high-sensitivity WBC analysis using a single tube approach, CD45 is employed for pattern recognition and to exclude unlysed RBCs, other debris not excluded by light scatter thresholding. Thereafter, carefully selected/validated conjugates of CD15 and CD64 are used to accurately delineate/'gate' neutrophils and monocytes, respectively. To detect GPI-deficient CD15-gated neutrophils, FLAER is used in combination with either carefully selected/validated CD24 or CD157 conjugates, and to detect GPI-deficient CD64-gated monocytes, FLAER is used in combination with either carefully selected/validated CD14 or CD157 conjugates (**Table 2** and **3**) [13–16].

Target	Antibody Conjugates	Purpose	Clone (Vendor)
WBC	FLAER-Alexa488	GPI-linked (Neuts + Monos)	NA (Cedarlane)
	CD24-PE CD24-APC	GPI-linked (Neuts)	SN3 (eBio), ALB9 (BC) SN3 (eBio, EXBIO)
	CD14-PE CD14-APC700	GPI-linked (Monos)	61D3 (eBio), RMO52 (BC) Tuk4 (Invitrogen) RMO52 (BC)
	CD157-PE	GPI-linked (Neuts + Monos)	SY11B5 (eBio, EXBIO, BD, BC, Sysmex)
	CD64-PC5 CD64-ECD CD64-PC7	Gating on Monocytes	22 (BC) 22 (BC) 22 (BC), 10.1 (EXBIO)
	CD15-PC5 CD15-PerCP-eF710 CD15-PerCPCy5.5	Gating on Neutrophils	80H5 (BC) MMA (eBio) MEM158 (EXBIO)
	CD45-PC7 CD45-KO CD45-eF450	Debris/unlysed RBC exclusion + pattern recognition	J33 (BC) J33 (BC) 2D1 (eBio)

Table 2. Recommended clones/conjugates to determine high-sensitivity detection of PNH WBC on Beckman Coulter Cytometers.

Target	Antibody Conjugates	Purpose	Clone (Vendor)
WBC	FLAER-Alexa488	GPI-linked (Neuts + Monos)	NA (Cedarlane)
	CD24-PE CD24-APC	GPI-linked (Neuts)	SN3 (eBio), ML5 (BD) SN3 (eBio, EXBIO)
	CD14-PE CD14-APC	GPI-linked (Monos)	61D3 (eBio), Tuk4 (Invitrogen) MoP9 (BD)
	CD157-PE	GPI-linked (Neuts + Monos)	SY11B5 (eBio, EXBIO, BD, BC, Sysmex)
	CD64-APC CD64-PECy7	Gating on Monocytes	10.1 (BD, eBio) 10.1 (EXBIO), 22 (BC)
	CD15-APC CD15-PerCP-eF710 CD15-PerCPCy5.5	Gating on Neutrophils	HI98 (BD) MMA (eBio) MEM 158 (EXBIO)
	CD45-eF450 CD45-PerCP CD45-APC-H7	Debris/unlysed RBC exclusion + pattern recognition	2D1 (eBio) 2D1 (BD) 2D1 (BD)

Table 3. Recommended clones/conjugates for high-sensitivity detection of PNH WBC on Becton Dickinson Cytometers.

2.2.2. Staining procedure

Undiluted anti-coagulated whole blood is the preferred sample source for the analysis of PNH phenotypes in WBCs. Reverse pipetting is used to dispense 100 μL of sample into the

staining tube, taking all the precautions noted above for the RBC assay to avoid aerosols and ensure that the sample is not left on the wall of the tube. The reagent set in use should be cocktailed, once optimal volumes of each reagent have been determined by titrations. The appropriate volume of cocktail is added directly into the blood sample at the bottom of the tube and gently admixed by up-and-down pipetting. After gentle swirling to avoid aerosols, the sample is incubated in the dark for 20–30 minutes at room temperature before RBC lysis. There are a variety of commercial lysing agents available such as Versalyse, FACSLyse and Immunoprep and most do a very good job. After lysis following manufacturers' recommendations, the sample is centrifuged and washed with PBS supplemented with 1% serum albumin. The sample is resuspended in 0.5–1 ml of PBS and acquired.

3. Analytical phase and data reporting

3.1. Instrument setup and standardization

Optimal instrument setup and standardization is a prerequisite for reproducible results over time and among laboratories. For the analysis of RBCs, the forward scatter (FS) and side scatter (SS) voltages are set in logarithmic mode and voltages adjusted to bring all unstained RBCs into the middle of the plot and above any FS threshold/discriminator. For WBCs, light scatter voltages are set in linear mode at such values that all unstained leukocyte subsets including lymphocytes scatter above the FS threshold and are clearly clustered on scale. Photomultiplier tube (PMT) voltage optimization, standardization and computer-assisted spectral overlap compensation are mandatory steps for instrument standardization of multiparameter assays and can be performed using an instrument platform-based approach (BD Biosciences, Beckman Coulter) or interplatform-based approach [17–20].

3.2. Data acquisition and analysis

3.2.1. Red blood cells

For high-sensitivity RBC analysis, the ICCS Guidelines recommended the use of CD235a (for RBC gating) and CD59 (to detect GPI-deficient cells) [9]. Based on subsequent publications that included rigorous testing and validation of various CD235a and CD59 clones and conjugates, optimal reagent combinations of CD235a-FITC and CD59-PE were identified [13]. Once extensively titrated, these reagents in combination did not cause major aggregation of RBCs while still maintaining a good signal-to-noise ratio and the ability to adequately separate Type II and Type III PNH RBCs from normal (Type I) RBCs [13–15]. Red blood cells are analyzed by a series of gating dot plots beginning with TIME versus SS, FS versus SS with detectors set in logarithmic mode, and CD235a-FITC versus FS to gate singlet RBCs and to quantify and exclude any remaining RBC aggregates (**Figure 1**). TIME is collected as a parameter and monitored during acquisition so that if fluidics problems are encountered, the sample can be reacquired if possible, or if not, data acquired prior to the fluidics hiatus can be 'gated' and only that portion of the data file subsequently analyzed. It is important to adjust the threshold (discriminator) for the FS so that no RBCs are excluded from acquisition. The diagnostic plots include a bivariate CD59 versus CD235a dot plot, a bivariate CD59 versus CD235a density

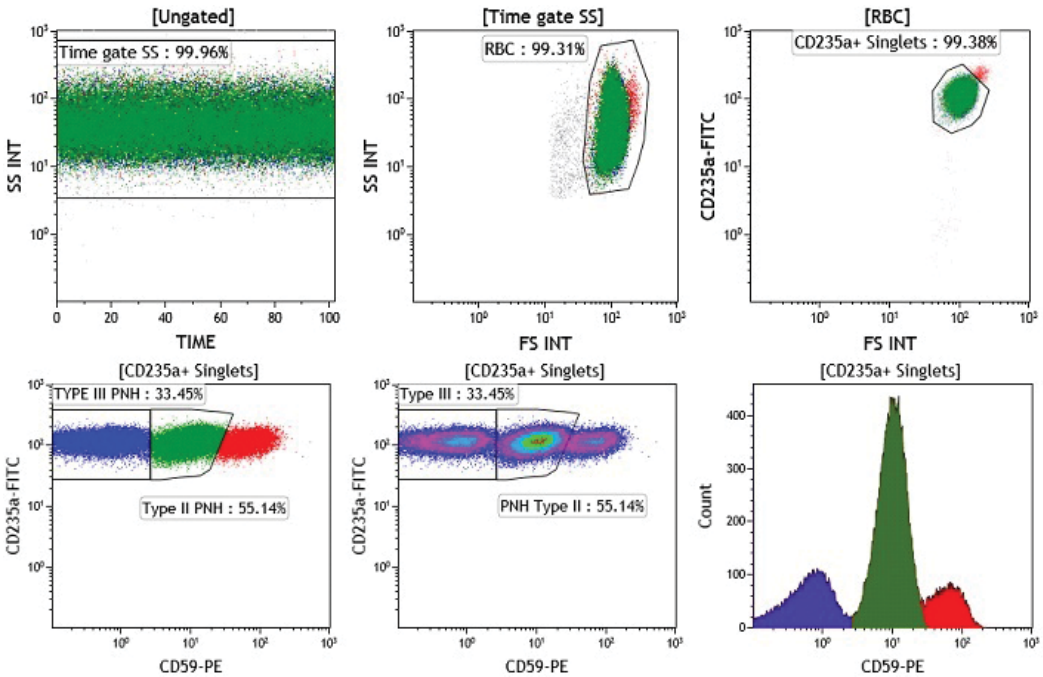

Figure 1. Sequence of bivariate gating and diagnostic dot-plots for analysis of PNH RBCs.

plot and a single parameter histogram of CD59 staining (**Figure 1**). Bivariate dot plots and/or density plots are recommended over single-parameter histograms, especially for samples containing small numbers of PNH phenotypes, for identifying poorly stained samples that need to be re-stained and for detecting media contamination and troubleshooting instrumentation issues [13]. However, while data regarding clone sizes come predominantly from the two-dimensional plots, in which the gating regions are linked across the dot plot and density plots, the single parameter histogram can also be useful in some situations. All three plots work in concert for optimal adjustment of the regions for Type III PNH cells and Type II PNH cells. An additional utility of the single parameter histogram is in comparing old versus new plots of CD235a-FITC/CD59-PE cocktails when tested on non-PNH samples.

3.2.2. White blood cells

High-sensitivity methodologies to detect PNH phenotypes in neutrophils and monocytes have been published previously. These methods were initially based on two separate 4-color neutrophil (FLAER, CD24, CD15 and CD45) and monocyte (FLAER, CD14, CD64 and CD45) tubes. In this earlier setting, samples were stained first with the RBC and neutrophil cocktails and if PNH phenotypes were detected, the 'reflex' monocyte tube was thereafter set up. The current document uses the same gating strategy used in earlier assays but discuss the more modern single tube assays on newer flow cytometers with 5, 6, or more PMTs that allow the simultaneous detection and quantification of both neutrophils and monocytes.

3.2.2.1. FLAER/CD24/CD14-based assay

For laboratories equipped with modern cytometers with 6-, 8- or 10 PMTs (Canto, Canto II and Navios), it is possible to configure 6-color cocktails based on FLAER, CD24 and CD14 (**Tables 2** and **3**). **Figure 2** shows the sequence of bivariate gating and diagnostic dot-plots from a Navios-specific reagent set comprising FLAER-Alexa488, CD24-PE (clone ALB9), CD15-PC5 (clone 80H5), CD64-PC7 (clone 22), CD14-APCA700 (clone RMO52) and CD45-KO (clone J33). The FS versus SS plot is gated from TIME versus SS plot (not shown) and light scatter voltages are set so that all WBC subsets are clearly visible and optimally separated; the threshold/discriminator is set to ensure that no lymphocytes are excluded. A debris exclusion gate (or WBC inclusion gate) can then be established to exclude any debris above the threshold/discriminator but below the

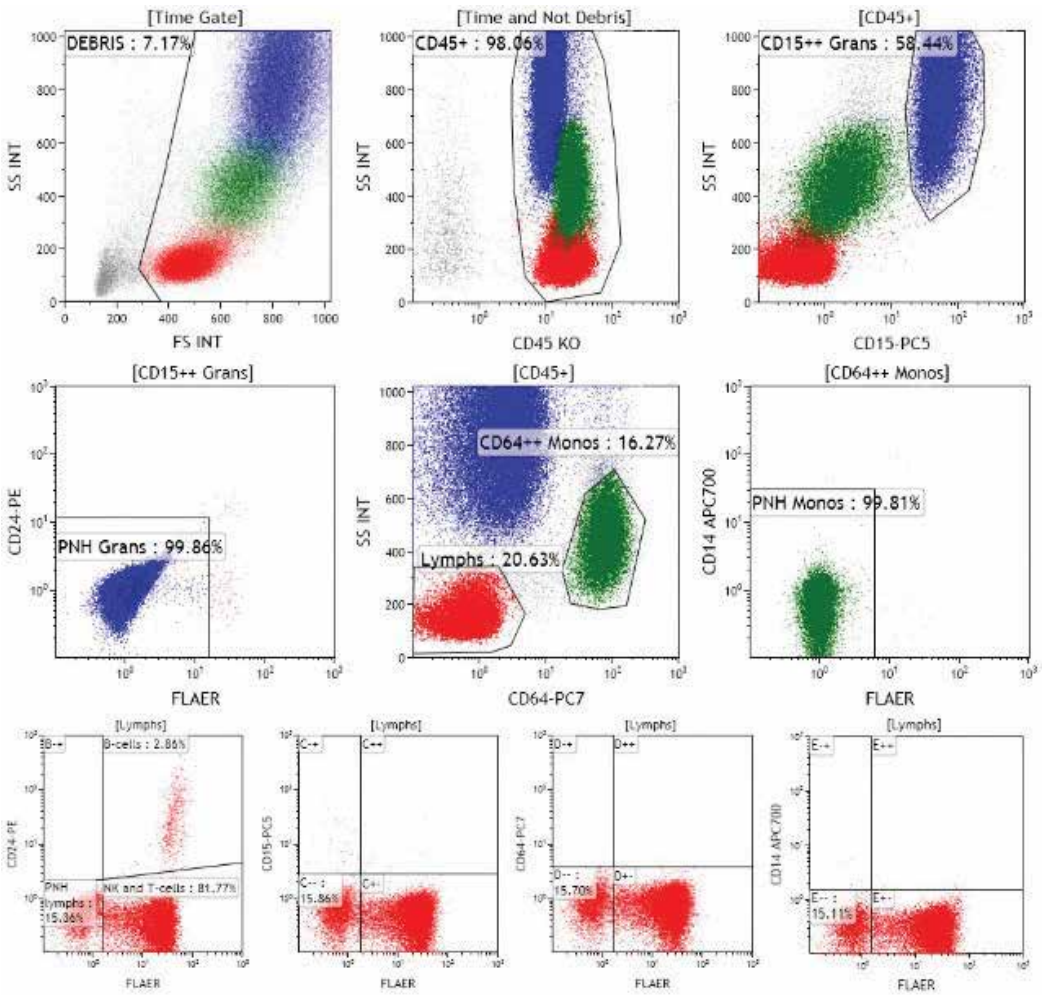

Figure 2. Sequence of bivariate gating and diagnostic dot-plots for FLAER/CD24/CD14- based analysis of PNH neutrophils and monocytes.

smallest lymphocytes. The CD45 versus SS plot is then gated through Boolean gating on Time and "not debris" with a gate drawn around the CD45+ cells. The CD45 versus SS plot is useful not only for pattern recognition but also for excluding any unlysed RBCs and other debris not removed by the debris exclusion gate. The CD15 versus SS plot is gated on the CD45+ populations and includes a gate drawn around the CD15++ neutrophils excluding as well as possible the CD15 dim + eosinophils visible to the left of the neutrophil/granulocyte population. The diagnostic FLAER/CD24 plot is gated on the CD15++ neutrophils and a region is drawn to encompass the FLAER-negative/CD24-negative cells, which represent the PNH neutrophils. The CD64 versus SS plot is also gated on the CD45+ cells and a region is drawn around the CD64++ monocytes. The FLAER versus CD14 dot plot is gated on the CD64++ monocytes and a region is drawn to delineate the FLAER-negative/CD14-negative cells, which represent the PNH monocytes. The lymphocytes gated on the CD64-negative/low SS plot are not a suitable target population for the PNH clone quantification due to their long lifespan. However, they serve as internal controls for verification of antigen expression and compensation settings. Plotting FLAER versus CD24, CD14, CD15 and CD64 verifies the instrument voltage and compensation settings as visible and clustered populations in the "correct" location. Plot FLAER versus CD24 shows B-cells (FLAER+/CD24+) verifying that both reagents were added, FLAER+/CD24-negative NK and T-cells and no dual-negative cells as this is a PNH-negative sample.

3.2.2.2. FLAER/CD157-based assay

ADP-ribosyl cyclase 2 (CD157) is a GPI-anchored cell surface enzyme encoded by the bone marrow stromal cell antigen-1 gene, which plays a role in pre-B cell growth [21]. Within the hematopoietic system, CD157 is highly expressed on both mature neutrophils and monocytes [22] leading to the possibility that CD157 could replace both CD24 and CD14, allowing the development of a single tube, high sensitivity 5C assay to identify and quantify both PNH neutrophils and PNH monocytes on cytometers with five or more PMTs [14–16]. The ability to perform simultaneous evaluation of both PNH neutrophils and PNH monocytes is particularly attractive to laboratories equipped with 5-C instruments such as the FC500 due to the major cost and time savings involved over running two separate 4-color assays for neutrophils and monocytes [14–16]. The gating and analysis strategies are similar to the ones used for the above described single-tube 6-color assay, except for the diagnostic FLAER/CD157 dot plots gated on CD15++ neutrophils and CD64++ monocytes (**Figure 3**). Three control lymphocyte plots (FLAER/CD15, FLAER/CD64 and FLAER/CD157) are also shown to monitor instrument setup and compensation.

It is important to note that several CD157-negative, non-PNH cases have been observed in the authors' laboratories (unpublished data). For these rare cases, the inclusion of the second GPI reagent (FLAER) as part of the built-in robustness of the assay prevents the misinterpretation of the data as a PNH clone-containing sample. Furthermore, in keeping with current state-of-the-art guidelines [12, 13], the RBC lineage should also be analyzed on every sample tested for the presence of PNH WBCs. As these rare CD157-negative non-PNH samples only contain normal (Type I) RBCs, there is even less chance of misinterpretation. An example of a CD157-negative case is shown in **Figure 4**. The sample was stained with a 7-color combination

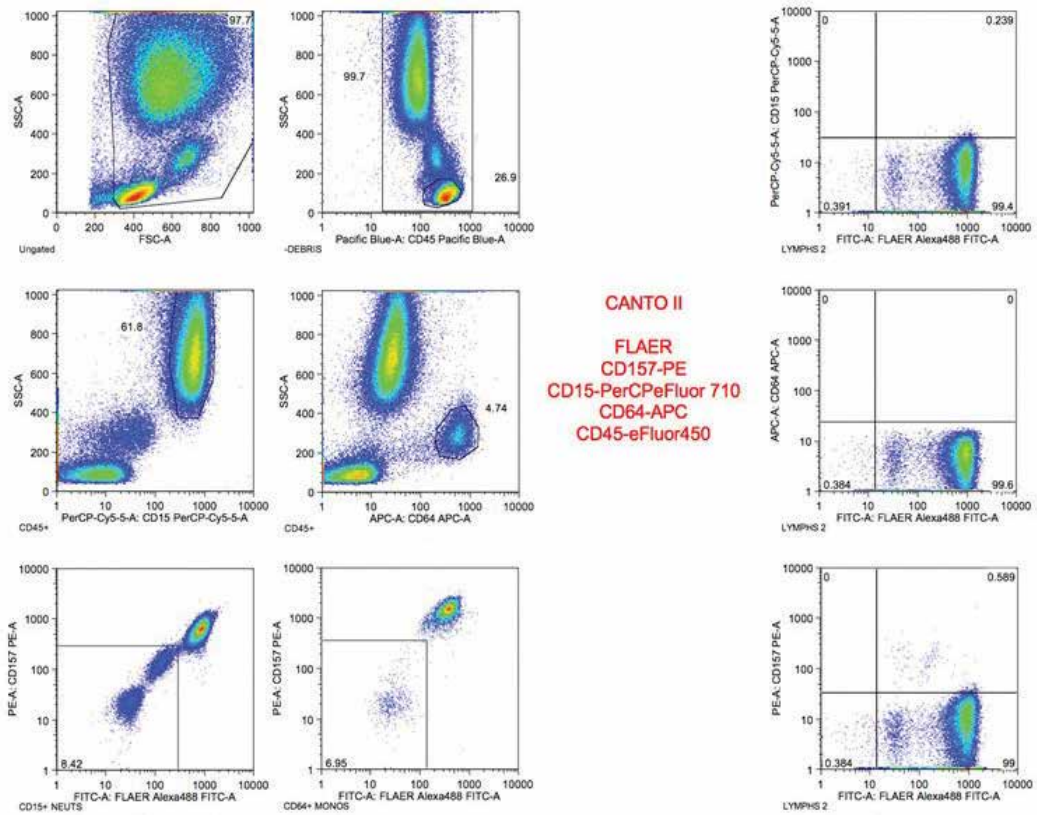

Figure 3. Sequence of bivariate gating and diagnostic dot-plots for FLAER/CD157- based analysis of PNH neutrophils and monocytes.

of FLAER, CD157, CD24, CD14, CD15, CD64 and CD45. While the CD157 failed to stain normal neutrophils in this sample, FLAER and CD24 stained the neutrophils in the expected manner. Similarly, while CD157 failed to stain normal monocytes in this sample, FLAER and CD14 stained monocytes in the expected manner.

3.3. Reporting

The following components are recommended for a PNH report:

1. The presence or absence of PNH clones. It is important to be clear and to avoid potentially misleading ambiguous terminology. A report stating that a CD59 test is negative may imply to some providers that the target population is negative for the GPI marker CD59 (thus indicating a PNH clone) or that absence of CD59 is not seen (thus indicating the absence of a PNH clone).
2. PNH clone size in the RBCs (total PNH clone size as well as the percentages for Type II and Type III PNH populations). There is a clinical significance associated for Type II and

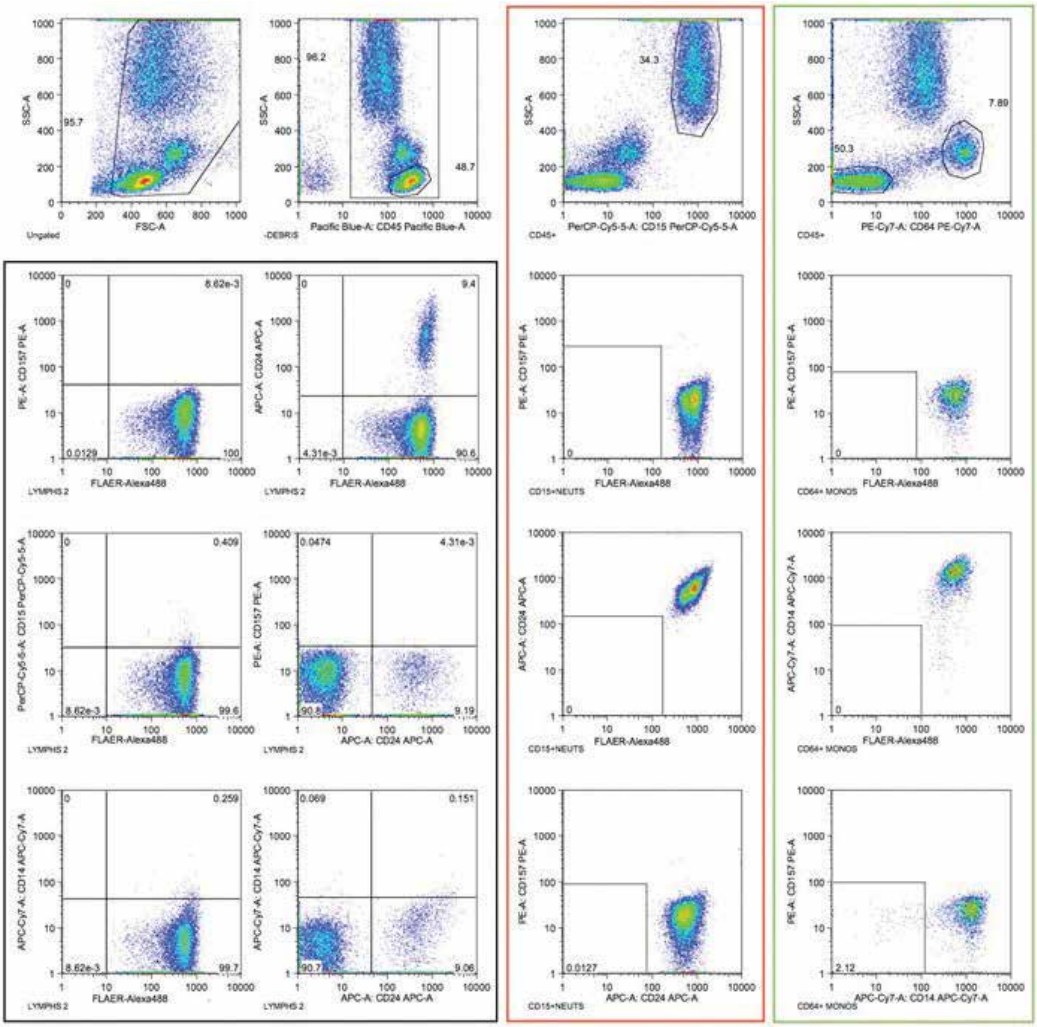

Figure 4. Example of CD157-negative, non-PNH case, 7-color FLAER/CD24/CD14/CD157-based protocol.

Type III RBCs. Type I RBCs are normal red blood cells with bright CD59 expression and a lifespan of approximately 120 days. Type III PNH RBCs have complete CD59 deficiency, which results in no protection from complement-mediated lysis and a shortened lifespan of 10–15 days. Type II PNH RBCs have partial CD59 deficiency resulting in partial protection from complement-mediated lysis. Just as the expression of CD59 on Type II RBCs varies considerably from patient to patient, the lifespan of Type II cells reflects this being intermediate between Type I normal RBCs and Type III PNH RBCs. Since the clinical significance of Type II PNH RBCs and Type III PNH RBCs is well established, it is recommended to report them separately and combined as the total PNH RBC clone.

3. PNH clone size in both lineages for the WBCs (neutrophils and monocytes). The PNH monocyte clone is often larger than the neutrophil PNH clone and reporting only the PNH neutrophil/granulocyte clone may underestimate the PNH clone size in the WBCs. Neutrophils

and monocytes may also show the presence of Type II populations but the clinical and biological significance of these populations has not been established at this time. It is therefore recommended to report only the total PNH clone size in the neutrophils and monocytes.

4. Interpretive terminology of reporting PNH clones based on CSLI H52-A2 [23]:
   a. PNH population > 1%: "PNH clone."
   b. PNH population 0.1–1%: "minor population of PNH cells" or "minor PNH clone."
   c. PNH population < 0.1%: "rare cells with GPI deficiency" or "rare cells with PNH phenotype.
5. List of all gating and diagnostic markers used for the PNH assay.
6. Levels of the limit of quantification (LOQ) for the neutrophil assay and the RBC assay, stating the recommended LOQ of 0.05% or better for RBCs (100,000 gated cells) and 0.1% or better for neutrophils (50,000 gated cells). It is important to include this information to the provider as an LOQ of 1% means that the possibility of a minor clone (less than 1%) cannot be excluded based on this LOQ.
7. Histograms or dot plots if possible because the dot plots may provide powerful visual supportive evidence of the PNH clone and also provide evidence of the quality of the assay.

4. Post-analytical phase and assay validation

The results of PNH testing by flow cytometry are usually reported as percentage of type II and III PNH cells from the total gated neutrophils, monocytes and red blood cells. Assays reporting numeric data are considered as semi-quantitative, therefore the post-analytical validation process should comprise confirmation of accuracy, specificity, sensitivity, repeatability, reproducibility and stability [24, 25].

4.1. Accuracy of PNH assays

The accuracy of a measurement is described by its trueness, which refers to the closeness of agreement between the average value of a large number of test results and the true or accepted reference value [25]. For PNH assays, we do not have cellular reference standard, therefore accuracy cannot be determined directly. Alternatively, interlaboratory comparison and/or external quality assessment represent the only available option for assay validation and mandatory step for ISO accreditation [26].

4.2. Specificity of PNH assays

4.2.1. Analytical specificity

The analytical specificity of PNH testing assays reflects the choice and validation of all antibodies/reagents and corresponding fluorochromes (**Tables 1–3**).

4.2.2. Clinical specificity

The clinical specificity or the ability to exclude abnormal specimen defined by true negatives/true negatives + false positives should be determined by assay of a series of samples and scoring for abnormality in comparison to a suitable reference method, such as clinical diagnosis [27]. The clinical specificity of well-established PNH assays is usually >99%.

4.3. Sensitivity of PNH assays

4.3.1. Analytical sensitivity

The analytical sensitivity of PNH assays is determined by the limit of blank (LoB) defined by the highest apparent signal detected in replicates of a sample containing no measurand and the limit of detection (LoD) defined by the lowest level of measurand that can be reliably distinguished from the LoB [28]. LoB for PNH assays could be determined by measuring a few replicates of a few negative specimens run over a few separate days and calculating the mean and standard deviation (SD) according to: LoB = mean of blank +1.645 SD of blank, assuming that 95% of negative values will be below this limit. Typically, the LoB for well-established PNH assays is <0.001% (<10 PNH phenotypes out of 1,000,000 acquired events). LoD for PNH assays is closely related but usually greater than LoB and could be determined by measuring a few replicates of a few negative specimens run over a few separate days and calculating the mean and SD according to: LoD = mean of blank + 2SD (3SD) of blank or by measuring a few replicates of a few low positive specimens run over a few separate days and calculating the SD according to: LoD = LoB + 1.645 SD of low positive. Alternatively, target LoD could be estimated by measuring a few replicates of a few low positive specimens run over a few separate days and calculating the reproducibility (inter-assay imprecision) expressed as coefficient of variation (CV%) or by confirming that no more than 5% of the values for a target LoD fall beyond the LoB. The generally accepted smallest number of events required to reproducibly detect a PNH population and determine LoD is 20 PNH events, lower levels should be validated in each laboratory.

4.3.2. Functional sensitivity

The functional sensitivity of PNH assays is determined by the limit of quantification (LoQ), which is the lowest level of measurand that can be reliably detected at predefined levels of bias and imprecision [28]. LoQ is usually greater than LOD and for PNH assays could be determined by measuring a few replicates of a few positive (near the expected LoQ) specimens run over a few separate days and calculating the reproducibility (inter-assay imprecision) expressed as CV%, which should be acceptable at levels below 10%. The generally accepted smallest number of events required to reproducibly quantify a PNH population and determine LoQ is 50 PNH events, lower levels should be validated in each laboratory.

4.3.3. Clinical sensitivity

The clinical sensitivity or the ability to detect an abnormal specimen and distinguish from normal specimens defined by true positive/true positive + false negative should be determined

by assay of a series of abnormal samples and scoring for abnormality in comparison to a suitable reference method, such as clinical findings [27]. The values for clinical sensitivity of well-established PNH assays is usually >99%.

4.4. Repeatability and reproducibility

The validation of assay performance characteristics comprises the determination of repeatability (intra-assay imprecision) and reproducibility (inter-assay imprecision). It is generally recommended to assay a few replicates from at least five samples within a single analytical run for repeatability and a few replicates from at least five samples in separate analytical runs for reproducibility [29]. For confirmation of good performance characteristics, CV% below 10% should be obtained for samples with more than 1% target PNH cells and below 20% for samples with minor clones (<1%).

4.5. Stability

The validation of specimen, processed specimen and reagent stability has been reviewed in Section 2 [13, 16, 23].

5. Accreditation

Flow cytometry is a highly versatile and complex technology, which is routinely applied in clinical diagnostic laboratories. The vast majority of assays are laboratory developed tests based on publications, without any gold standard reference [30] mostly with poor validation. For the purpose the ICSH/ICCS workgroup published in 2013 the practice guidelines for validation of cell-based fluorescence assays [31], subsequently several relevant publications addressed various aspects of the validation of PNH testing by flow cytometry [12, 13, 32]. Each laboratory applying for ISO 15189 accreditation should confirm optimal validation of instrument setup, assay performance characteristics, laboratory information system and result reporting [33].

6. Conclusion

Highly sensitive and specific PNH testing of all three lineages (RBC, neutrophils and monocytes) has become the standard of care for patients with suspected PNH. This is a rare disease and therefore often overlooked as a diagnostic possibility. It is important for the ordering physician to test the high-risk patients for PNH [12] and also to receive informational reports as an important part for best patient management. The laboratories are challenged with the validation of multiple steps, including instrument optimization, selection of best antibody clones/conjugates, panel design and targeted acquisition and interpretation of data. Developing competency in PNH testing and reporting is critical for laboratories and is directly related to awareness of best practices, following guidelines which are developed by experts based on extensive evaluation of

various approaches. Standardized reporting based on currently available guidelines is important to communicate to the physician the size of the PNH clone, which aids him/her in the decision-making for optimal treatment of the patient.

Author details

Iuri Marinov[1]*, Andrea Illingworth[2] and D. Robert Sutherland[3]

*Address all correspondence to: iuri.marinov@uhkt.cz

1 Institute of Hematology and Blood Transfusion, Prague, Czech Republic

2 Dahl-Chase Diagnostic Services, Bangor, Maine, USA

3 University Health Network/Toronto General Hospital, Toronto, Canada

References

[1] Takeda J, Miyata T, Kawagoe K, Iida Y, Endo Y, Fujita T, Takahashi M, Kitani T, Kinoshita T. Deficiency of the GPI anchor caused by a somatic mutation of the PIG-A gene in paroxysmal nocturnal hemoglobinuria. Cell. 1993;**73**:703-711. DOI: 10.1016/0092-8674(93)90250-T

[2] Nicholson-Weller A, March JP, Rosenfeld SI, Austen KF. Affected erythrocytes of patients with paroxysmal nocturnal hemoglobinuria are deficient in the complement regulatory protein, decay acceleration factor. Proceedings of the National Academy of Sciences of the United States of America. 1983;**80**:5066-5070. DOI: 10.1073/pnas.80.16.5066

[3] Holguin MH, Frederick LR, Bernshaw NJ, Wilcox LA, Parker CJ. Isolation and characterization of a membrane protein from normal human erythrocytes that inhibits reactive lysis of the erythrocytes of paroxysmal nocturnal hemoglobinuria. The Journal of Clinical Investigation. 1989;**84**:7-17. DOI: 10.1172/JCI114172

[4] Yamashina M, Ueda E, Kinoshita T, Takami T, Ojima A, Ono H, Tanaka H, Kondo N, Orii T, Okada N, Okada H, Inoue K, Kitani T. Inherited complete deficiency of 20-kilodalton homologous restriction factor (CD59) as a cause of paroxysmal nocturnal hemoglobinuria. The New England Journal of Medicine. 1990;**323**:1184-1189. DOI: 10.1056/NEJM199010253231707

[5] Parker C, Omine M, Richards S, Nishimura J, Bessler M, Ware R, Hillmen P, Luzzatto L, Young N, Kinoshita T, Rosse W, Socie G, International PNH Interest Group. Diagnosis and management of paroxysmal nocturnal hemoglobinuria. Blood. 2005;**106**:3699-3709. DOI: 10.1182/blood-2005-04-1717

[6] Dunn DE, Tanawattanacharoen P, Boccuni P, Nagakura S, Green SW, Kirby MR, Kumar MS, Rosenfeld S, Young NS. Paroxysmal nocturnal hemoglobinuria cells in patients with

bone marrow failure syndromes. Annals of Internal Medicine. 1999;**131**:401-408. DOI: 10.7326/0003-4819-131-6-199909210-00002

[7] Raza A, Ravandi F, Rastogi A, Bubis J, Lim SH, Weitz I, Castro-Malaspina H, Galili N, Jawde RA, Illingworth A. A prospective multicenter study of paroxysmal nocturnal hemoglobinuria cells in patients with bone marrow failure. Cytometry B. 2014;**86B**:175-182. DOI: 10.1002/cyto.b.21139

[8] Hillmen P, Lewis SM, Bessler M, Luzzatto L, Dacie JV. Natural history of paroxysmal nocturnal hemoglobinuria. The New England Journal of Medicine. 1995;**333**:1253-1258. DOI: 10.1056/NEJM199511093331904

[9] Richards SJ, Rawstron AC, Hillmen P. Application of flow cytometry to the diagnosis of paroxysmal nocturnal hemoglobinuria. Cytometry. 2000;**42**:223-233. DOI: 10.1002/1097-0320(20000815)42:4%3C223::AID-CYTO2%3E3.0.CO;2-D

[10] van der Schoot CE, Huizinga TW, van't Veer-Korthof, Wijmans R, Pinkster J, von dem Borne AE. Deficiency of glycosyl-phosphatidylinositol-linked membrane glycoproteins of leukocytes in paroxysmal nocturnal hemoglobinuria, description of a new diagnostic cytofluorometric assay. Blood. 1990;**76**:1853-1859 PMD: 2145990

[11] Hall SE, Rosse WF. The use of monoclonal antibodies and flow cytometry in the diagnosis of paroxysmal nocturnal hemoglobinuria. Blood. 1996;**87**:5332-5340 PMD: 8652849

[12] Borowitz MJ, Craig FE, DiGiuseppe JA, Illingworth AJ, Rosse W, Sutherland DR, Wittwer CT, Richards SJ, On Behalf of the Clinical Cytometry Society. Guidelines for the diagnosis and monitoring of paroxysmal nocturnal hemoglobinuria and related disorders by flow cytometry. Cytometry. Part B. 2010;**78B**:211-230. DOI: 10.1002/cyto.b.20525

[13] Sutherland DR, Keeney M, Illingworth A. Practical guidelines for the high-sensitivity detection and monitoring of paroxysmal nocturnal hemoglobinuria clones by flow cytometry. Cytometry. Part B. 2012;**82B**:195-208. DOI: 10.1002/cyto.b.21023

[14] Sutherland DR, Acton E, Keeney M, Davis BH, Illingworth A. Use of CD157 in FLAER-based assay for high sensitivity PNH granulocyte and PNH monocyte detection. Cytometry. Part B. 2014;**86B**:44-55. DOI: 10.1002/cyto.b.21111

[15] Marinov I, Kohoutová M, Tkáčová V, Pešek A, Čermák J, Cetkovský P. Clinical relevance of CD157 for rapid and cost-effective simultaneous evaluation of PNH granulocytes and monocytes by flow cytometry. International Journal of Laboratory Hematology. 2015;**37**:231-237. DOI: 10.1111/ijlh.12271

[16] Sutherland DR, Richards SJ, Keeney M, Illingworth A. High-sensitivity detection of PNH red blood cells, red cell precursors and white blood cells. Current Protocols in Cytometry. 2015;**72**: Unit 6.37.1-6.37.29. DOI: 10.1002/0471142956.cy0637s72

[17] Kalina T, Flores-Montero J, van der Velden VH, Martin-Ayuso M, Böttcher S, Ritgen M, Almeida J, Lhermitte L, Asnafi V, Mendonça A, de Tute R, Cullen M, Sedek L, Vidriales MB, Pérez JJ, te Marvelde JG, Mejstrikova E, Hrusak O, Szczepański T, van Dongen JJ, Orfao A; EuroFlow Consortium (EU-FP6, LSHB-CT-2006-018708). EuroFlow standardization of flow

cytometer instrument settings and immunophenotyping protocols. Leukemia 2012;**9**:1986-2010. DOI: http://dx.doi.org/10.1038/leu.2012.122

[18] F. Solly, Rigollet L, Baseggio L, Guy J, Borgeot J, Guérin E, Debliquis A, Drenou B, Campos L, Lacombe F, Béné MC. Comparable flow cytometry data can be obtained with two types of instruments, Canto II, and Navios. A GEIL study. Cytometry. Part A 2013;**83**:1066-1072. DOI: http://dx.doi.org/10.1002/cyto.a.22404

[19] Lacombe F, Bernal E, Bloxham D, Couzens S, Porta MG, Johansson U, Kern W, Macey M, Matthes T, Morilla R, Paiva A, Palacio C, Preijers F, Ratei R, Siitonen S, Allou K, Porwit A, Béné MC. Harmonemia: A universal strategy for flow cytometry immunophenotyping-A European LeukemiaNet WP10 study. Leukemia 2016;**8**:1769-1772. DOI: http://dx.doi.org/10.1038/leu.2016.44

[20] Byrd T, Carr KD, Norman JC, Huye L, Hegde M, Ahmed N. Polystyrene microspheres enable 10-color compensation for immunophenotyping of primary human leukocytes. Cytometry. Part A 2015;**87**:1038-1046. DOI: http://dx.doi.org/10.1002/cyto.a.22717

[21] Kajimoto Y, Miyagawa J, Ishihara K, Okuyama Y, Fujitani Y, Itoh M, Kaisiho T, Mtsuoka T, Watada H, Hanafusa T, Yamasaki Y, Kamada T, Matsuzawa Y, Hirano T. Pancreatic islet cells express BS-1, a CD38-like surface molecule having ADP-ribosyl cyclase activity. Biochemical and Biophysical Research Communications 1996; **219**:941-946. DOI: http://dx.doi.org/10.1006/bbrc.1996.0327

[22] Hernandez-Campo PM, Almeida J, Sanchez ML, Malvezzi M, Orfao A. Normal patterns of expression of glycosylphosphatidylinositol-anchored proteins on different subsets of peripheral blood cells: A frame of reference for the diagnosis of paroxysmal nocturnal hemoglobinuria. Cytometry. Part B, DOI. 2006;**70B**:71-81. http://dx.doi.org/10.1002/cyto.b.20087

[23] Davis BH, Keeney M, Brown R, Illingworth AJ, King MJ, Kumpel B, Meier ER, Sandler SG, Shaz BH, Sutherland DR. CLSI H52-A2 Red Blood Cell Diagnostic Testing Using Flow Cytometry; Approved Guideline, 2nd ed. Wayne, PA: Clinical and Laboratory Standards Institute. 2014. ISBN: 1-56238-957-2.

[24] Owens MA, Vall HG, Hurley AA, Wormsley SB. Validation and quality control of immunophenotyping in clinical flow cytometry. Journal of Immunological Methods. 2000;**243**:33-50. DOI: 10.1016/S0022-1759(00)00226-X

[25] ISO 3534-1:2006. Statistics-Vocabulary and Symbols. General Statistical Terms and Terms Used in Probability. Geneva: ISO; 2006

[26] Libeer J-C. Role of external quality assurance schemes in assessing and improving quality in medical laboratories. Clinica Chimica Acta. 2001;**309**:173-177. DOI: 10.1016/S0009-8981(01)00518-6

[27] CLSI EP12-A2: User Protocol for Evaluation of Qualitative Test Performance—Second Edition—Approved Guideline. Wayne, PA: National Committee for Clinical Laboratory Standards, 2008. ISBN 1-56238-468-6

[28] NCCLS. Protocols for Determination of Limits of Detection and Limits of Quantitation Approved Guideline. NCCLS document EP17-A. 2004. ISBN 1-56238-551-8

[29] CLSI EP06-A: Evaluation of the Linearity of Quantitative Measurement Procedures—Approved Guideline. Wayne, PA: National Committee for Clinical Laboratory Standards, 2003. ISBN 1-56238-498-8

[30] Spitzenberger F, Edelhaeuser R. Accreditation of medical laboratories in Europe: Statutory framework, current situation and perspectives. Transfusion Medicine and Hemotherapy. 2006;**33**:384-392. DOI: 10.1159/000094738

[31] Validation of cell-based fluorescence assays: practice guidelines from the international council for standardization of haematology and international clinical cytometry society. Cytometry, Part B (Clinical Cytometry). 2013;**84B**:Special Issue. ISSN: 1552/4949

[32] Marinov I, Kohoutová M, Tkáčová V, Pešek A, Pešek A, Čermák J, Cetkovský P. Performance characteristics of consensus approaches for small and minor paroxysmal nocturnal hemoglobinuria clone determination by flow cytometry. Clinical Chemistry and Laboratory Medicine. 2013;(11):2133-2139. DOI: 10.1515/cclm-2013-0251

[33] ISO 15189-1012. Medical Laboratories—Requirements for Quality and Competence. Geneva: ISO; 2012

Chapter 2

Insight into the Leukemia Microenvironment and Cell-cell Interactions Using Flow Cytometry

Katarzyna Piwocka,
Paulina Podszywalow-Bartnicka, Julian Swatler,
Marta D. Kolba, Agata Kominek and Ewa Kozlowska

Additional information is available at the end of the chapter

http://dx.doi.org/10.5772/intechopen.76481

Abstract

Cancer cells, including leukemia cells, reside in a complex microenvironment, which influences biology and activity of the cells. The protective role of bone marrow stromal cells is already commonly recognized. Remodeling of stroma cell functions by leukemia cells is also well documented. In this respect, different routes of interactions were defined, such as direct cell-cell interactions or indirect cross talk, by release of soluble factors or vesicular particles containing proteins, RNAs and other molecules. Since intercellular communication seems to play a role in various biological processes, it might be important to conduct studies in co-culture systems, which at least mimic partially more physiological conditions, and enables this intercellular exchange to occur. Thus, it is crucial to improve analytical methods of investigation of co-cultured cells, to study their interactions and so to understand biology of leukemia in order to understand molecular mechanisms and offer novel therapeutic strategies. The present chapter outlines the importance of modern, multiparameter flow cytometry methods, which allow to analyze interactions between different types of cells within the leukemia microenvironment. Importantly, the proposed experimental setups can be easily transformed to study different cell types and different biological systems.

Keywords: co-culture, cell-cell interactions, cell tracking, tracking dyes, proliferation dyes, viability dyes, barcoding, cancer microenvironment, stroma, regulatory T cells, extracellular vesicles (EVs), tunneling nanotubes (TNTs)

1. Introduction

Cancer cells, including leukemia cells, reside in a microenvironment, which influences biology and activity of these cells. The importance of microenvironment in leukemia cells biology is widely accepted. Leukemia microenvironment is a complex and dynamic network, comprising different types of cells [1]. There is a direct and indirect cross talk between these cells, which modulates cell function, signal transduction and response to therapy. This intercellular interactions can contribute to leukemogenesis [2]. Thus, unraveling of interplay between all types of cells and the microenvironment is crucial for understanding the biology of leukemia.

Because of its key regulatory role, the cross talk between leukemia and bystander cells is of interest as possible therapeutic target [3]. It is critically important to take such cell-cell interactions into account in the studies of potential therapeutic strategies, novel therapeutic targets and novel treatment regimes. To partially mimic the physiological conditions, an increasing number of the basic research as well as preclinical studies in the cancer biology area use the *in vitro* cell co-culture systems, in which two or more types of cells are cultured together [4]. This allows natural interactions to occur between different types of cells, which normally coexist within the microenvironment.

Therefore, it becomes crucial to improve analytical methods of investigation of co-cultured cells to study their interactions and so to understand biology of leukemia in order to offer novel therapeutic strategies. The principle of flow cytometry is separation of cells/events based on their fluorescence signals. Using different types of cell tracking techniques, combined with modern, multiparameter flow cytometry methods, it has become possible to analyze interactions between different types of cells within the leukemia microenvironment. Flow cytometry allows for gating cells of interest from the whole cell mixture based on the fluorescence parameter to study different cell features, cellular processes and signaling in separated subpopulations.

2. Bone marrow niche in leukemia

The concept of "niche" has been introduced in 1978 by Schofield to describe the possibility of association of hematopoietic stem cell (HSC) with its surroundings that regulates and determines HSC fate, such as self-renewal, differentiation, proliferation and survival [5]. Since then, many evidences appeared showing its composition and function. The bone marrow microenvironment (BMM) is complex and consists of the extracellular matrix and multiple cell populations, including different types of endothelial cells, osteolineage cells, osteoclasts, adipocytes, sympathetic neurons, non-myelinating Schwann cells, mesenchymal cells and macrophages [1, 6]. Interactions between leukemia cells and their niche are bi-directional. They represent either direct interactions by cell-cell contact or indirect interactions by secreted soluble factors and extracellular vesicles.

Over the years, our understanding of the BMM role in leukemogenesis has greatly increased. Bone marrow microenvironment supports proleukemic features of cells. Regulation of leukemia stem/progenitor cells (LS/PC) strongly depends on the signals from the bone marrow microenvironment [3, 7]. They promote leukemia progression as well as development of resistance

to therapy. Bone marrow microenvironment is a key player in the pathogenesis and leukemia development by creating conditions which promote survival and proliferation of leukemic blasts [8].

There are many evidence confirming protective role of the bone marrow stroma. Several mechanisms leading to chemoresistance in leukemia cells mediated by BMM have been described. Among these, stroma fibroblasts represent one of the main population within the bone marrow niche, strongly supporting leukemogenesis. Interaction of leukemia cells with stroma fibroblasts results in the increased resistance to cell death in response to drug treatment, changes in metabolism and decreased clonogenic potential [9, 10]. Leukemia cells can also shape the bone marrow microenvironment. We have observed that leukemia cells participate in the remodeling of stroma extracellular matrix [11]. Due to secretion of stroma-modifying enzymes, leukemia cells support disarrangement in the leukemic bone marrow. Another aspect of the leukemia microenvironment is development and promotion of the inflammatory microenvironment [12, 13]. Activation of intrinsic factors like NF-κB as well as extrinsic components including cytokines, chemokines and adhesion molecules leads to complex responses promoting proinflammatory state. In general, this supports the process of transformation, survival and proliferation of leukemia cells.

Altogether, due to their importance and key role, targeting the leukemia-stroma interactions has gained big interest as a novel and attractive strategy for anti-leukemia treatment. Currently, our understanding of the function and importance of the bone marrow niche in hematological neoplasms has increased due to improved murine models and development of imaging tools [14–16]. Nevertheless, the *in vitro* studies are still necessary to investigate mechanisms and signaling between leukemia and stromal cells as well as a proof of concept experiments in the drug designing and testing of novel therapeutic strategies.

Our group is involved in the studies of leukemia-stroma interactions and remodeling of stroma cell functions mediated by leukemia cells. We have used experimental setups to investigate leukemia cells *in vitro*, either cell lines or primary cells from patients, in the conditions mimicking the bone marrow millieu, thus hypoxia and co-culture with stroma fibroblasts. Herein we present and discuss some of the experimental systems utilized to study the role of the cross talk between leukemia and stromal cells to which multiparameter flow cytometry can be adapted. Importantly, these experimental approaches can be transferred to other cell types and different biological systems.

3. Fluorescent cell tracking to follow cell type, function, and state in co-cultures

Upon co-culture conditions, when different types of cells are cultured together, the key component of the experimental strategy enabling cell analysis is to separate both cell types, either physically by sorting or by flow cytometry gating. For this, cells have to express some fluorescent protein or have to be stained and tracked by fluorescent dye. This allows to separate signals from each type of cell based on the different fluorochromes using flow cytometry. The scheme and typical histograms to analyze tracked cells in co-culture are presented in **Figure 1**.

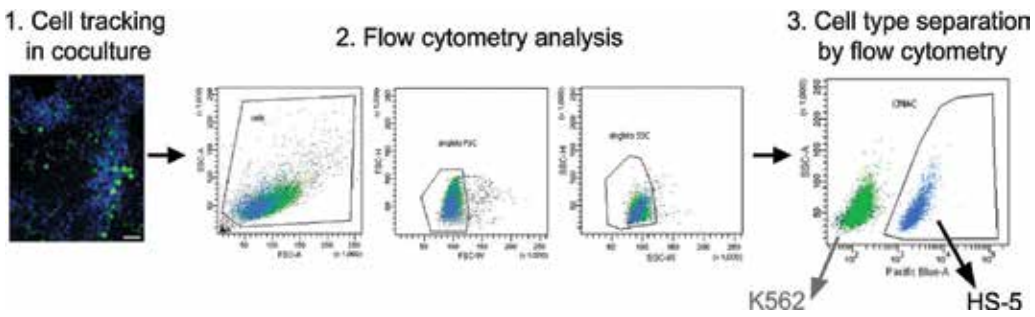

Figure 1. Scheme of the cell type separation by fluorescent tracking followed by flow cytometry gating.

3.1. Fluorescent cell trackers

Cell trackers have been successfully used for years in multiple studies, starting from immunology, which intensively utilized flow cytometry techniques [17–19]. Today, there is a broad spectrum of commercially available tracking dyes, which simultaneously allow to track cells and study proliferation and/or viability. Cell tracking dyes vary widely in their chemistries and fluorescence properties but the great majority fall into one of two classes based on their mechanism of cell labeling. They are represented by "membrane dyes," which are highly lipophilic dyes that go stably but noncovalently into cell membranes or "protein dyes," which are amino-reactive dyes that form stable covalent bonds with cell proteins [20]. They are safe and can be used in viable cells even in the long-term cultures. Big variability allows excitation by any available laser and usage in combination with other fluorochromes in multiparameter studies. **Table 1** presents the tracking dyes currently available for different lasers. These dyes can be used separately or combined due to their different excitation signals. It is important to mention that due to its nature, the fluorescent signal of labeled population is decreasing, depending on the growth rate of cells. So, quickly dividing cells will lose tracing signal faster than cells with longer cell cycle. This feature, on the one hand, enables monitoring of cell proliferation rate in co-culture setups but on the other hand limits the time frame within which the subpopulation of dye-labeled cells can be distinguished. **Figure 2** presents an example of the time-course of CMAC fluorescence measured by flow cytometry, when different concentrations of CMAC dye were used. After 72 h, two populations were not clearly separated anymore when the lower concentration of CMAC was used. Therefore, also concentration of the dye used for labeling of different types of cells should be chosen accordingly to the level of fluorescence detected at the end time point of planned experiment and verified in the toxicity assay.

Another strategy to track cells is expression of fluorescent proteins. Green fluorescent protein (GFP) has been purified in the 60-ties from *Aequorea victoria* [21]. This has started a new era of studies, in which original or engineered GFP as well as other fluorescent proteins were utilized to tag proteins of interest. Today, GFP derivatives, yellow fluorescent protein (YFP) and a big family of red fluorescence proteins (RFP), which are derivatives of DsRed isolated from *Discosoma* sp. [22], are commonly used in many different studies. The advantage of this strategy is stable fluorescent signal; however, the stable expression of fluorescent proteins has some limitations, requires transfection of cells and is connected with the nonphysiological

Function	Excitation laser [nm]	Dye	Emission (nm)
Proliferation	405 (violet)	CellTrace violet cell proliferation kit	450
		Violet proliferation dye 450	450
	488 (blue)	CFSE	520
		EdU proliferation kit (iFluor 488)	520
	530 (yellow-green)	CellTrace yellow cell proliferation kit	579
	560 (yellow)	CellTrace yellow cell proliferation kit	579
	633/640 (red)	CellTrace far red cell proliferation kit	661
Viability	355 (UV)	CellTrace calcein blue	425
		Hoechst 33258	450
		DAPI	470
	405 (violet)	CellTrace calcein violet	452
		SYTOX blue dead cell stain	480
	488 (blue)	CellTrace calcein green	515
		SYTOX green dead cell stain	523
		TO-PRO™-1 iodide	530
		SYTOX orange dead cell stain	570
		Propidium iodide	617
		7-AAD (7-aminoactinomycin D)	647
	530 (yellow-green)	SYTOX orange dead cell stain	570
		Propidium iodide	617
		7-AAD (7-aminoactinomycin D)	647
	560 (yellow)	Propidium iodide	617
		7-AAD (7-aminoactinomycin D)	647
	633/640 (red)	TO-PRO™-3 iodide	661
Fixable viability	355 (UV)	Live/dead fixable dead cell stain kit (450)	450
	405 (violet)	Live/dead fixable dead cell stain kit (450)	450
		Fixable viability stain 450	450
		Fixable viability stain 510	510
		Live/dead fixable dead cell stain kit (525)	525
		Live/dead fixable dead cell stain kit (575)	575
		Fixable viability stain 575 V	575
	488 (blue)	Fixable viability stain 520	520
		Live/dead fixable dead cell stain kit (530)	530
		Live/dead fixable dead cell stain kit (585)	585

Function	Excitation laser [nm]	Dye	Emission (nm)
	530 (yellow-green)	Fixable viability stain 620	620
	560 (yellow)	Fixable viability stain 570	570
	633/640 (red)	Fixable viability stain 660	660
		Live/dead fixable dead cell stain kit (660)	660
		Fixable viability stain 700	700
		Live/dead fixable dead cell stain kit (780)	780
Cell tracking	355 (UV)	Hoechst 33342	450
		CytoPainter blue cell tracking staining kit	455
		CellTracker™ blue CMF2HC	464
		CellTracker™ blue CMAC	466
	405 (violet)	CellTracker™ violet BMQC	516
		CytoPainter green cell tracking staining kit	520
	488 (blue)	CellTracker™ green CMFDA	517
	530 (yellow-green)	CytoPainter orange cell tracking staining kit	560
	560 (yellow)	CellTracker™ CM-DiI	570
		CellTracker™ orange CMRA	575
		CytoPainter red cell tracking staining kit	600
		CellTracker™ CMTPX	602
	633/640 (red)	CellTracker™ deep red	650
		CytoPainter deep red cell tracking staining kit	650

Table 1. Tracking dyes used for fluorescent cell staining; function, excitation, and emission spectra as well as full name are shown.

overexpression of novel form of protein. On the other hand, the signal from the expressed fluorescent protein is relatively stable over time. Thus, this attitude might have advantage over cell tracking in case of long-term experiments.

Recently, a highly advanced methodology based on the lentiviral fluorescent genetic barcoding system for flow cytometry-based multiplex cell tracking has been used to follow clonal subpopulations in the real time [23]. Cells transduced with the lentiviral vectors are individually marked by a highly characteristic pattern of insertion sites inherited by all their progeny. The system allows creation of 26, 14, or 6 unique labels, and the color-coded populations can be tracked for up to 28 days.

Another strategy to perform high-content multiplex analysis is based on the fluorescent cell barcoding (FCB) technique [24, 25]. In FCB, each sample is labeled with a unique fluorescent signature (barcode), of different fluorescence intensity (due to dilutions) and/or emission wavelength, mixed together with other samples, then stained with antibodies or probes and analyzed by flow cytometry as a single sample. Today, there is a variability of FCB dyes

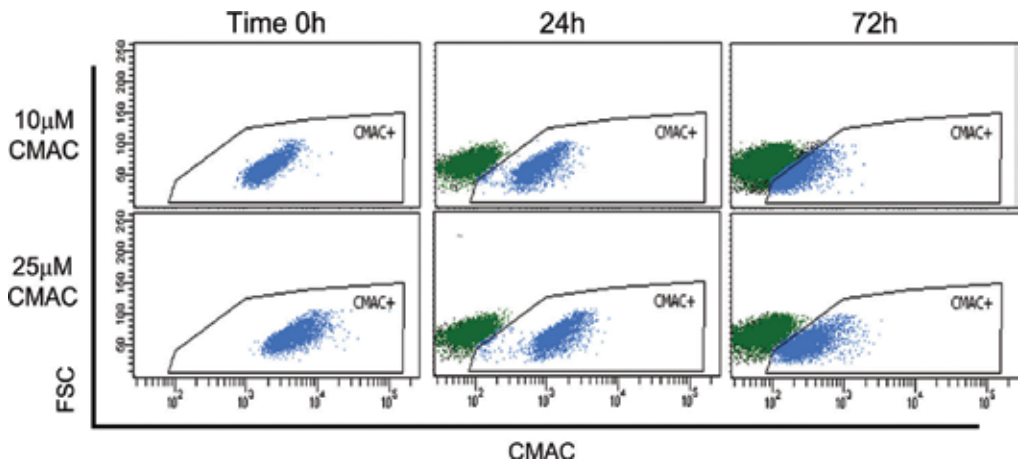

Figure 2. The time-course of CMAC fluorescence measured by flow cytometry upon conditions when different concentrations (10 and 25 μM) of CMAC dye were used. CMAC-positive (CMAC+, blue) subpopulation is gated. Green subpopulation represents CMAC-negative cells in co-culture.

which can be utilized, such as CBD500, Pacific Orange NHS ester, DyLight 350 NHS ester, and DyLight 800 NHS ester, Pacific Blue dyes, Alexa dyes, eFluor, and others. Using this technique allows to perform multiplate assays in relatively short time and with economical use of reagents, as mixing sample prior to staining, antibody consumption is reduced 10- to 100-fold. Importantly, either viable or fixed samples can be barcoded, thus giving broad possibilities to combine FCB with other multiparameter protocols. Such strategy can be used to analyze samples under treatments, co-cultured, or stimulated with different agents. FCB has been successfully utilized for different studies, including drug screening and cell signaling profiling studies [26], intracellular cytokine production [27], immunophenotyping [28], and others.

3.2. Cell proliferation dyes

Quantitative assessment of proliferation is an important parameter in leukemia and other cancer studies. Especially, when co-culture with stroma provides protective signaling, proliferation is analyzed as one of the major parameters to estimate cytostatic effects. Moreover, proliferation dyes can also be utilized to fluorescently track cells in co-culture. So, in addition to detection and quantifying cell divisions, these dyes can be used to distinguish one type of cells from the other. The measurement, independently on the tracking dye used, relies on the same mechanism, namely permanent labeling of cells without affecting morphology or physiology to trace generations or divisions *in vivo* or *in vitro*. Dilutions of the dye equally distributed to daughter cells as a result of cell divisions can be measured by flow cytometry [17, 20]. The scheme of CFSE dilution with each cell division and flow cytometry measurement is presented in **Figure 3**.

For many years, CFSE dye (carboxyfluorescein succinimidyl ester) was a gold standard for tracking cell divisions [29]; however, today there is a variety of tracking dyes allowing to measure the proliferation index. Proliferation dyes are available for the UV, violet, blue, yellow, and red lasers, giving more flexibility in multiplexed experiments [29, 30] (see **Table 1**, Proliferation). Compared to the classical CFSE, modern proliferation trackers are less cytotoxic

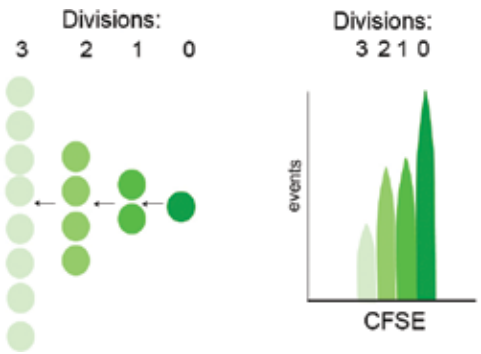

Figure 3. The scheme of tracking cells with proliferation dye. Dilution of CFSE with cell divisions (left panel) and CFSE detection by flow cytometry (right panel) are shown.

and more stable. Importantly, what has been already mentioned above, decrease of the fluorescence signal resulting from dye dilution with every division has to be considered when tracking cells with proliferation dyes.

In our studies, in which GFP-expressing CML cells have been co-cultured with stroma fibroblasts labeled with CMAC dye, tracking of subpopulations has been combined with analysis of proliferation (**Figure 4**). To do so, subpopulations have been gated based on the fluorescent signal of the cell tracker, either GFP (A) or CMAC (B), followed by separate analysis of cell divisions in each subpopulation. Such strategy allowed to investigate the impact of co-culture conditions on the proliferation index of either leukemia or stromal cells. This protocols can also be utilized in co-cultures under treatment with anticancer drugs to verify the protective effect of stroma. Similar strategy has been used to investigate interactions of lymphocytes with mesenchymal stem cells [31] as well as in the co-cultures of healthy or malign breast tissue-derived stromal cells with human breast adenocarcinoma cell line MCF-7 [32]. Altogether, proliferation dyes represent a very potent group of tracking dyes analyzed with a broad range of available lasers and cytometers.

3.3. Multiparameter studies

Modern flow cytometry, due to development of multiple laser systems, provides possibility for polychromatic analysis of many parameters in single cells. The key to success, particularly in the studies, in which multiple dyes are used to track different types of cell, is therefore to understand the critical issues enabling optimal use of different tracking dyes. It has to be noticed that some limitations appear when using tracking dyes in co-culture experiments. Each class of commercially available cell trackers—lipophilic "membrane" dyes and amino-reactive "protein" dyes possess advantages and limitations. Thus, there is a need for optimization of different proliferation tracking dyes especially when combined together [33]. Recently, a novel edition of protocols to study cell proliferation by dye dilution, alone or in combination with other methods, has been published [34]. The authors discuss currently available tracking dyes, with suppliers and new spectral properties, as well as describe evaluations to be performed when selecting one for use in multicolor proliferation monitoring. The protocols presented by the authors address the critical issues related

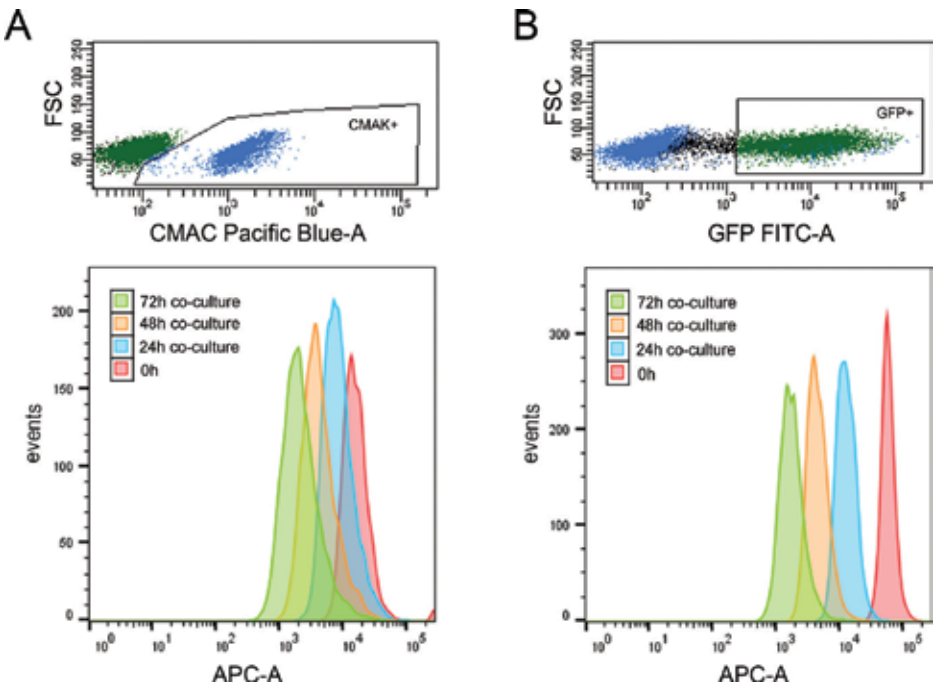

Figure 4. Analysis of cell proliferation estimated upon tracking with CMAC, combined with cell-type gating in co-culture of leukemia and stromal cells. (A) Leukemia cells expressed GFP protein (GFP+) and (B) stromal cells were tracked with CMAC (CMAC+). Labeling with CMAC allowed for cell-type gating and simultaneous analysis of cell divisions. CMAC was detected in the APC channel; histograms show CMAC dilution at different time points of co-culture.

to suboptimal tracking combinations, reproducible labeling, combining of cell tracking dyes with fluorescent antibodies staining and others. Briefly, the recommendations include evaluating the dye's spectral profile and available cytometers/lasers to optimize compatibility with other fluorochromes and to minimize compensation problems, evaluating the effect of labeling on cell growth rate, testing cell divisions and dye dilutions to determine the maximum number of generations to be included when using dye dilution profiles, and verifying that relevant cell functions remain unaltered by tracking dye labeling.

As proliferation is tracked in living cells, it enables to combine analysis of cell proliferation with other live-cell applications, such as immunophenotyping, cell sorting, cell cycle analysis, mitochondrial potential, ROS studies, and others. This possibility has been utilized, for example, in the studies in which myelin-phagocytosing macrophages were co-cultured with CFSE-labeled T lymphocytes followed by analysis of surface receptors and role of nitric oxide [35]. In other studies, cell tracker has been used to investigate immune cells proliferation and cytotoxicity [36].

Another group of trackers is represented by the fixable viability dyes, enabling the post-fixation discrimination of dead cells, which lost plasma membrane integrity before fixation (see **Table 1**, Viability). This gives a novel opportunity to combine them with staining procedures which require fixation. Thus, analysis of internal targets, like as intracellular protein levels or γH2AX, within the population of cells which was alive prior fixation, was possible. In our

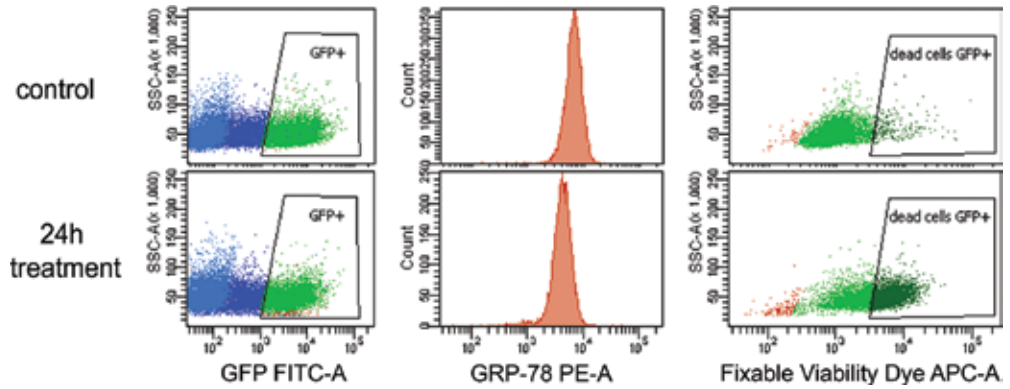

Figure 5. Combination of cell tracking by expression of GFP protein (GFP+, green), with analysis of apoptosis by using fixable viability dye and estimation of intracellular level of Grp78 protein (red histograms). Subpopulation expressing high level of GFP was gated (GFP+) and further analyzed. Cells were untreated (control) or treated with antileukemic drug for 24 h.

studies, we have combined cell tracking with GFP expression together with analysis of apoptosis by fixable viability dye and detection of intracellular level of Grp78 protein (**Figure 5**). Cells were co-cultured and the subpopulation expressing high level of GFP (GFP+) was gated and further analyzed. Additionally, as cells were treated with anti-leukemia drug, this procedure enabled to estimate sensitivity to treatment by detection of dead cells.

4. Application of flow cytometry in the studies of cell-cell cross talk by extracellular vesicles

4.1. Extracellular vesicles

In recent years, extracellular vesicles (EVs) have emerged as an important mean of intercellular communication, both in physiological conditions and in disease. They seem to play a crucial role in the cell-cell communication between cancer cells and the neighboring cells and they have been shown to be important for the development of cancer [37, 38]. Extracellular vesicles are released by most cell types and contain lipids, proteins, and different nucleic acids—mRNAs, ncRNAs (including miRNAs), and fragments of DNA. EVs are classified depending on their origin: released from multivesicular bodies (exosomes, 30–100 nm), shed from plasma membrane (microvesicles, usually 50–500 nm), or formed during apoptosis (apoptotic bodies, about 1 μm) [39, 40]. EVs can influence targeted cells both locally and in distant tissues. They regulate multiple biological processes, such as cell differentiation, tissue homeostasis, immune response, and cell signaling, and can contribute to disease progression, for example, by affecting tumor microenvironment [41]. Recently, the role of EVs in tissue repair, immunotherapy, and drug delivery has also been evaluated.

Extracellular vesicles play a significant role in pathology of hematological malignancies, including chronic myeloid leukemia (CML) [42]. It has been demonstrated that exosomes produced by

CML cells support leukemic cell growth and survival in an autocrine manner, both *in vitro* and *in vivo* [43]. Moreover, factors facilitating leukemic transformation have been identified within vesicles released by leukemia cells [44]. Extracellular vesicles not only directly supported leukemia cell growth but also potently modified components of CML microenvironment to further promote leukemia progression. CML-derived exosomes activated EGFR signaling in stromal cells, which led to IL-8 production by stroma bone marrow fibroblasts and which in turn stimulated leukemia cell adhesion to stromal cells [45, 46]. CML exosomes have been widely studied in terms of their influence on neovascularization process, which has previously been shown to support progression of leukemia [47]. Our own unpublished data suggest that extracellular vesicles released by murine BCR-ABL-expressing progenitor cells may also influence function of cells in distant tissues. Altogether, this supports the notion that leukemic EVs constitute an important mechanism of disease progression both by direct influence on CML cells and by indirect modification of leukemic niche components and immune cells. Moreover, EVs components, such as proteins and microRNAs, have recently become of interest as biomarkers in hematological malignancies [42, 48, 49]. Thus, analysis of EVs number, size, and composition may soon be used to diagnose, stage, and even analyze relapse of hematological malignancies in the clinical setting.

4.2. Analysis of EVs uptake and binding by flow cytometry

Multiple studies underline functional relevance of different extracellular vesicles. Thus, a significant aspect of research is analysis of fluorescently labeled EVs uptake or binding to different cells, both in *in vitro* and *in vivo* experiments. It allows to confirm biological relevance of experiments and exclusion of indirect effects on target cells. Different analytical techniques are used to study extracellular vesicles, as there is no one single method which can be proposed to analyze these particles [50]. Confocal microscopy is widely used to analyze EVs uptake by cells [51]. However, the flow cytometry provides a very good and fast method for quantification of EVs uptake or binding to cells.

Flow cytometry allows to quickly assess if association of EVs with target cells is dose- and time-dependent. This may incline biologically active doses of EVs and thus help choose appropriate amounts of EVs for further functional studies. Multicolor flow cytometry allows to monitor association of EVs to different subpopulations of cells, especially *in vivo* or in *ex vivo* cultures of, for example, immune cells. This is doable if a combination of fluorescent EVs labeling is used in parallel with staining of protein markers of subpopulations with fluorochrome-conjugated antibodies. Moreover, flow cytometry analysis enables correlation of EVs uptake with various biological parameters, such as cell viability, apoptosis, proliferation, and expression of signaling molecules. Such approach allows more precise and direct observation of functional effects of EVs. On the other hand, opposed to confocal microscopy, flow cytometry does not distinguish between uptake and binding of extracellular vesicles to target cells, but rather gives information on association of EVs with target cells. Such information may be relevant in terms of mechanism of influence on target cells, as solely binding to surface of target cell suggests regulation through mediators (mostly proteins) on EVs surface rather than by, for example, non-coding RNAs in the lumen.

Various methods and reagents may be used to fluorescently label extracellular vesicles for analysis using flow cytometry (**Table 2**). EVs staining can either lead to labeling of all types of

Function	Excitation laser (nm)	Dye	Emission (nm)
Lumen labeling	488 (blue)	CFDA-SE (CFSE)	517
		CalceinAM	515
Membrane labeling	488 (blue)	PKH67	504
		DiO	501
	560 (yellow)	PKH26	567
		Dil	565
	633/640 (red)	DiD	665

Table 2. Fluorescent dyes used to fluorescently label extracellular vesicles for analysis by flow cytometry; function, excitation, and emission spectra as well as full name are shown.

vesicles or any of the specific populations, like exosomes or microvesicles. To stain EVs lumen, widely used dyes such as CFSE and CalceinAM may be used. Those dyes in non-fluorescent form passively enter EVs and due to esterase activity in the EV lumen are transformed into fluorescent molecules. Gray et al. demonstrated that CalceinAM stains only intact EVs, which may be advantageous for its use in both EVs uptake studies and direct flow cytometry of EVs [52]. CFSE staining was applied to quantitatively show differential association of cancer EVs with myeloid cells depending on their differentiation into various stages of monocyte and dendritic cell development [53]. In our experiments, we have used CFSE labeling to study the dose-dependent uptake of EVs released by murine BCR-ABL-expressing cells by thymocytes (**Figure 6**). It is clearly visible that increasing amounts of fluorescently labeled EVs correlate with increased fluorescence of CFSE signal detected in acceptor thymocytes.

Membrane staining is also widely used to label EVs with the use of dyes such as PKH67, PKH26, DiD, Dil, and DiO. They allow a wider choice of fluorescence spectra but, as they are lipophilic, can form various aggregates and micelles. Thus, in this case, EVs need to be carefully washed to avoid adding unbound dye which may nonspecifically label cells. PKH67

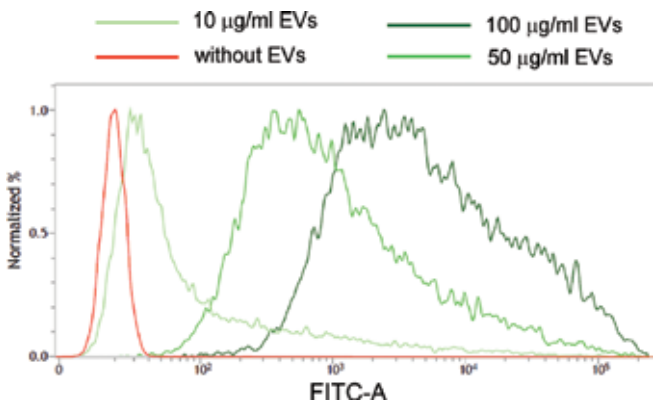

Figure 6. CFSE labeling to study uptake of EVs. Leukemia-released EVs were labeled with CFSE and different amounts of EVs were added to thymocytes. Fluorescence of CFSE in thymocytes was detected by flow cytometry in FITC channel.

was used for EVs labeling to track time-dependent uptake of mantle cell lymphoma-derived exosomes by different immune cells and cell lines and to investigate their possible therapeutic potential. Lai et al. took another approach on staining of EV membrane by fusing GFP at N-terminus with palmitoylation signal and thus directing it to plasma and EV membrane. This enabled more specific staining than with the use of PKH67 dye. Additionally, it allows effective *in vivo* tracking of EVs released by tumors [51]. Furthermore, fusion of specific EV-enriched proteins (such as tetraspanins—CD9, CD63, CD81; ESCRT proteins—Tsg101; proteins widely expressed on cells producing EVs—e.g. HLA proteins) with GFP/RFP or other fluorescent proteins can be applied. CD63-GFP and CD81-GFP have already been used by different groups to track exchange of EVs using flow cytometry [54].

4.3. Flow cytometry analysis of extracellular vesicles

Flow cytometry has emerged as one of the tools for analysis of extracellular vesicles and their composition. As detection limit of conventional flow cytometers is around 500 nm, bead capture of EVs has been used to facilitate, for example, analysis of proteins expressed on their surface. However, direct flow cytometry of extracellular vesicles has also been widely performed [55]. As light scatter triggering itself is not sufficient to distinguish nanoscale vesicles, fluorescence triggering has been used to directly identify EVs on flow cytometers. Commercially available flow cytometer (BD Influx) has been adapted for high-throughput analysis of fluorescently labeled vesicles. PKH67 staining of EVs allowed fluorescence-based thresholding of events, and by modifying cytometer elements, the authors were also able to observe size distribution of exosomes in the FSC channel. The described technique allowed to identify molecules expressed on the surface of EVs [56] and then apply the method to perform quantitative and qualitative analyses of dendritic cell-released EVs upon different stimulations and culture conditions [57]. Direct flow cytometry of fluorescently labeled EVs using conventional flow cytometers has been applied to study mesenchymal stromal cell markers (CD90, CD44, CD73) on EVs released by HS-5 and K562 cells as well as to analyze surface molecules expressed on microvesicles isolated from patient sera with hematological tumors (CD20, CD38, CD30) [48].

However, direct flow cytometry of EVs needs to be used cautiously, as different sample parameters and cytometer settings may affect measurements. It was demonstrated that due to high concentration of very small molecules in suspension, the measurement may not be precise, due to analysis of multiple events as one. Flow cytometry is emerging as a tool for direct analysis of EVs and their surface markers, allowing fast and precise measurements. Various aspects of EVs analysis by FACS are demonstrated in a special issue of Cytometry Part A Journal "Measurement of Extracellular Vesicles and Other Submicron Size Particles by Flow Cytometry" [58]. It is noteworthy that due to small size of EVs precise fluorescent labeling needs to be applied and conventional flow cytometer settings need to be cautiously optimized, for example, by using fluorescent beads of different sizes (e.g. 200 and 100 nm beads).

4.4. Fluorescent tracking and flow cytometry analysis of direct, intercellular transfer of vesicular cargo

Recently, a novel way of intercellular communication has been described. This is mediated by the long intercellular connections called tunneling nanotubes (TNTs), which link two cells

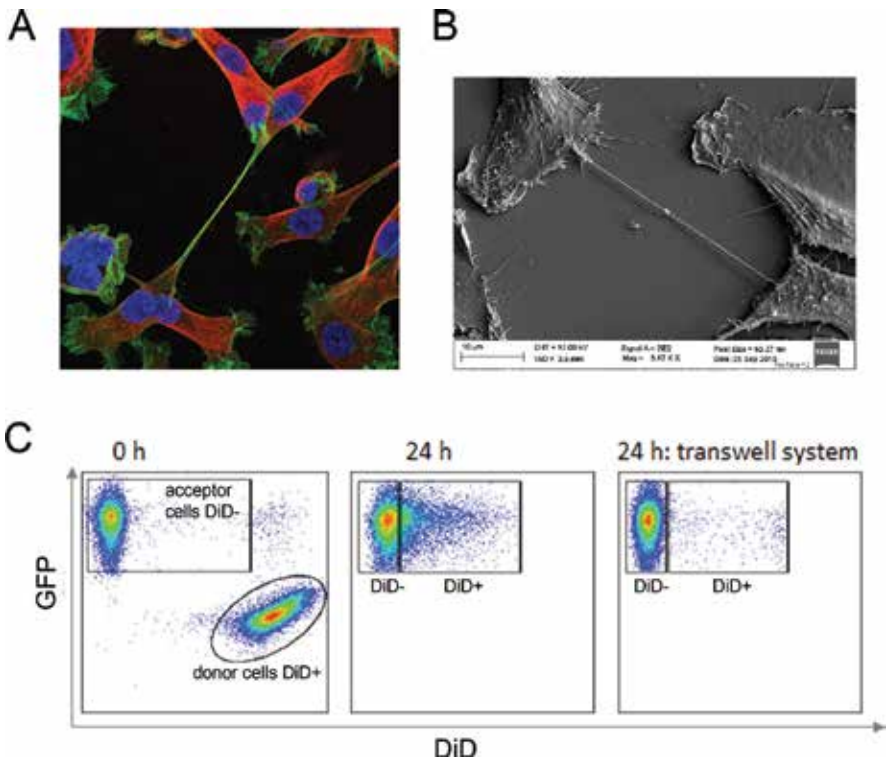

Figure 7. (A) Overlay of confocal images presenting formation of tunneling nanotube (TNT); actin—green, microtubules—red, nuclei—blue); (B) SEM micrograph of a TNT formed between two distant cells; (C) flow cytometry dot plots showing the gating strategy to separate the donor and acceptor populations upon labeling of vesicular cargo by DiD (0 h), the uptake of vesicular cargo visible as appearance of DiD+ acceptor cells (24 h), and the absence of uptake upon donor and acceptor populations physical separation in control experiment (24 h: transwell system).

and enable long-range, direct communication between distant cells [59]. Formation of this structure has been observed between different types of cells by different groups including ours [60–63] and **Figure 7A** and **B**. They have been shown to mediate the cell-to-cell transfer of vesicles, organelles, electrical stimuli, and small molecules [64–66]. The proposed functions of TNTs and mechanism are still not well understood; however, there is growing evidence that cell-cell communication *via* TNTs might play an important role in the cancerogenesis. They are actively formed between leukemia cells and bone marrow-derived mesenchymal stromal cells to promote viability and chemoresistance of leukemia cells [67].

Vesicular cargo can be actively transferred by TNTs between two distinct cells. For now, the flow cytometry is one of the best methodologies to track and analyze cells, which obtained vesicles from donor cells [68–70]. For this, methods to label vesicles has been adapted (**Table 2**) and combined with cell type tracking to distinguish donor and acceptor cells. First, vesicles in donor cells are labeled with lipophilic dyes, such as DiD, DiO, and others, and mixed with acceptor cell population. Flow cytometry allows to separate both subpopulations—positive population of donor cells (DiD+) and negative population of acceptor cells (DiD-), together with additional combination with cell-type tracking with GFP (**Figure 7C**, time 0 h). After

incubation, the fluorescence signal appears in the acceptor cells (GFP+, DiD+), indicating uptake of the vesicular cargo transferred from donor cells (**Figure 7C**, time 24 h). To confirm that vesicles were transferred by direct cell-cell contact, not secreted into the medium, the trans-well control has been performed. In this case, the vesicle uptake has not been observed (**Figure 7C**, transwell). Such methodology has been already successfully used in different cellular systems [60, 69, 71] to analyze direct transfer of vesicles between cells.

5. Interactions of leukemia cells with immunosuppressive regulatory T cells

Immune responses against hematological cancers are less characterized than those against solid tumors. Among them, chronic myeloid leukemia (CML) is not an exception [72]. Little is known about mechanisms of innate and acquired immunity exerted against CML. Although, the involvement of CD4+ and CD8+ T cell as well as NK cells and humoral response in the immunity against CML is widely accepted. Recently, CML-specific antigens exerting cellular and humoral response have been identified [73, 74]. The growing body of evidences is pointing the role of cytotoxic CD8+ T cell as a central player in the anti-CML response. [3, 8] Moreover, CML is considered as one of the diseases which are most sensitive to immunological manipulation [75].

Analysis of blood of untreated patients diagnosed with CML reveals decreased number of NK-cells, which are antitumor effector cells [76]. Moreover, the increased number of inhibitory cells such as T regulatory (T_{reg}) cells and myeloid-derived suppressor cells were present [77]. Also, it has been shown that CML cells (including CD34+ leukemia stem cells) express programmed death receptor ligand 1 (PD-L1). Binding of PD-L1 to the PD-1 receptor expressed on T cells suppresses their effector function.

Immune evasion is a major obstacle for effective anticancer therapy. T regulatory (T_{reg}) cells are recognized as one of the most promising targets for therapy, which could reverse the unresponsiveness of the immune system during malignancy [73]. T_{reg} cells are essential for maintaining homeostasis of the immune system during the steady state and inflammation. The balance between immune activation and tolerance mediated by T_{reg} cells is crucial for maintaining proper responses. The suppression exerted by T_{reg} cells to different types of immune cells has been extensively studied. Activity of T_{reg} cells is beneficial for maintaining self-tolerance, during resolution of inflammation, and for limiting inadequate immune responses. However, their ability to suppress different types of immune cells may also restrain beneficial responses by limiting the anti-tumor immunity. T_{reg} cells constitute a major component of the tumor-infiltrating lymphocytes in human malignancies as well as in mouse experimental models of cancer. Moreover, the increased number of T_{reg} cells among tumor-infiltrating lymphocytes correlates with a poor prognosis and an increased risk of recurrence in majority of solid tumors. In CML patients, the increased number of T_{reg} cells is linked to limited anti-tumor immune effector responses [78, 79]. Data suggest that a balance between the effector and suppressor arms of the immune system could be important in mediating a successful and treatment-free remission (TFR). However, a major goal in CML treatment is to identify the uppermost target to maximize beneficial immune response and promote TFR success [74]. In this context, the study of T regulatory cells is critical.

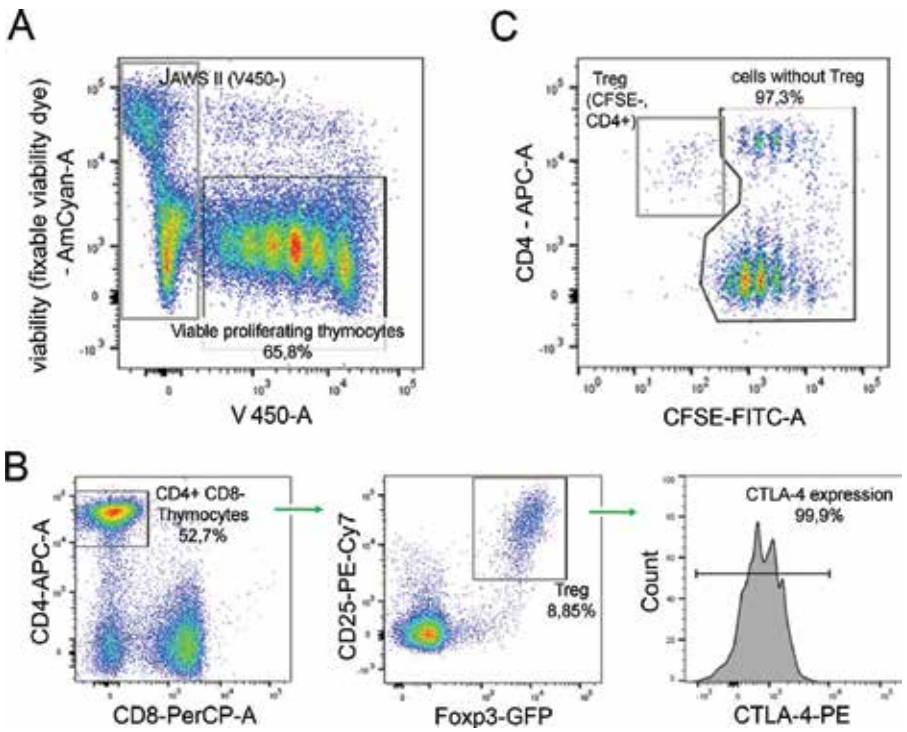

Figure 8. Flow cytometry analysis of T regulatory (T_{reg}) cells differentiation and function. (A) Analysis of cell viability and proliferation (AmCyan channel—fixable viability stain eFluor 506, V450—violet proliferation dye 450). V450 staining allows to track thymocyte proliferation and distinguish them from JAWS II cells (V450-). (B) Identification of T regulatory cells by sequential gating and analysis of CTLA-4 expression. (C) CFSE staining allows to track proliferation of responder cells in an *in vitro* suppression test. An example of combination with CD4-APC staining, which helps eliminate remaining Treg cells (CFSE-, CD4+) in analysis, is presented.

To explore the CML-derived extracellular vesicles impact on T regulatory cell development and activity, we adjust two *in vitro* assays, both based on the flow cytometry.

5.1. Flow cytometry analysis of T regulatory (T_{reg}) cells differentiation and function

To study the effect of CML extracellular vesicles on the differentiation of thymic regulatory T cells (tT_{reg}), we have employed a previously described *in vitro* assay of tT_{reg} differentiation on JAWS II immature dendritic cells [80]. Briefly, during the step of preactivation of thymocytes on αCD3-coated plates, we added extracellular vesicles to allow their uptake or binding solely by thymocytes. Thymocytes were additionally stained with a violet proliferation dye 450, which would allow to track their proliferation and distinguish them from JAWS II cells. After 24 h of preactivation, thymocytes were washed and co-cultured with JAWS II cells. Afterwards, tT_{reg} differentiation using multicolor flow cytometry was analyzed. This analysis allowed to track viability, proliferation (**Figure 8A**), differentiation of tT_{reg}, as well as their phenotype (**Figure 8B**). Extracellular vesicles can also potentially influence suppressive activity of mature, already differentiated tT_{reg}. To study this phenomenon, we sorted tT_{reg} and cultured them, first with CML extracellular vesicles for 24 h and afterwards with conventional T cells (responder cells) stimulated for proliferation, to observe differences in suppressive activity manifested by decreased

proliferation. Labeling of responder cells with CFSE allowed to track their proliferation after co-culture with tT_{reg}, which have been preincubated with either CML-derived or control extracellular vesicles. This in turn allowed to assess differences in tT_{reg} suppressive activity due to influence of EVs. Combination with additional staining of surface receptors such as CD4 or CD8 enabled to distinguish between suppression towards helper (CD4+) or cytotoxic (CD8+) T cells (**Figure 8C**).

6. Summary

Many studies already confirmed that leukemia cells behave differently whether they are cultured alone or in co-culture with stromal cells. This mimics some elements of the bone marrow microenvironment and represents more physiological conditions. Also, the cross talk between leukemia and immune cells is an example showing importance of the interactions within the leukemia microenvironment. Thus, in our opinion, analysis of cell signaling in the co-culture conditions is highly informative and might have some therapeutic implications.

Studies of leukemia cells *in vitro*/*ex vivo*, including analysis of primary cells and stem/progenitor subpopulations, represent an important step in development of novel therapeutic strategies. Different parameters, such as viability, proliferation, DNA damage, clonogenic potential, and others, are investigated after treatment with drugs or drug candidates. Pretreatment with investigated drugs can also be followed by mice Xenograft *in vivo* studies to investigate their therapeutic potential. All these studies are critically important as a first step in analysis of potential therapeutic strategies.

Nevertheless, we propose that in the next step or simultaneously, some of these studies might be performed also upon co-culture conditions to add an essential element of the cross-talk with stroma components, which normally exist *in vivo*. These conditions allow to verify whether the treatment is still effective even upon protective impact of stroma. This fulfills, at least partially, the big gap between *in vitro* experiments and *in vivo* conditions.

In this chapter, we described and discussed flow cytometry applications, which can be used to perform co-culture studies to analyze some signaling elements within the leukemia microenvironment. This strategy enables to distinguish between the cell types and to investigate the cross talk between cancer and surrounding cells, signaling pathways regulated by the cell-cell interactions, as well as sensitivity to treatment with anticancer drugs in the stroma-mimicking conditions. Utilizing modern flow cytometry and a broad spectrum of currently available dyes/trackers allows to perform highly informative studies not only because of the use of multiparameter cytometry but also because of more complex cellular context, which is taken under consideration. Moreover, even if the described flow cytometry applications rely on the leukemia microenvironment studies, they are uniform and can be broadly applied into another biological context.

Acknowledgements

This work was supported by the National Science Centre research grants: UMO-2013/10/E/NZ3/00673 to K.P. and UMO-2014/15/D/NZ3/05187 to P. P.-B.

Conflict of interest

The authors declare no conflict of interest.

Author details

Katarzyna Piwocka[1]*, Paulina Podszywalow-Bartnicka[1], Julian Swatler[1], Marta D. Kolba[1], Agata Kominek[1] and Ewa Kozlowska[2]

*Address all correspondence to: k.piwocka@nencki.gov.pl

1 Laboratory of Cytometry, Nencki Institute of Experimental Biology, Polish Academy of Sciences, Warsaw, Poland

2 Department of Immunology, Faculty of Biology, University of Warsaw, Poland

References

[1] Krause DS, Scadden DT. A hostel for the hostile: The bone marrow niche in hematologic neoplasms. Haematologica. 2015;**100**(11):1376-1387

[2] Ayala F et al. Contribution of bone microenvironment to leukemogenesis and leukemia progression. Leukemia. 2009;**23**(12):2233-2241

[3] Konopleva MY, Jordan CT. Leukemia stem cells and microenvironment: Biology and therapeutic targeting. Journal of Clinical Oncology. 2011;**29**(5):591-599

[4] Dhami SPS et al. Three-dimensional ex vivo co-culture models of the leukaemic bone marrow niche for functional drug testing. Drug Discovery Today. 2016;**21**(9):1464-1471

[5] Schofield R. The relationship between the spleen colony-forming cell and the haemopoietic stem cell. Blood Cells. 1978;**4**(1-2):7-25

[6] Yin T, Li L. The stem cell niches in bone. The Journal of Clinical Investigation. 2006; **116**(5):1195-1201

[7] Agarwal P, Bhatia R. Influence of bone marrow microenvironment on leukemic stem cells: Breaking up an intimate relationship. Advances in Cancer Research. 2015;**127**:227-252

[8] Shafat MS et al. The bone marrow microenvironment – Home of the leukemic blasts. Blood Reviews. 2017;**31**(5):277-286

[9] Bendall LJ et al. Bone marrow adherent layers inhibit apoptosis of acute myeloid leukemia cells. Experimental Hematology. 1994;**22**(13):1252-1260

[10] Sexauer A et al. Terminal myeloid differentiation in vivo is induced by FLT3 inhibition in FLT3/ITD AML. Blood. 2012;**120**(20):4205-4214

[11] Podszywalow-Bartnicka P et al. Increased phosphorylation of eIF2alpha in chronic myeloid leukemia cells stimulates secretion of matrix modifying enzymes. Oncotarget. 2016;**7**(48):79706-79721

[12] Giles FJ et al. The role of inflammation in leukaemia. Advances in Experimental Medicine and Biology. 2014;**816**:335-360

[13] Imbert V, Peyron JF. NF-kappaB in hematological malignancies. Biomedicines. 2017; **5**(2). pii: E27. DOI: 10.3390/biomedicines5020027

[14] Abarrategi A et al. Versatile humanized niche model enables study of normal and malignant human hematopoiesis. The Journal of Clinical Investigation. 2017;**127**(2):543-548

[15] Hawkins ED et al. T-cell acute leukaemia exhibits dynamic interactions with bone marrow microenvironments. Nature. 2016;**538**(7626):518-522

[16] Passaro D et al. Increased vascular permeability in the bone marrow microenvironment contributes to disease progression and drug response in acute myeloid leukemia. Cancer Cell. 2017;**32**(3):324-341 e6

[17] Parish CR. Fluorescent dyes for lymphocyte migration and proliferation studies. Immunology and Cell Biology. 1999;**77**(6):499-508

[18] Parish CR et al. Use of the intracellular fluorescent dye CFSE to monitor lymphocyte migration and proliferation. Current Protocols in Immunology. 2009;**Chapter 4**:Unit 4.9

[19] Quah BJ, Parish CR. New and improved methods for measuring lymphocyte proliferation in vitro and in vivo using CFSE-like fluorescent dyes. Journal of Immunological Methods. 2012;**379**(1-2):1-14

[20] Lyons AB. Divided we stand: Tracking cell proliferation with carboxyfluorescein diacetate succinimidyl ester. Immunology and Cell Biology. 1999;**77**(6):509-515

[21] Shimomura O, Johnson FH, Saiga Y. Extraction, purification and properties of aequorin, a bioluminescent protein from the luminous hydromedusan, Aequorea. Journal of Cellular and Comparative Physiology. 1962;**59**:223-239

[22] Fradkov AF et al. Novel fluorescent protein from Discosoma coral and its mutants possesses a unique far-red fluorescence. FEBS Letters. 2000;**479**(3):127-130

[23] Maetzig T et al. A lentiviral fluorescent genetic barcoding system for flow cytometry-based multiplex tracking. Molecular Therapy. 2017;**25**(3):606-620

[24] Giudice V et al. Optimization and standardization of fluorescent cell barcoding for multiplexed flow cytometric phenotyping. Cytometry. Part A. 2017;**91**(7):694-703

[25] Krutzik PO et al. Fluorescent cell barcoding for multiplex flow cytometry. Current Protocols in Cytometry. 2011;**Chapter 6**:Unit 6.31

[26] Krutzik PO, Nolan GP. Fluorescent cell barcoding in flow cytometry allows high-throughput drug screening and signaling profiling. Nature Methods. 2006;**3**(5):361-368

[27] Stam J et al. Fluorescent cell barcoding as a tool to assess the age-related development of intracellular cytokine production in small amounts of blood from infants. PLoS One. 2011;**6**(10):e25690

[28] Lekishvili T, Campbell JJ. Rapid comparative immunophenotyping of human mesenchymal stromal cells by a modified fluorescent cell barcoding flow cytometric assay. Cytometry. Part A. 2017

[29] Lyons AB, Doherty KV. Flow cytometric analysis of cell division by dye dilution. Current Protocols in Cytometry. 2004:**Chapter 9**:Unit 9.11

[30] Begum J et al. A method for evaluating the use of fluorescent dyes to track proliferation in cell lines by dye dilution. Cytometry. Part A. 2013;**83**(12):1085-1095

[31] Svirshchevskaya EV et al. Interaction of lymphocytes with Mesenchymal stem cells. Bulletin of Experimental Biology and Medicine. 2016;**161**(4):571-579

[32] Saglam O et al. IL-6 originated from breast cancer tissue-derived mesenchymal stromal cells may contribute to carcinogenesis. Tumour Biology. 2015;**36**(7):5667-5677

[33] Tario Jr JD et al. Optimized staining and proliferation modeling methods for cell division monitoring using cell tracking dyes. Journal of Visualized Experiments. 2012;**70**:e4287

[34] Tario Jr JD et al. Monitoring cell proliferation by dye dilution: Considerations for probe selection. Methods in Molecular Biology. 2018;**1678**:249-299

[35] Bogie JF et al. Myelin-phagocytosing macrophages modulate autoreactive T cell proliferation. Journal of Neuroinflammation. 2011;**8**:85

[36] Tario Jr JD et al. Tracking immune cell proliferation and cytotoxic potential using flow cytometry. Methods in Molecular Biology. 2011;**699**:119-164

[37] Ciardiello C et al. Focus on extracellular vesicles: New frontiers of cell-to-cell communication in cancer. International Journal of Molecular Sciences. 2016;**17**(2):175

[38] Kosaka N et al. Versatile roles of extracellular vesicles in cancer. The Journal of Clinical Investigation. 2016;**126**(4):1163-1172

[39] Gangadaran P et al. Extracellular vesicles from mesenchymal stem cells activates VEGF receptors and accelerates recovery of hindlimb ischemia. Journal of Controlled Release. 2017;**264**:112-126

[40] Robbins PD, Morelli AE. Regulation of immune responses by extracellular vesicles. Nature Reviews. Immunology. 2014;**14**(3):195-208

[41] Raposo G, Stoorvogel W. Extracellular vesicles: Exosomes, microvesicles, and friends. The Journal of Cell Biology. 2013;**200**(4):373-383

[42] Caivano A, Del Vecchio L, Musto P. Do we need to distinguish exosomes from microvesicles in hematological malignancies? Leukemia. 2017;**31**(9):2009-2010

[43] Raimondo S et al. Chronic myeloid leukemia-derived exosomes promote tumor growth through an autocrine mechanism. Cell Communication and Signaling. 2015;**13**:8

[44] Cai J et al. Transferred BCR/ABL DNA from K562 extracellular vesicles causes chronic myeloid leukemia in immunodeficient mice. PLoS One. 2014;**9**(8):e105200

[45] Corrado C et al. Exosome-mediated crosstalk between chronic myelogenous leukemia cells and human bone marrow stromal cells triggers an interleukin 8-dependent survival of leukemia cells. Cancer Letters. 2014;**348**(1-2):71-76

[46] Corrado C et al. Chronic myelogenous leukaemia exosomes modulate bone marrow microenvironment through activation of epidermal growth factor receptor. Journal of Cellular and Molecular Medicine. 2016;**20**(10):1829-1839

[47] Taverna S et al. Role of exosomes released by chronic myelogenous leukemia cells in angiogenesis. International Journal of Cancer. 2012;**130**(9):2033-2043

[48] Caivano A et al. High serum levels of extracellular vesicles expressing malignancy-related markers are released in patients with various types of hematological neoplastic disorders. Tumour Biology. 2015;**36**(12):9739-9752

[49] Ohyashiki K et al. Downregulation of plasma miR-215 in chronic myeloid leukemia patients with successful discontinuation of Imatinib. International Journal of Molecular Sciences. 2016;**17**(4):570

[50] Erdbrugger U, Lannigan J. Analytical challenges of extracellular vesicle detection: A comparison of different techniques. Cytometry. Part A. 2016;**89**(2):123-134

[51] Lai CP et al. Visualization and tracking of tumour extracellular vesicle delivery and RNA translation using multiplexed reporters. Nature Communications. 2015;**6**:7029

[52] Gray WD, Mitchell AJ, Searles CD. An accurate, precise method for general labeling of extracellular vesicles. MethodsX. 2015;**2**:360-367

[53] Czernek L, Chworos A, Duechler M. The uptake of extracellular vesicles is affected by the differentiation status of myeloid cells. Scandinavian Journal of Immunology. 2015;**82**(6):506-514

[54] Luo X et al. Exosomes are unlikely involved in intercellular Nef transfer. PLoS One. 2015;**10**(4):e0124436

[55] Gardiner C et al. Techniques used for the isolation and characterization of extracellular vesicles: Results of a worldwide survey. Journal of Extracellular Vesicles. 2016;**5**:32945

[56] Nolte-'t Hoen EN et al. Quantitative and qualitative flow cytometric analysis of nano-sized cell-derived membrane vesicles. Nanomedicine. 2012;**8**(5):712-720

[57] Nolte-'t Hoen EN et al. Dynamics of dendritic cell-derived vesicles: High-resolution flow cytometric analysis of extracellular vesicle quantity and quality. Journal of Leukocyte Biology. 2013;**93**(3):395-402

[58] Lannigan J, Nolan P, Zucker R. Measurement of extracellular vesicles and other submicron size particles by flow cytometry. Cytometry. Part A. 2016;**89**(2):109-110

[59] Ariazi J et al. Tunneling nanotubes and gap junctions-their role in long-range intercellular communication during development, health, and disease conditions. Frontiers in Molecular Neuroscience. 2017;**10**:333

[60] Gousset K et al. Prions hijack tunnelling nanotubes for intercellular spread. Nature Cell Biology. 2009;**11**(3):328-336

[61] Lou E et al. Tunneling nanotubes provide a unique conduit for intercellular transfer of cellular contents in human malignant pleural mesothelioma. PLoS One. 2012;**7**(3):e33093

[62] Onfelt B et al. Cutting edge: Membrane nanotubes connect immune cells. Journal of Immunology. 2004;**173**(3):1511-1513

[63] Rustom A et al. Nanotubular highways for intercellular organelle transport. Science. 2004;**303**(5660):1007-1010

[64] Onfelt B et al. Structurally distinct membrane nanotubes between human macrophages support long-distance vesicular traffic or surfing of bacteria. Journal of Immunology. 2006;**177**(12):8476-8483

[65] Vallabhaneni KC, Haller H, Dumler I. Vascular smooth muscle cells initiate proliferation of mesenchymal stem cells by mitochondrial transfer via tunneling nanotubes. Stem Cells and Development. 2012;**21**(17):3104-3113

[66] Wang X et al. Animal cells connected by nanotubes can be electrically coupled through interposed gap-junction channels. Proceedings of the National Academy of Sciences of the United States of America. 2010;**107**(40):17194-17199

[67] Polak R et al. B-cell precursor acute lymphoblastic leukemia cells use tunneling nanotubes to orchestrate their microenvironment. Blood. 2015;**126**(21):2404-2414

[68] Domhan S et al. Intercellular communication by exchange of cytoplasmic material via tunneling nano-tube like structures in primary human renal epithelial cells. PLoS One. 2011;**6**(6):e21283

[69] Gurke S et al. Tunneling nanotube (TNT)-like structures facilitate a constitutive, actomyosin-dependent exchange of endocytic organelles between normal rat kidney cells. Experimental Cell Research. 2008;**314**(20):3669-3683

[70] Pasquier J et al. Preferential transfer of mitochondria from endothelial to cancer cells through tunneling nanotubes modulates chemoresistance. Journal of Translational Medicine. 2013;**11**:94

[71] Sowinski S et al. Membrane nanotubes physically connect T cells over long distances presenting a novel route for HIV-1 transmission. Nature Cell Biology. 2008;**10**(2):211-219

[72] Curran EK, Godfrey J, Kline J. Mechanisms of immune tolerance in Leukemia and lymphoma. Trends in Immunology. 2017;**38**(7):513-525

[73] Facciabene A, Motz GT, Coukos G. T-regulatory cells: Key players in tumor immune escape and angiogenesis. Cancer Research. 2012;**72**(9):2162-2171

[74] Ilander M, Hekim C, Mustjoki S. Immunology and immunotherapy of chronic myeloid leukemia. Current Hematologic Malignancy Reports. 2014;**9**(1):17-23

[75] Kurbegov D, Molldrem JJ. Immunity to chronic myelogenous leukemia. Hematology/Oncology Clinics of North America. 2004;**18**(3):733-752 xi-xii

[76] Chen CI et al. NK cells are dysfunctional in human chronic myelogenous leukemia before and on imatinib treatment and in BCR-ABL-positive mice. Leukemia. 2012;**26**(3):465-474

[77] Bachy E et al. Quantitative and functional analyses of CD4(+) CD25(+) FoxP3(+) regulatory T cells in chronic phase chronic myeloid leukaemia patients at diagnosis and on imatinib mesylate. British Journal of Haematology. 2011;**153**(1):139-143

[78] Plitas G, Rudensky AY. Regulatory T cells: Differentiation and function. Cancer Immunology Research. 2016;**4**(9):721-725

[79] Shevach EM. Biological functions of regulatory T cells. Advances in Immunology. 2011;**112**:137-176

[80] Bienkowska A et al. Thymus-deriving natural regulatory T cell generation in vitro: Role of the source of activation signals. Immunology Letters. 2014;**162**(2 Pt B):199-209

Chapter 3

High Throughput Screen for Inhibitors of Rac1 GTPase by Flow Cytometry

Catherine Bardelle, Vincent Sauzeau, Mark B. Carter, Zhaoping Liu, Gervaise Loirand and David Murray

Additional information is available at the end of the chapter

http://dx.doi.org/10.5772/intechopen.71074

Abstract

High throughput (HT) screening is at the starting point for most drug discovery programs. As the range of targets being pursued widens new technologies have to be deployed to enable assays built to measure the activity of proteins previously deemed challenging. Flow cytometry is a technology providing multi-parametric analysis of single cells or other particles in suspension, such as beads. High throughput (HT) flow cytometry has become a very attractive screening platform for drug discovery. In this chapter we describe a 1536 well format high throughput screen of 500,000 compounds to find inhibitors of Rac1 GTPase to prevent allergic airway hyper-responsiveness in asthma. We discuss the assay development, miniaturization and validation carried out prior to the full screening campaign. We then describe how we have automated our iQue® HD screener instruments and how we proceed with the data analysis and explain why we chose to run this screen on a flow cytometer and how it enabled us to reduce cost and timelines for the project.

Keywords: HTS, drug discovery, bead-based assay, GTPase

1. Introduction

Asthma is a heterogeneous inflammatory disorder of the airways characterized by chronic deregulated inflammation, bronchial hyperreactivity, and symptoms of recurrent wheezing, coughing, and shortness of breath. Its prevalence has increased considerably over the past three decades, particularly in Western countries. Asthma is a major public health problem that affects 300 million people worldwide [1, 2].

Airway hyperresponsiveness (AHR), one of the hallmarks of asthma, directly results from excessive contraction of airway smooth muscle cells (aSMC). The degree of AHR always correlates with asthma severity and the need for therapy [3, 4]. Regular treatment of chronic asthma consists of a combination of inhaled anti-inflammatory corticosteroids and long-acting beta2-adrenergic receptor agonists for bronchodilation. However, severe asthma escapes to usual treatments or frequently requires higher doses. In acute asthma, short-acting beta2 agonists or anticholinergics are used as bronchodilators. These drugs are rapidly effective but can be insufficient in some cases of severe acute asthma attack. Despite available therapies, many patients with severe asthma remain uncontrolled and the number of asthma deaths is still elevated [5]. There is thus an obvious need for new drugs acting through other pathways to prevent or reverse AHR and decrease severe asthma attacks, hospitalizations and deaths.

The molecular mechanisms regulating aSMC contraction and proliferation involved in AHR are still largely unknown. Understanding the intracellular signaling pathways responsible for AHR is thus essential to identify new targets and design new treatments. In this way, the Rho protein Rac1 has been identified as a promising candidate.

The Rho/Rac proteins constitute a family of small GTPases of more than 25 members in mammals. So far, the best characterized members of this family include the members of the Rho (RhoA, RhoB, RhoC), Rac (Rac1, Rac2, RhoG), and Cdc42 (Cdc42) subfamilies. Rho/Rac proteins share a common structure (40–95% identity) composed of a six-stranded mixed β sheet flanked by five α helices. The core G domain is made up of five polypeptide loops (G1–G5) involved in nucleotide, regulators and effectors interactions. Like the majority of Ras superfamily GTPases, most members of the Rho/Rac family behave as molecular switches that cycle between inactive (GDP-bound) and active (GTP-bound) states. In basal conditions, these proteins are inactive and sequestered in the cytosol due to their binding to Rho GDP dissociation inhibitors (RhoGDIs). Upon cell stimulation, Rho proteins became GTP-bound, translocate to the plasma membrane after release from RhoGDI, and interact with their primary effector molecules to trigger different signal transduction pathways. In addition to RhoGDIs, the activation/inactivation cycle of Rho/Rac proteins is regulated by a complex set of regulatory proteins that include GDP/GTP exchange factors (GEFs) and GTPase activating protein (GAPs) (**Figure 1**). Interaction of Rho/Rac protein with a GEF promotes the exchange of GDP for GTP molecules, thus leading to the rapid activation of Rho/Rac proteins during cell stimulation events. By contrast, GAPs promote the hydrolysis of the bound GTP molecules to GDP, thus allowing the transfer of the GTPases back to the inactive state at the end of the stimulation cycle [6].

During the last decade, Rho/Rac protein signaling pathways have been recognized as major regulators of essential cellular functions. Rac1 is a key regulator of cytoskeletal structure and dynamics, leading to lamellipodia and ruffle formations [6, 7]. Thanks to this last function, Rac1 controls cellular migration and adhesion. Recently, we demonstrated that Rac1 regulates vascular SMC contraction, and consequently modulates arterial pressure [8]. Accordingly, we hypothesized that Rac1 could also be involved in aSMC contraction. We demonstrated that the specific SMC deletion of Rac1 (SM-Rac1-KO) in mice prevents bronchoconstriction *ex* and *in vivo*. Our results showed that the decreased expression or activity of Rac1 in aSMC impairs

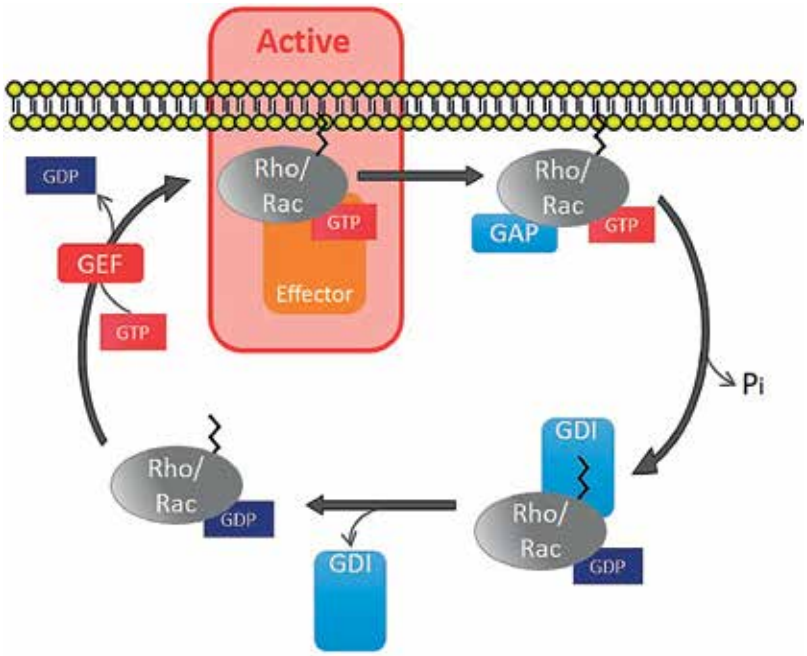

Figure 1. Activation cycle of Rho/Rac proteins and their regulatory proteins. Activation of Rho/Rac proteins is mediated by a guanine nucleotide exchange factor (GEF) leading to GTP loading and to the translocation of Rho/Rac proteins to the plasmatic membrane. This active configuration of Rho/Rac proteins promotes effector interactions. To "turn off" the cycle, a GTPase-activating protein (GAP) accelerates the intrinsic GTPase activity of Rac, allowing Rac to return to its inactive state in the cytosol. The guanine nucleotide-dissociation inhibitor (GDI) binds specifically to GDP-bound Rho/Rac proteins, prolonging the inactive state and sequestering the GTPase in the cytosol.

agonist-induced rise in intracellular Ca^{2+} concentration through a mechanism involving Rac1-dependant control of PLC activity. Interestingly, Rac1 deficiency has no impact on the respiratory system in basal, physiological condition. However, deletion of Rac1 expression in aSMC or nebulization of the Rac inhibitor NSC23766 prevented AHR in an allergic asthma model in mouse. These data indicate that (1) Rac1 is a critical component in aSMC contraction and (2) inhibition of Rac1 activity or expression may represent a novel therapeutic approach for patients with airway AHR such as asthma.

Unfortunately, the currently available drugs that inhibit Rac1 (EHT 1864 and NSC23766) have low affinity and induce critical off-target effects, thus highlighting the obvious need to discover new Rac inhibitors [9, 10].

In this chapter we describe how a published flow cytometry assay was taken and converted to a 1536 well format suitable for high throughput screening (HTS) to enable the screening of 500,000 compounds in the AstraZeneca Global HTS Centre to attempt to find new Rac1 inhibitors. We describe the whole protocol from receiving assay ready plates through to the data analysis and discuss the criteria that are important for an assay to be suitable for a high throughput screen by flow cytometry and describe the validation process we go through prior to starting a high throughput screening campaign.

2. Assay development

Several papers have demonstrated the utility of a bead-based flow cytometric GTP-binding assay for screening GTPase targets for small molecule inhibitors in both singleplex and multiplex formats [11–13]. As part of AstraZeneca's Open Innovation initiative, we collaborated with researchers at l'Institut du thorax to identify small molecule inhibitors of Rac1 GTPase. We therefore set out to develop a bead-based assay for screening Rac1 in a singleplex fashion (**Figure 2**) for a screening campaign in 1536 well plates on an iQue® Screener HD. The Intellicyt iQue® Screener HD is a flow cytometer with an autosampler able to sample from 96, 384 and 1536 well plates. Using proprietary technology the instrument separates well samples with an air bubble allowing the software to determine what sample comes from what well making the instrument a true high throughput instrument.

The assay is based on glutathione-coated beads used to capture GST-tagged Rac1. Bodipy-labeled GTP (FL-GTP, ThermoFisher Scientific), is then used as a tracer for the detection of compounds that compete with its binding to the GTPase resulting in a decreased fluorescence signal.

We purchased commercially-available glutathione coated particles (GSH beads, size 4.0–4.9 μm, Spherotech) that have glutathione covalently coupled to their surface and glutathione S-transferase tagged Rac1 protein (human wild type) (GST-Rac1, ThermoFisher Scientific) and bound the GST-Rac1 onto the GSH beads overnight. Assay development was performed in 384 well plates before miniaturizing the assay for 1536 well plates. We optimized the concentration of FL-GTP to use in the assay to achieve the largest signal to background window and also confirmed that FL-GTP did not bind to unconjugated beads to demonstrate Rac1/GTP binding specificity. Based on the data shown in **Figure 3** and associated table, 100 nM FL-GTP was selected.

To validate that the beads were coated with GST-Rac1 and that they would bind bodipy-labeled GTP the prepared beads were mixed with serial dilutions of unlabeled GTP (ThermoFisher

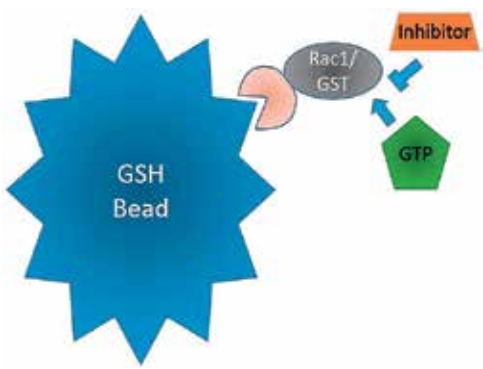

Figure 2. Pictorial representation of GST-Rac1 bound to GSH beads. Inhibitors of fluorescent GTP binding result in decreased FL1-H signal.

A

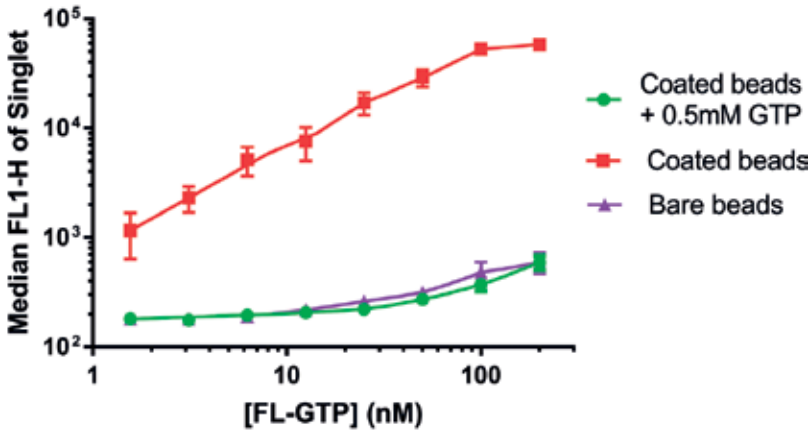

B

Bodipy-FL GTP Concentration (nM)	S/B
1.5625	6
3.125	13
6.25	27
12.5	37
25	78
50	107
100	142
200	99

Figure 3. Optimization of FL-GTP concentration and confirmation of binding specificity. (A) Unconjugated or Rac1-coated beads were incubated with varying amounts of FL-GTP in the presence or absence of 0.5 mM unlabeled GTP and bead fluorescence measured on the iQue®. ■: Rac1 coated beads in the presence of 0.5 mM unlabeled GTP, ▲: bare beads, and ●: Rac1 coated beads. (B) Signal to background table for each concentration of FL-GTP.

Scientific) as a competitor followed by the addition of FL-GTP. To prepare the assay, 5 μL of coated beads were dispensed into wells on a 384 well plate followed by 5 μL of buffer containing unlabeled GTP in serial dilutions in triplicate, then 5 μL of 100 nM FL-GTP was added for a final volume of 15 μL and incubated for 30 min. The methods described in Refs. [11–13] included a final incubation for up to 60 min at 4°C. We wanted to be able to prepare and incubate the plates at room temperature (RT) for large scale screening, so we incubated plates both at 4°C or RT and then read the plates on the iQue Screener HD immediately after incubation or after 2 h at RT to determine if the signal window was still adequate for screening at that time. The beads are not fluorescently labeled, therefore exhibit low fluorescence intensity in the FL-1 channel (excitation 488 nm; emission filter 530/30 nm). Beads with bound FL-GTP exhibit a marked increase in fluorescence (approximately 200–500 fold). Inhibitors of GTP binding decrease the FL-1 fluorescence which is the measured signal for the samples read on the iQue® Screener HD. For analysis, beads were gated on forward scatter height (FSC-H) vs. side scatter height (SSC-H), then doublets were excluded by gating on the singlet population on forward scatter height vs. forward scatter area (FSC-A). **Figure 4** shows representative data for the gating scheme and the decrease in bead fluorescence with three concentration response curves (0–333.3 μM unlabeled GTP).

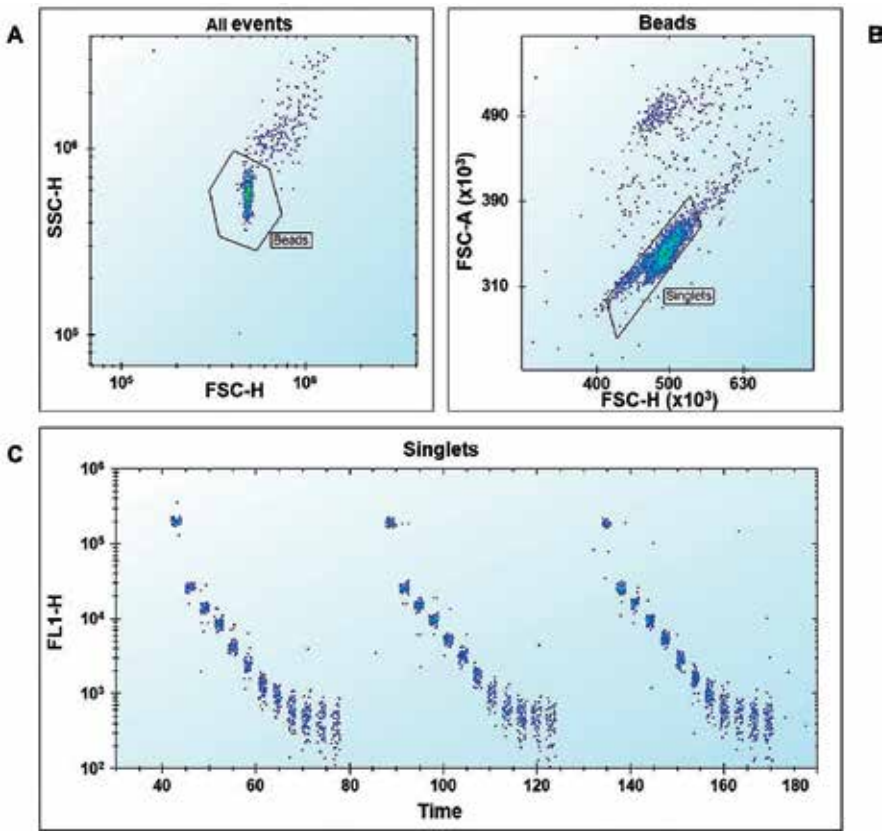

Figure 4. Gating scheme for Rac1 assay. (A) Beads gated on FSC-H versus SSC-H, (B) then on FSC-H versus FSC-A for singlet beads, (C) time-resolved serial dilution curves (time versus log(Median FL1-H fluorescence) of singlet beads. Wells treated with 0–333.3 μM unlabeled GTP show decreasing FL-GTP bound to beads (data in triplicate).

Addition of unlabeled GTP was able to compete with FL-GTP under all assay conditions in a concentration-dependent manner (**Figure 5**). Samples incubated at 4°C and read immediately afterward showed the highest binding of FL-GTP as well as the greatest decrease in fluorescence in the presence of unlabeled GTP. All other conditions showed a slight increase in FL-GTP intensity, but very similar competition curves. Assay Z′ was greater than 0.75 for all conditions. These data in a final volume of 15 μL demonstrated that the assay was adequate to move forward with miniaturization, so the assay was tested again in small volumes using 2 μL of GST-Rac1 coated beads, 2 μL of buffer containing unlabeled GTP in serial dilutions, and 2 μL of FL-GTP for a total assay volume of 6 μL in low volume 384 well plates. The miniaturized assay was comparable to the preliminary tests (data not shown) so we moved forward with miniaturization to 1536 well plates.

The challenge for us was to perform the assay in a 1536-well format in order to minimize both cost and timelines of the screen.

Miniaturization to 1536 well format was first performed by using blank GSH beads to test dispensing, inter-well shake speeds, and sip times. Runs were repeated under various conditions

http://dx.doi.org/10.5772/intechopen.71074

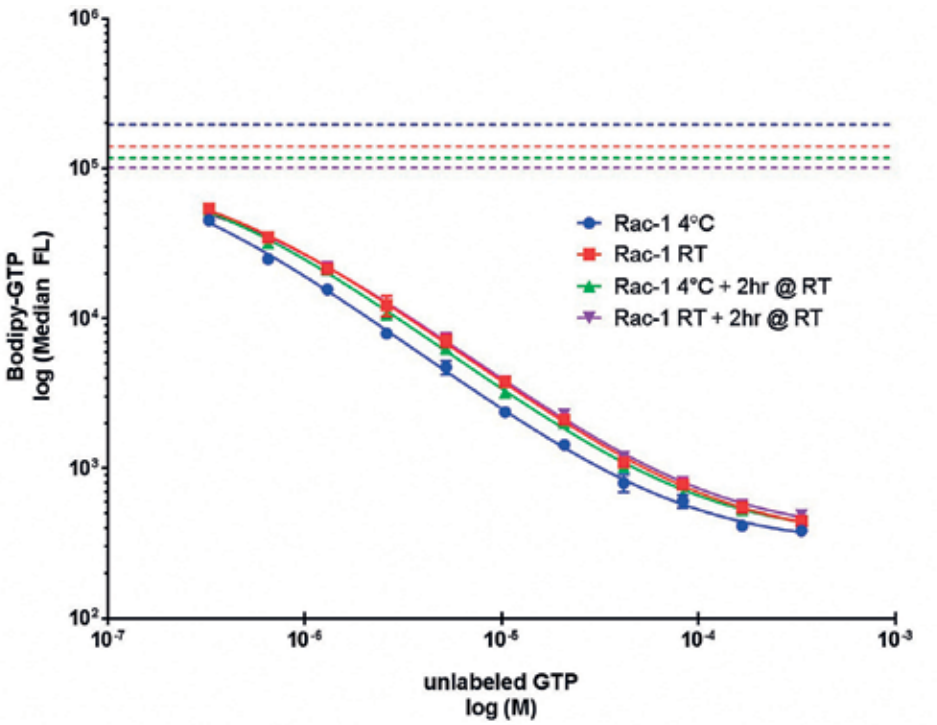

Figure 5. Comparison of incubation on competition of FL-GTP. Bead fluorescence measured by competition of FL-GTP by unlabeled GTP. GST-Rac1 coated beads with FL-GTP were incubated in the presence of varying amounts of unlabeled GTP in triplicate. Dotted lines indicate bead fluorescence in the presence of no unlabeled GTP. ●: incubated at 4°C for 30 min, ■: incubated at RT for 30 min, ▲: incubated at 4°C for 30 min then stored for 2 h at RT and ▼: incubated at RT for 30 min then stored for 2 h at RT.

to determine the optimum protocol. During these runs it was determined that it was best to use the bead sample buffer 0.1% (w/v) BSA in NP-HPS (30 mM HEPES pH 7.2, 100 mM KCl, 20 mM NaCl, 0.01% NP-40) supplemented with 1 mM DTT to prime the system before acquisition and during inter-well shaking. We found that we could decrease the sip time during which the sample probe aspirates from the well to 0.5 s per well, resulting in the acquisition of an entire 1536 well plate in under 50 min. Once the iQue® Screener HD protocol was optimized with blank GSH beads, we ran 3 separate plates with ½ of the plate with negative control (sample buffer) and ½ of the plate with positive control (unlabeled GTP). Briefly, the assay was performed by dispensing 2 μL of GST-Rac1 coated beads to each well of a 1536 well plate, followed by either 2 μL of sample buffer (negative control) or 2 μL of 500 μM unlabeled GTP (positive control; final concentration 166.7 μM). Finally, 2 μL FL-GTP was added to each well, then the plate was heat sealed with a pierceable foil seal and incubated at RT for 30 min. Each plate's Z′ factor was calculated as greater than 0.5 with an average of 0.68 across the three plates (**Figure 6**).

We optimized the coating of Rac1 on the beads by testing the signal strength and assay window achieved over a 15 fold range of initial protein concentration from saturation down to zero (**Table 1**).

The aim was to identify the optimum concentration to use while maintaining best signal to background ratio. Following optimization i.e. check that the assay was suitable for running

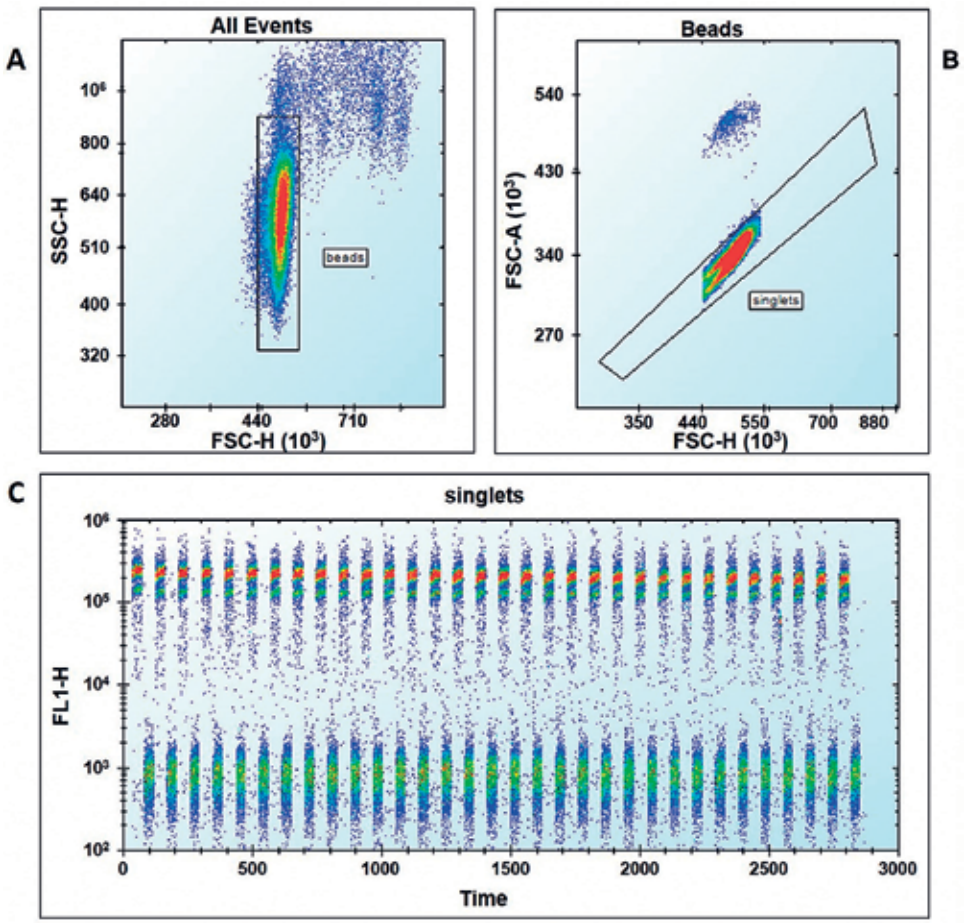

Figure 6. Representative data from 1536 well Rac1 assay. (A) Beads gated on FSC-H versus SSC-H, (B) then on FSC-H versus FSC-A for singlet beads, (C) time-resolved data (time versus log(Median FL1-H fluorescence) of singlet beads. Wells treated with 0 or 166.7 μM unlabeled GTP show decreasing FL-GTP bound to beads.

Rac1 concentration (μM)	Max signal	Min signal	Z′	S/B
5	107,304	15,623	0.57	6.87
2.5	106,718	14,885	0.82	7.17
1.25	66,630	8559	0.79	7.79
0.625	39,836	5630	0.60	7.08
0.3175	21,087	3518	0.24	5.99

Table 1. Optimization of bead coating. Beads were coated with various concentrations of Rac1, incubated with FL-GTP and the bead fluorescence measured on the iQue®. Max refers to signal in the absence of 0.5 mM unlabeled GTP, min refers to signal in the presence of 0.5 mM unlabeled GTP.

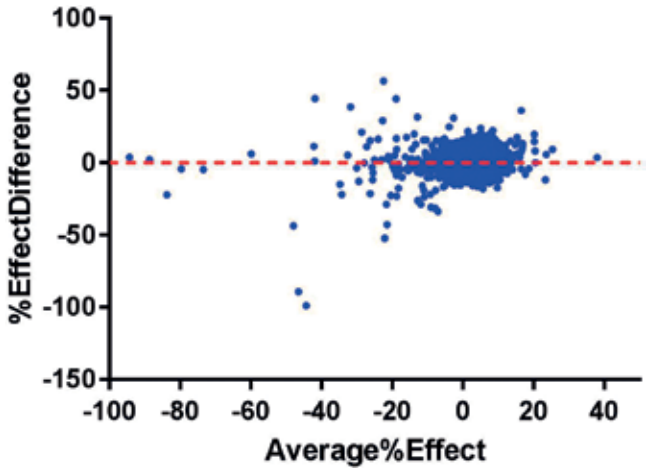

Figure 7. Bland-Altman plot of validation data.

at large scale, the assay was validated by running a set of 7000 core compounds and a set of 3000 low molecular weight compounds (LMW) (mol.wt. below 325) (see Section 3) on 2 separate occasions to assess variability. These compounds encompass the diversity of the collections that will be screened. Running an HTS campaign is a costly and fairly demanding process. For this reason we need to ensure an assay is robust (Z′ factor greater than 0.5, signal to background greater than 3, low coefficient of variation across whole plate) and reproducible i.e. active compounds will be found repeatedly if the assay was run multiple times. We therefore defined a set of criteria we need to satisfy prior to embarking on a screen [14]. Core compounds were run at 12.5 μM and LMW at 100 μM. We use an in-house designed Tibco Spotfire® tool to analyze the data and visualize the repeatability of the assay. Validation showed the assay was performing well resulting in good agreement between the repeat runs as depicted in **Figure 7** which shows a Bland-Altman plot comparing data from the 2 runs; the average difference is 0.3 and the standard deviation of the difference around 7%. We were confident that this assay was now amenable to full scale screening.

3. Screening

The iQue® Screener HD increases the capabilities of flow cytometry with rapid sampling and assay miniaturization with a final assay volume of 6 μL per well, using as little as 1 μL per sample with no dead volume. The iQue® Screener HD has an autosampler that delivers samples in an air gap delimited stream to the cytometer engine. The plate loading area is accessible to robotic integration and an easy to use interface allows integration of laboratory automation. The entire plate of data is processed at one time. ForeCyt® software that controls the iQue® Screener HD allows plate level annotation, analysis, and visualization of the acquired data, enabling rapid, high content, multiplexed analysis of cells and beads in suspension. To enable the throughput required, we have linked two iQue® Screener HD to an

ACell benchtop automation system (HighRes Biosolutions), as shown in **Figure 8**, comprising a Nanoserve plate carousel and an ambient nest integrated by the Cellario® scheduling software. This simple small footprint automation system allows unattended operation as well as automatically clean the cytometers at the end of each run and has a capacity of up to 28 plates per working day. We also used a third iQue® Screener HD as a standalone instrument for backup and additional throughput.

Prior to first use, a daily clean was run on the iQue® consisting of 5 min in decontamination solution (Intellicyt), a mildly basic solution, followed by 5 min in cleaning solution (Intellicyt), a mildly acidic and surfactant solution that neutralizes the decontamination solution and a final 10 min in water. This ensures cleaning of the entire fluidics path from probe to detector. Following this procedure a QC test was run to check the performance of the iQue instruments consisting of a 2 min water test to check cleanliness of the system followed by an 8 peak (Intellicyt) and 6 peak (Intellicyt) beads test to check laser alignment and performance of the 4 fluorescence channels. The 8 peak product contains a mixture of several similar size particles with 8 different fluorescence intensities. Every particle contains a mixture of fluorophores that enables their excitation with the blue laser (488 nm) to validate the FL1, FL2 and FL3 channels of the iQue. Similarly, the 6 peak product contains a mixture of particles with 6 different fluorescence intensities excitable by the red laser to validate the FL4 channel.

All compounds for HTS in AstraZeneca are delivered in what are known as assay ready plates. Assay ready plates have the correct volume of compound in them such that on addition of

Figure 8. Automation platform used with our iQue® Screener HD. (A) and (B) iQue® Screener HD, (C) ACell robotic arm, (D) NanoServe™ stacker carousel.

the assay reagents the correct final compound concentration is achieved. Compound volumes are in the nL range and are added by a Labcyte Echo® acoustic dispenser. Using assay ready plates removes the need for intermediate dilution steps to get compounds and vehicle to the correct concentration making plate processing much simpler and faster in HTS screens.

Within the AstraZeneca HTS Centre we have 2 main collections of compounds that we screen. We have what we call the core collection that is screened at a single final concentration of 10 μM or a concentration close to this balancing solubility of the compounds with detecting weaker activity. We also have a low molecular weight collection [15] where we have separated out compounds with molecular weights below 325 Da that pass solubility filters. These compounds are screened at higher concentrations (typically 100 μM) to ensure we detect the activity of these compounds that potentially have better ligand efficiencies than hits that may be found in the core collection.

Rac1-coated beads were prepared by vigorously vortexing the glutathione beads, then transferring 7 mL into a 50 mL centrifuge tube. The beads were centrifuged (1000 × *g*, 5 min) and the supernatant removed, taking care not to disturb the pellet. 7 mL of wash buffer (0.1%, w/v BSA in NP-HPS) were added and vortexed vigorously to wash the beads. Beads were then incubated at room temperature for 30 min. Lyophilized Rac1 protein was reconstituted to 0.25 mg/mL final concentration (~5 μM) by adding 25 μL of wash buffer and mixing gently until the protein is completely dissolved. After the 30 min incubation of the beads they were pelleted by centrifugation (1000 × *g*, 5 min) and the supernatant discarded, taking care not to disturb the pellet. Beads were resuspended in 700 μL of wash buffer +175 μL of Rac1 protein to a final concentration of 1 μM. The sample was vortex mixed gently and incubated overnight at 4°C. After incubation at 4°C, beads were washed twice with 14 mL sample buffer (wash buffer +1 mM DTT) pelleted by centrifugation (1000 × *g*, 5mins) between washes and finally resuspended in 14 mL wash buffer. Labeled beads were stored at 4°C. An accurate bead count was made using the iQue® Screener HD with beads diluted to a density of 1.33 × 10^6 beads/mL prior to running the assay. The method described here should provide enough beads for 16 plates a day for 6 days.

The primary screen was performed at compound concentration of 12.5 μM (100 μM for LMW) against a diversity collection of 500,000 compounds. All assay ready plates of compounds were prepared by our compound management team. The plate layout included on-board controls in the four central columns (64 wells of either 12.5 μM unlabeled GTP or 1% (v/v) DMSO as inhibitor and neutral controls, respectively). Each remaining well contained a single compound from the library, resulting in single shot screening of 1408 compounds per plate.

To assemble the assay, the Rac1-coated beads were vigorously vortexed to mix and dispensed 3 μL/well to each well of the 1536 well assay ready plate (polypropylene deep well V-bottom microplates, Greiner Bio-One) using a Multidrop™ dispenser and a small tube cassette. Assay ready plates for this assay had 7.5 nL (60 nL for low molecular weight compounds) of a 10 mM stock of compound dispensed to each well. 3 μL/well of 200 nM Bodipy-FL GTP in sample buffer was added and plates were centrifuged (250–500 × *g*, 10 s) to ensure that samples are at the bottom of the plate and not adhered to the walls of the wells. Plates were sealed using a pierceable heat seal (recommend Thermo Cat No AB-1720 or equivalent) and incubated for 120 min

at room temperature shielded from light. Samples were acquired on the iQue® HD Screener using the "Rac1 template" acquisition and analysis template. Rac1 Sample Buffer (0.1% BSA in NP-HPS supplemented with 1 mM DTT) in the iQue HD Buffer station gave the best sampling results. The cytometer protocol was set up with 0.6 s sip time, 0 s up time, standard pump speed, and medium detector speed as can be seen in **Figure 9**. Reading time per plate is 45 min.

In the Intellicyt ForeCyt® software, we acquired flow cytometric light scatter as well as fluorescence emission in the FL1 channel (Ex 488 nm, Em 530 ± 30 nm). We gated on forward scatter and side scatter to identify the bead populations followed by forward scatter area vs. height to identify the singlet bead subpopulation. The median fluorescence of the singlet bead population was then extracted. Data files were exported from the ForeCyt® software as multiple plates in 1536 grid format as a comma-delimited text file. The files were manually imported into Genedata Screener® for analysis.

Data were normalized on a plate by plate basis using the on-board controls to calculate a % effect value and by robust Z Score. Robust Z Score is a derivation of the original Z Score calculation [16] substituting median for average and robust standard deviation for standard deviation and is used routinely for normalization and hit calling in the AstraZeneca HTS Centre alongside the more common 2-point normalizations using positive (inhibitor) and negative (neutral) control wells. By using robust statistical measures the calculation is resistant to outliers which are, of course, the hits in an HTS which can be missed if using the

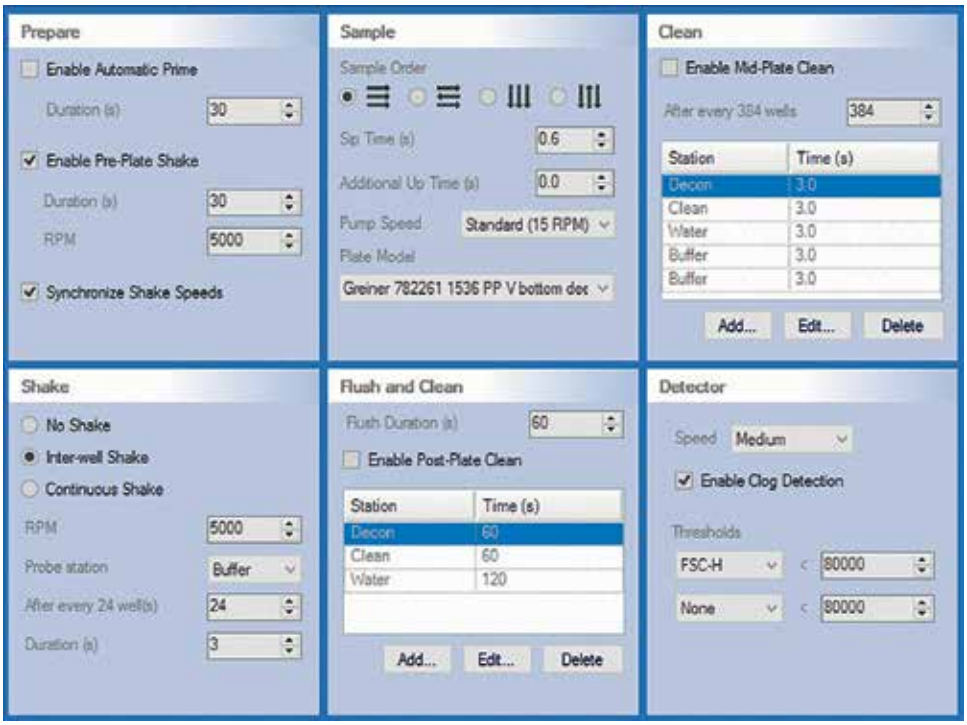

Figure 9. ForeCyt® protocol on iQue® Screener HD.

non-robust version of the equation. Robust Z Score is calculated according to the equation below (Eq. (1)) and normalizes individual wells by calculating the number of robust standard deviations the well value is away for the median of the plate central reference. In most HTS screens this central reference is the median of all the compound wells on a plate as >99% of the wells will be inactive and will define the central reference.

$$N(x) = \frac{x - \langle CR \rangle}{\langle\langle CR \rangle\rangle} \tag{1}$$

x is the measured raw signal value of a well; $\langle CR \rangle$ is the median of the measured signal values for the central reference values on a plate; $\langle\langle CR \rangle\rangle$ is the robust standard deviation of the measured signal values for the central reference values on a plate.

Hits were identified using a cut-off of −10 in robust Z score; this corresponded to an approximate change of fluorescence greater than 30% (50% for LMW) from controls.

The primary screen of 500,000 compounds took 4 weeks to complete and some summaries of the data are presented in **Figure 10**.

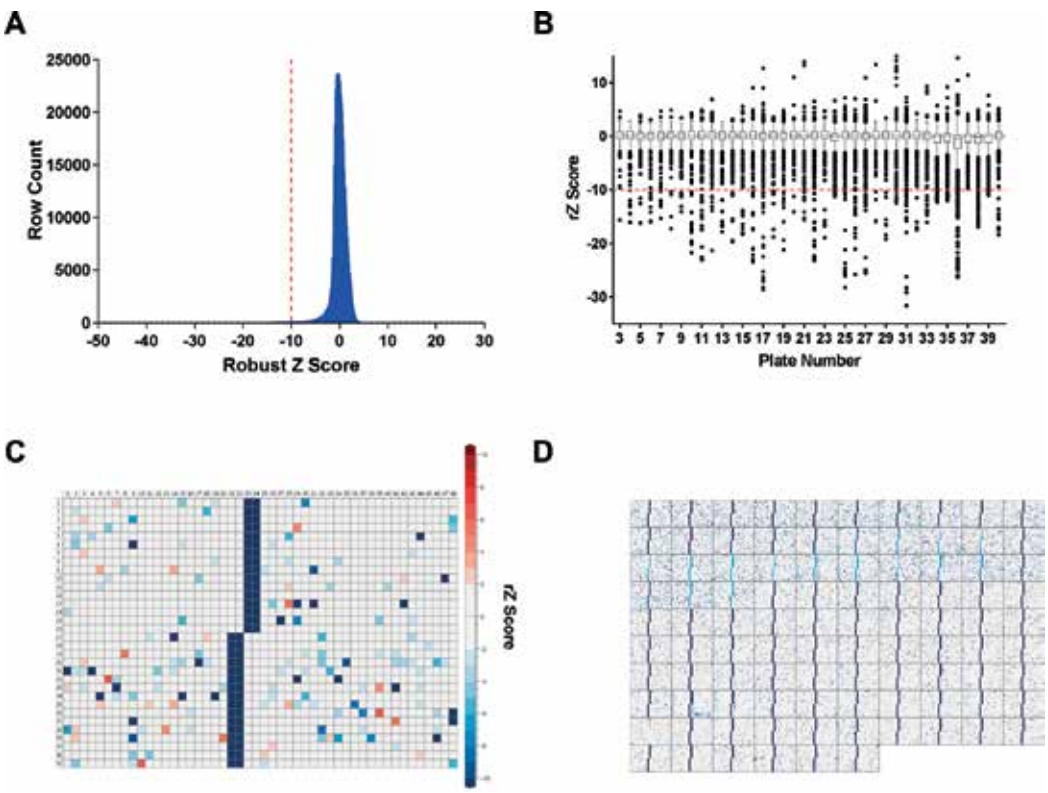

Figure 10. Primary screen data. (A) Distribution plot, (B) box plot, (C) plate view in Genedata Screener® and (D) assay overview in Genedata Screener®.

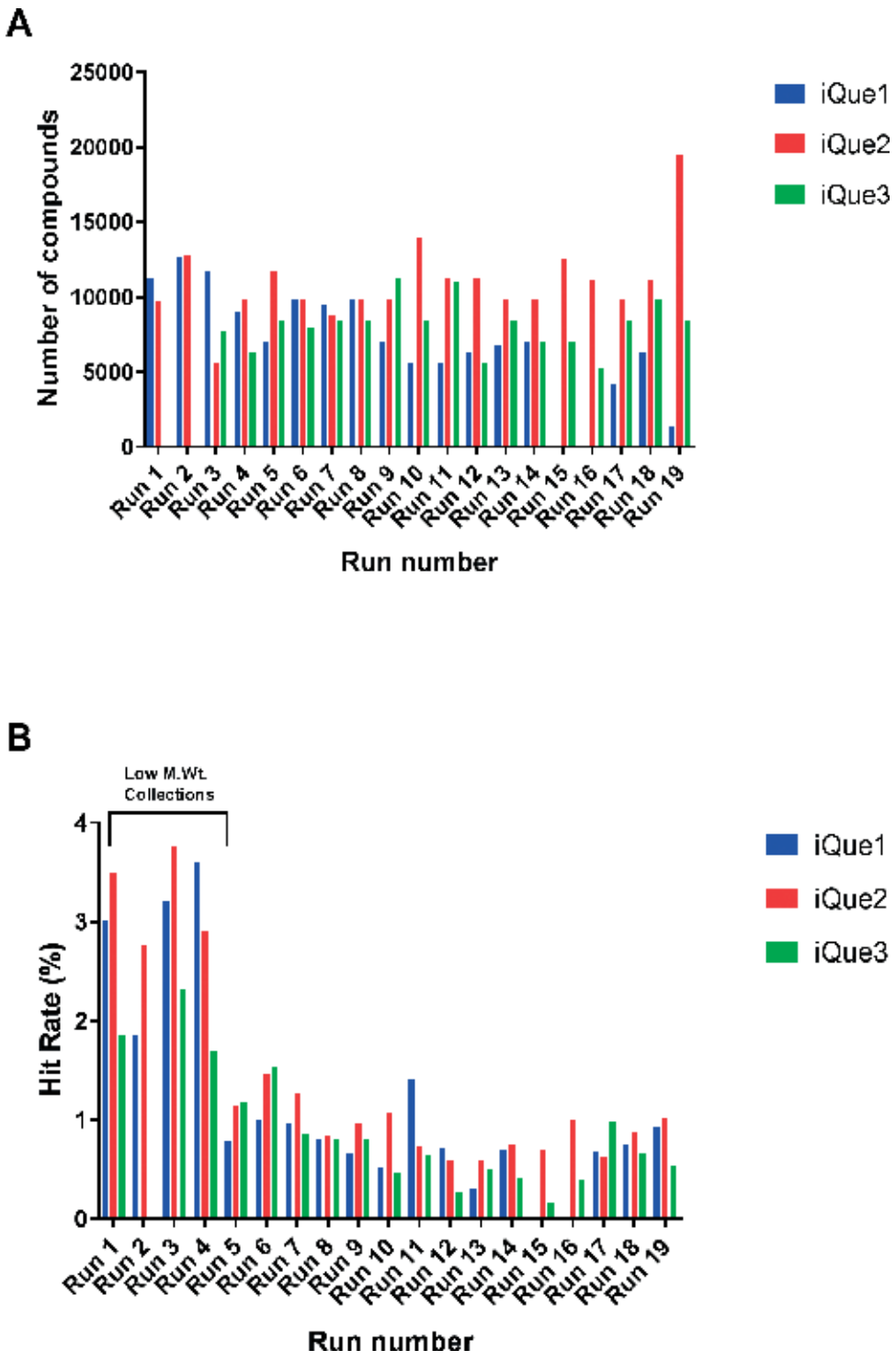

Figure 11. Primary screen data analysis plots. (A) Number of compounds analyzed per run and (B) hit rate per run.

The screen ran at a throughput of 20 plates per day equivalent to 31,000 compounds per day. The overall distribution in **Figure 10** shows a narrow central peak centered on zero with the left tail containing potential hits. This is a typical distribution shape seen in HTS screens and clearly shows that the assay was capable of identifying hits. The box plots shows the stability and consistency of the assay and tightness of the data across multiple plates and also allows visualization of the hits represented as the outliers on the plot. A typical plate analysis is shown depicting the controls in the central columns and a few hits scattered across the plate as dark blue wells with the histogram showing the heat map scale of the robust Z score. The assay overview (**Figure 11**) shows the whole set of plates (with the low molecular weight collection highlighted) run on one iQue® Screener HD highlighting the hit rate variation with the collection subset. It can be clearly seen that the hit rate in the low molecular weight set, found in the first 32 plates, is elevated above that of the core collections. This can occur due to the higher screening concentration leading to more non-specific inhibition due to common contaminants such as metals which are then ruled out by further downstream assays and SAR analysis Although not shown, the assay signal to background as well as Z′ factor [17] are monitored throughout the screen as markers of data quality and again indicated that this assay was of high quality.

5870 hits were identified after the primary screen representing a 1.2% overall hit rate. All hits were then tested as 10-point concentration responses (100–0.003 μM) against Rac1 as well as RhoA and CDC42 so we could assess selectivity of the compounds for Rac1. The assay is performed as described for the primary screen. All hits identified in the primary

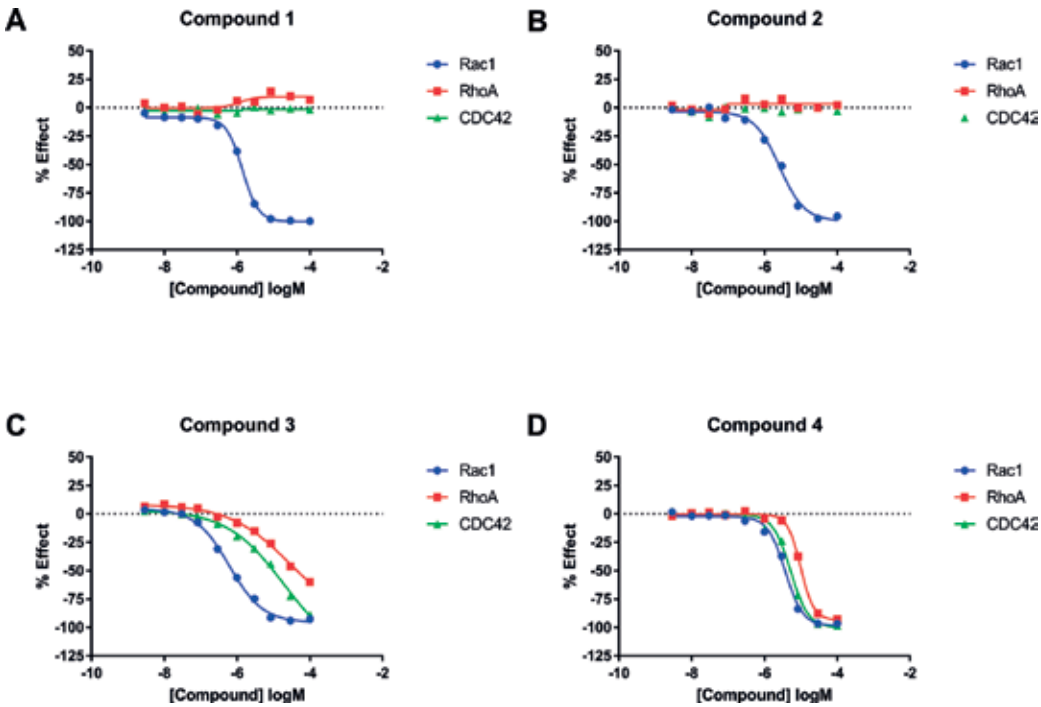

Figure 12. Representative curves of selective and non-selective compounds.

screen were serially diluted 1:3 to construct a 10-point concentration response curve. Compound concentration curves are dispensed using acoustic dispensing into assay ready plates at 150 compound curves per plate. Wells are backfilled with DMSO to keep the DMSO concentration constant in all wells. The plates were sealed and stored in the controlled atmosphere and temperature working plate store before use as for primary screen plates. 1 mM $MgCl_2$ was added to the buffer for the RhoA assay. 82% of the tested compounds were confirmed as active with 44 identified as Rac1 selective using a ≥10 fold ratio of Rac1 IC_{50} vs. RhoA and Cdc42 as a cutoff. These compounds encompass a variety of chemical structures. **Figure 12** shows representative curves of selective and non-selective compounds. Selected hits are being further characterized through a panel of cellular assays by the team at INSERM.

4. Conclusions

Until recently flow cytometry was considered a powerful technology dedicated to bespoke assays where just a few samples were to be measured. No medium throughput let alone high throughput screen could be run on this technology due to lack of plate handling features, time needed per sample and therefore cellular imaging was the preferred method for any high content screen. Increases of interest in phenotypic screening combined with a desire to access relevant cell models, often suspension cells, and development of plate-based sampling flow cytometers have led to the opportunity to use flow cytometry as a drug screening technology platform. The ability to perform multiplexing where different cells or particles labeled with distinct fluorophores are analyzed in parallel and multiple endpoints are measured leads to in-depth analysis of subpopulations within a sample. Such an approach results in increased productivity by decreasing timelines and cell requirements, two critical parameters for high throughput screening.

We chose to run a screen for Rac1 inhibitors on our iQue® Screener HD as it enabled us to miniaturize and run a simple and robust assay on one of our automation platforms.

We have run a successful 500,000 compound screen using the iQue® HD screener as summarized in **Figure 13**. By optimizing the protocol, we were able to retain high-quality data while decreasing read time per 1536 well plate to under 50 min. This allowed us to run the primary screen within 4 weeks. Although time is not the most critical criteria we consider it remains an important factor as we need to maintain the overall flow of projects through our portfolio and therefore we must decide on a suitable time frame for completion of each screen.

High throughput screening is a key method for the identification of hit and lead compounds and remains at the start of most of our drug discovery programs. As we pursue a wide range of targets we also use a wide range of assays and technologies. We have invested into several iQue® Screener systems as we updated and replaced previous detection systems and to fill a capability gap for screening suspension cells or primary cells in small sample volumes. We have successfully used the iQue® Screener systems in a variety of applications from phenotypic screening to more complex multiplex profiling. The technology has enabled several projects due to the ability to reduce cell requirement, cost and timelines.

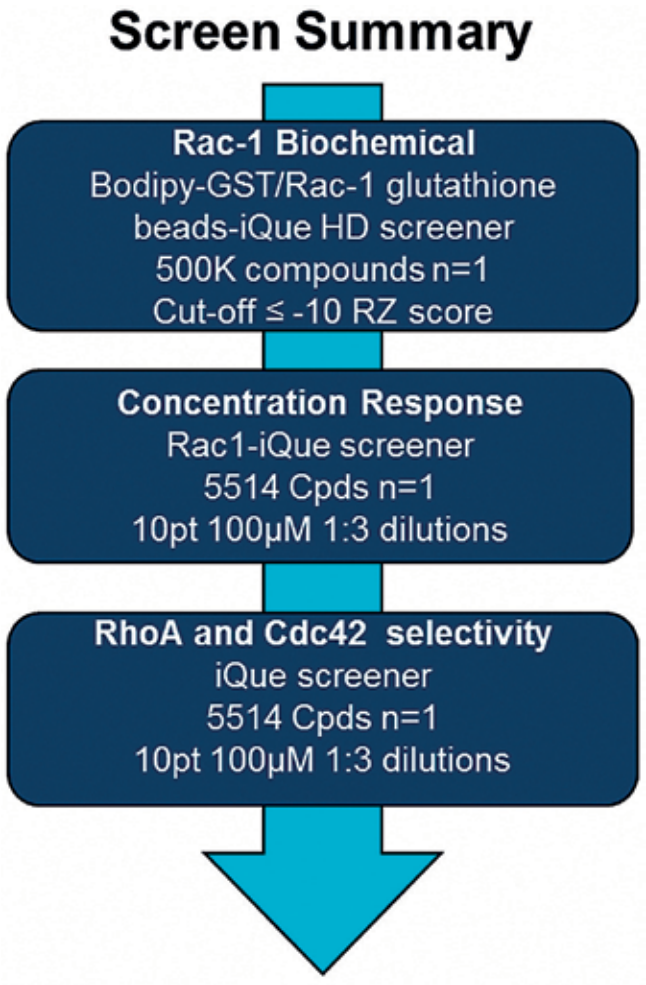

Figure 13. Screen summary.

The screen we have described here would have not been possible a few years ago but, thanks to the development of high throughput capable instruments, flow cytometry has found its place within the drug discovery process and high throughput screening in AstraZeneca. Although we decided not to multiplex our concentration response assays, it should be noted that the use of flow cytometry technology does allow for such multiplexing and indeed has been described in the literature [12].

Acknowledgements

The authors would like to thank Matthew Collier for his assistance during the high throughput screen and Kim Luu for her technical support with the iQue®.

Author details

Catherine Bardelle[1]*, Vincent Sauzeau[2], Mark B. Carter[3], Zhaoping Liu[3], Gervaise Loirand[2] and David Murray[1]

*Address all correspondence to: catherine.bardelle@astrazeneca.com

1 AstraZeneca, Discovery Sciences, Macclesfield, Cheshire, UK

2 L'institut du thorax, Inserm 1087, CNRS UMR 6291, Université de Nantes, Nantes, France

3 IntelliCyt Corporation, Albuquerque, NM, USA

References

[1] Busse WW, Lemanske RF Jr. Asthma. The New England Journal of Medicine. 2001;**344**(5):350-362

[2] To T et al. Global asthma prevalence in adults: Findings from the cross-sectional world health survey. BMC Public Health. 2012;**12**:204

[3] Cockcroft DW, Davis BE. Mechanisms of airway hyperresponsiveness. The Journal of Allergy and Clinical Immunology. 2006;**118**(3):551-559. quiz 560-551

[4] Prakash YS. Airway smooth muscle in airway reactivity and remodeling: What have we learned? American Journal of Physiology. Lung Cellular and Molecular Physiology. 2013;**305**(12):L912-L933

[5] Barnes PJ. Immunology of asthma and chronic obstructive pulmonary disease. Nature Reviews. Immunology. 2008;**8**(3):183-192

[6] Loirand G et al. Small G proteins in the cardiovascular system: Physiological and pathological aspects. Physiological Reviews. 2013;**93**(4):1659-1720

[7] Bustelo XR et al. GTP-binding proteins of the Rho/Rac family: Regulation, effectors and functions in vivo. BioEssays. 2007;**29**(4):356-370

[8] Andre G et al. Smooth muscle specific Rac1 deficiency induces hypertension by preventing p116RIP3-dependent RhoA inhibition. Journal of the American Heart Association. 2014;**3**(3):e000852

[9] Carrizzo A et al. Rac-1 as a new therapeutic target in cerebro- and cardio-vascular diseases. Current Drug Targets. 2014;**15**(13):1231-1246

[10] Halaban R. RAC1 and melanoma. Clinical Therapeutics. 2015;**37**(3):682-685

[11] Hong L et al. A Pan-GTPase inhibitor as a molecular probe. PLoS One. 2015;**10**(8):e0134317

[12] Surviladze Z et al. Identification of a small GTPase inhibitor using a high-throughput flow cytometry bead-based multiplex assay. Journal of Biomolecular Screening. 2010;**15**(1):10-20

[13] Surviladze Z et al. High throughput flow cytometry bead-based multiplex assay for identification of Rho GTPase inhibitors. Methods in Molecular Biology. 2012;**827**:253-270

[14] Murray D, Wigglesworth M. Chapter 1 HTS methods: Assay design and optimisation. In: High Throughput Screening Methods: Evolution and Refinement. London: The Royal Society of Chemistry; 2017. p. 1-15

[15] Wigglesworth MJ et al. Increasing the delivery of next generation therapeutics from high throughput screening libraries. Current Opinion in Chemical Biology. 2015;**26**:104-110

[16] Malo N et al. Statistical practice in high-throughput screening data analysis. Nature Biotechnology. 2006;**24**(2):167-175

[17] Zhang JH et al. A simple statistical parameter for use in evaluation and validation of high throughput screening assays. Journal of Biomolecular Screening. 1999;**4**(2):67-73

Chapter 4

Multidimensional Flow Cytometry for Testing Blood-Handling Medical Devices

Ina Laura Pieper, Gemma Radley and
Catherine A. Thornton

Additional information is available at the end of the chapter

http://dx.doi.org/10.5772/intechopen.76437

Abstract

Blood handling devices such as left ventricular assist devices and total artificial hearts offer life-saving treatments for patients suffering from severe heart failure. Current devices have clinically proven that heart assist pumps are a safe and effective therapy, and indeed in many cases they are the only available method of treatment. However, current devices cause side effects including stroke, bleeding, infection, and thrombosis, preventing the technology from reaching its full potential. If the side effects could be reduced, then more patients could benefit from these devices. The complications are related to damage to blood cells and proteins as a result of contact with foreign materials and mechanical stress. There is a need for better devices with minimal blood impact to enable more patients to be safely treated; better tools, especially flow cytometry, could support the device development life cycle. In this chapter we review the clinical, in vivo, and in vitro flow cytometry data available for ventricular assist devices, conduct a gap analysis, and identify areas of future possibilities for device developers to establish new flow cytometry-based methodologies.

Keywords: multidimensional flow cytometry, translational research, ventricular assist, microparticles, multispecies

1. Introduction

Blood handling devices such as left ventricular assist devices and total artificial hearts offer life-saving treatments for patients suffering from severe heart failure. Current devices have clinically proven that heart assist pumps are a safe and effective therapy, and indeed in many

cases they are the only available method of treatment. However, current devices cause side effects including stroke, bleeding, infection, and thrombosis, preventing the technology from reaching its full potential [1]. If the side effects could be reduced, then more patients could benefit from these devices. The complications are related to damage to blood cells and circulating proteins as a result of contact with foreign materials and mechanical stress. There is a need for better devices with minimal negative effect on blood to enable more patients to be treated safely; better tools, especially flow cytometry, could support the device development life cycle.

The use of multidimensional flow cytometry during pre-clinical development of blood handling devices offers a powerful tool to monitor changes to erythrocytes, leukocytes, and platelets, as well as circulating mediators such as von Willebrand factor. A key challenge is the need to study these in cows, sheep and pigs which are used for pre-clinical studies. This is associated with markedly reduced reagent options compared to studies using human blood. While there are some species-specific antibodies suitable for flow cytometry, the preferential use of cross-reactive reagents and species non-specific tools enables multicolor panels to be developed that can be used with blood from multiple species. Such an approach also allows for comparisons at all stages of device development and implementation: in vitro, in vivo pre-clinical, and ex vivo clinical settings. Flow cytometry methods could also support personalised treatment strategies to potentially predict patients at risk of complications [2]. This could be prior to or following implantation of a device. Here, we will provide an overview of the development of flow cytometry tools to address this need including a review of work performed to date, as well as future possibilities for this technology platform.

2. Current use of flow cytometry for ventricular assist and total artificial heart research

The majority of the flow cytometry research performed in the area of blood-handling medical devices is to further the understanding of the complications that arise upon ventricular assist device implantation into heart failure patients. Since the aim of using flow cytometry during *in vitro* and

in vivo device testing is to maximise its haemocompatibility and minimise complications, it makes sense to start this review with the clinical data. The gaps in *in vitro* and *in vivo* research and development will then become evident and lay the foundation for the future possibilities for device developers.

2.1. Clinical flow cytometry data from ventricular assist devices

Flow cytometry has been used to analyse all major cellular components of the blood—i.e. erythrocytes, leukocytes, and thrombocytes—in VAD-patients.

2.1.1. Erythrocytes

Sansone et al. were the first group to use flow cytometry in the clinic to evidence VAD-related damage to erythrocytes, in addition to the standard method of measuring plasma free haemoglobin [3]. Patients implanted with continuous flow (CF) VADs (HVAD, HeartWare), showed significantly greater levels of $CD235^+$ erythrocyte MPs compared to controls (both age-matched healthy and patients with stable coronary artery disease, CAD). Their erythrocyte counts were not described, but the VAD-patients had significantly greater levels of free haemoglobin compared to controls. Increased levels of erythrocyte MPs have been found in patients suffering sickle cell disease and β-thalassemia major, which are diseases also characterised by haemolysis [3].

2.1.2. Leukocytes

From a flow cytometry perspective leukocytes have received more attention than erythrocytes. VAD-related leukocyte damage has been demonstrated using flow cytometry in all major leukocyte subsets. Using the pan-leukocyte marker CD45, leukocyte microparticles ($CD45^+$) were shown to be elevated in CF VAD patients compared to healthy and CAD controls [3]. This is indicative of overall leukocyte destruction and is supported by Woolley et al. who observed decreased total leukocyte counts in CF VAD patients [4]. In the same study, CD15+ neutrophils were found to become activated as measured by an increase in MAC-1 (CD11b) expression. The level of activated neutrophils was dependent on pump type: HeartMate II causing greater levels than HVAD and PVAD [4]. Neutrophil activation status might also influences the patient's susceptibility to infection as more HeartMate II patients than HVAD patients suffered from infection. The PVAD has a larger driveline exit area which contributes to infection rates, hence it cannot be directly compared to the other two pumps [5]. *In vitro,* neutrophils release $CD11b^+$ MPs during activation [6–8] and could therefore be the parental cell type for the $CD11b^+$ MPs that are elevated significantly in VAD-patients (mainly HeartMate II patients) compared to healthy controls [9].

Monocytes also become activated in VAD-patients with the expression of tissue factor (TF) increased significantly within the first month of pulsatile Novacor or HeartMate XVE support versus healthy controls [10, 11]. TF is a key element of the extrinsic coagulation cascade, and it is able to trigger coagulation, even with endothelial integrity virtually preserved. The major source of TF in blood is monocytes, and the expression is upregulated by for example lipopolysaccharides (LPS) [12]. As summarised by Angelillo-Scherrer: volunteers exposed to endotoxin, patients with meningococcal sepsis, and primates with Ebola fever, all show increased levels of $CD14^+/TF^+$ MPs, indicating a potential role for these MPs in disseminated intravascular coagulation associated with severe infections [12]. As driveline infections is a common problem in VAD-patients, there is a possibility that $CD14^+$ monocytes expressing TF and/or $CD14^+TF^+$ MPs, could be a thrombosis risk marker in patients with ongoing infection.

Lymphocytes are affected by both pulsatile and CF-VADs [13–15]. A general lymphopenia occurred in patients, implanted with the early pulsatile HeartMate XVE [14]. This was

accompanied by a significant reduction in the mean CD4/CD8 T cell ratios, and in the mean number of circulating CD4 T cells. The CD4/CD8 T cell ratio decreased rapidly within the first month and remained low at the 2 month follow-up assessment [14]. The decline in CD4 T cells was attributed to a heightened susceptibility to apoptosis as measured by surface expression of phosphatidylserine through annexin V binding [14]. These results were confirmed in a group of patients implanted with either the pulsatile HeartMate XVE or the Novacor, where the mean number of circulating CD4 T cells was significantly lower compared to medically managed heart failure patient controls. While the levels of CD8 T cells remained unaffected [15], both CD4 and CD8 T cells had increased CD95(Fas) expression and annexin V binding versus controls, indicating apoptosis. Furthermore, the LVAD-patients had a significantly greater risk of developing candidal infection compared to the controls or other patients undergoing cardiac surgery. Altogether, this suggests that the pulsatile LVADs cause T-cell defects, most notably CD4 T-cell defects, and that some of these defects are measurable through flow cytometry [14, 15]. How this translates to an effect on the function of T cells remains to be determined.

Patients with CF-VADs also have changes in their T cell levels. However, contrary to pulsatile LVAD-patients, those implanted with CF-VADs (specific device not published) and who suffered from infection had significantly higher levels of CD4+/CD25+ Tregs and increased lymphocyte reactive oxygen species (ROS) compared to VAD-patients without infection [13]. Whether these differences between pulsatile and CF VADs relates to pulsatility would be an interesting topic for further studies.

As far as we are aware, circulating B cells and NK cells have not been studied by flow cytometry in LVAD-patients. Nor have other minor populations such as dendritic cells or innate lymphoid cells. There are some data of the effect of VADs on B cells from in vitro studies (Schuster 2002) and these are discussed below.

2.1.3. Platelets

Platelets have been studied on their own and in microaggregates with leukocytes. Wilhelm et al. found that platelets were activated in patients with pulsatile VADs (Novacor and HeartMate XVE) compared to healthy controls [11]. This was measured as significantly increased CD62P expression. However, Dewald showed that increased platelet activation might not be due to the VAD as platelets in heart failure patients are already activated prior to implantation. This was shown using antibodies against CD62P, CD63, and antithrombospondin [16]. Similarly, Matsubayashi showed that CD62P and CD63 expression are elevated on platelets in Novacor-patients compared to healthy controls, but preoperative values were already high with no clear increase or decrease during implantation [17]. Further highlighting the impact of heart failure rather than VAD use on platelet activation *in vivo* granulocyte-platelet ($CD15^+/CD42b^+$) and monocyte-platelet ($CD14^+/CD42b^+$) aggregates were also increased significantly in the pulsatile VAD patients versus healthy controls before and after VAD implantation [11].

Platelet MPs also have been detected using flow cytometry in CF-LVAD patients [3, 9]. In 2010, Diehl P et al. showed that LVAD-patients, the majority of whom were implanted with the CF-LVAD HeartMate II, had significantly increased levels of CD31+/CD61+ platelet MPs compared to healthy controls [9]. Five years later, Sansone et al. showed that $CD31^+/CD41^+$ platelet MPs were elevated in patients 3 months post-implantation of a HVAD (a CF-LVAD) in comparison to both age-matched healthy controls and patients suffering from coronary artery disease (CAD) [3]. Hence, although the HeartMate II and the HVAD differ drastically in design, both were associated with platelet microparticle formation.

The focus has been on platelet activation and platelet MPs but these have so far not shown a utility as predictors of adverse events or stratifiers. However, there are other platelet parameters, all measurable by flow cytometry, that have potential as patient risk stratifiers, or even predictors, for bleeding complications in patients with CF-VADs [18–20]. These include significantly greater levels of reactive oxygen species, mitochondrial damage, surface phosphatidylserine (PS) expression/apoptosis, and significantly decreased expression of $\alpha 2b\beta 3$ on the platelet surface, in bleeders compared to non-bleeders [18–20]. The CF-VADs studied included the HeartMate II, Jarvik 2000, and the HVAD and no differences were found between the devices.

2.1.4. Endothelial cells and microparticles of unknown origin

$CD62E^+$ endothelial cell microparticles (EMPs) are increased in VAD-patients compared to healthy controls [3, 9] and CAD patients [3]. EMPs phenotyped as $CD31^+/CD41^-$, and $CD144^+$ are also elevated levels in VAD-patients [3].

Additional to the MPs of specific lineages described above—erythrocytes, leukocyte, platelet and endothelial—PS-expressing MPs of unknown lineage have been suggested as a potential biomarker of adverse events in VAD-patients implanted with a HeartMate II [2]. Patients who developed an adverse event, including ventricular tachycardia storm, non-ST elevation myocardial infarction, arterial thrombosis, gastrointestinal bleeding, and stroke had significantly higher levels of PS+ MPs than patients with no adverse events [2].

2.2. Pre-clinical in vivo haemocompatibility of blood-handling devices

The flow cytometry data from published pre-clinical *in vivo* studies of LVADs is focussed mainly on platelets with the exception of one study on leukocytes. There is no published data on erythrocytes.

2.2.1. Leukocytes

Snyder et al. have published the only *in vivo* leukocyte work wherein the aim was to develop assays for leukocyte-platelet aggregates and monocyte tissue factor expression [21]. Using an anti-bovine granulocyte antibody (CH138A) or anti-CD14 (TüK4) in combination with antibody CAPP2A (anti-ruminant CD41/61), calves implanted with CF-LVADs (HeartMate II

or EVAHEART) had significantly elevated levels of both neutrophil-platelet and monocyte-platelet aggregates compared to pre-operative [21]. Monocyte tissue factor expression monitored using an anti-bovine tissue factor antibody developed by Stephen Carson at University of Nebraska [22], also showed a dramatic increase immediately post-operatively and significantly elevated levels throughout the 30-day study [21].

2.2.2. Platelets

Bovine platelet activation and microaggregates have been studied using various markers in calves implanted with CF-VADs. Baker et al. developed a method using the antibodies BAQ56, BAQ125 and GC5A (platelet antigen, CD equivalent unknown, available from Washington State University) to measure platelet activation, and CAPP2A (anti-CD41/CD61) to measure platelet microaggregates in calves implanted with CF-LVADS (the Sun Medical centrifugal pump or the HeartMate II) [23]. Platelet microaggregates, i.e. platelet positive events (binding anti-bovine CD41/61 antibody) with forward scatter larger than single platelets, increased post-operatively and then showed some decline in calves implanted with Sun Medical whereas they remained elevated in the calves implanted with HeartMate II. Platelet activation increased post-operatively for both implants and remained elevated. BAQ56 provided the strongest signal and GC5 the weakest signal of the three antibodies, but BAQ125 and GC5 exhibited the strongest agreement with one another, and with the circulating microaggregates [23].

Snyder et al. used a modified version of Baker's methodology in two studies of calves implanted with the CF-LVADs—HeartMate II [24] and the EVAHEART [25]. Snyder showed that the microaggregate levels in surgical sham controls remained at pre-operative levels, confirming that the CF-LVAD and not the cardiac surgery cause elevated levels [24]. Microaggregate levels increased post-implantation, and decreased within the first week in all animals implanted with the EVAHEART [25], and in those animals implanted with the HeartMate II who had an uneventful post-operative course [24]. In calves who suffered adherent thrombi in the outflow region of the pumps, the microaggregate levels either remained elevated or increased before conclusion of the study [24].

Part of Snyder's modification was the inclusion of additional markers for platelet activation to address the limitations BAQ56, BAQ125, and GC5 with their unknown target antigens, namely Annexin V binding [24], anti-CD62P and anti-CD63 [25]. All platelet activation/apoptosis markers tested (BAQ125, GC5, Annexin V, CD62P, CD63) increased immediately after implantation and remained significantly elevated in CF-LVAD animals versus the pre-operative control [24, 25]. Those tested in sham animals (BAQ125, GC5, Annexin-V) decreased around 2 weeks post-operatively [24]. Although CD62P and CD63 successfully identified activated platelets in CF-LVAD calves, the signal was weaker than that of the BAQ125 and GC5 antibodies [25].

CAPP2A also binds to ovine platelets whereas anti-bovine platelet activation antibodies BAQ125 and GC5 do not. Hence, Johnson et al. used CAPP2A as a platelet lineage marker along with cross-reactive anti-human CD62P antibodies (clones Psel.KO.2.7 and Psel.KO.2.12)

to assess platelet activation in sheep implanted with paediatric CF-LVADs [26–28]. Johnson showed that, similarly to calves, platelet activation increases post-operatively in surgical sham control sheep and returns to pre-operative levels at around 2 weeks. The implanted sheep did not demonstrate a common pattern [28]. However, a finding also consistent with previous work was that platelet activation spiked in animals that suffered complications [26–28].

2.3. In vitro haemocompatibility of blood-handling devices

Similarly to the *in vivo* studies, the *in vitro* studies of VADs using flow cytometry are focussed on platelets, with some recent studies introducing leukocyte data. There is no published data on erythrocytes.

2.3.1. Leukocytes

Work from our group has shown that bovine leukocytes shed microparticles, measured as increasing levels of $CD45^+$ MPs (**Figure 1**), during *in vitro* pumping in the extracorporeal CF-LVADs CentriMag and RotaFlow, and the intracorporeal CF-LVAD VentrAssist [29, 30]. We have also shown that $CD45^+$ MPs increase significantly when sheep rather than bovine blood was pumped with the CentriMag [31]. Subtypes of leukocyte MPs were discovered

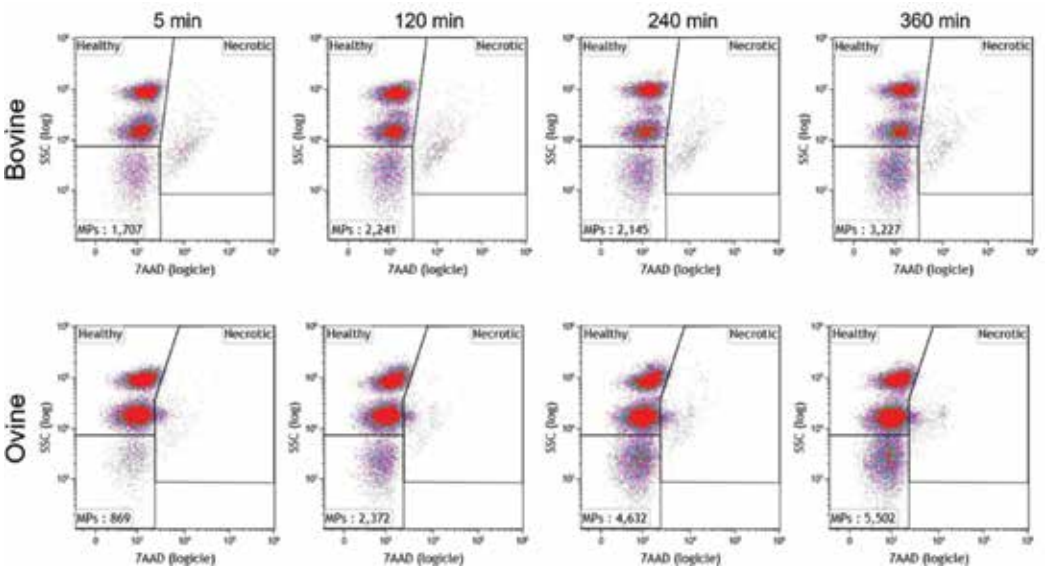

Figure 1. Flow plots showing bovine and ovine blood pumped through the CentriMag. Whole blood was collected into CPDA-1 anticoagulant primed with antibiotics/antimycotics and gentamicin. Blood was diluted with PBS to achieve a haematocrit of 30±2% according to ASTM standards and entered into the mock circulatory loop. The CentriMag was operated at a speed of 2200 rpm, flow of 5 L/min, and pressure 100 mmHg for both species. Samples were removed every 2 h and stained with CD45-PE and 7AAD. CD45+ events were gated on a SSC vs. 7AAD plot and events with a low SSC were identified as leukocyte-derived microparticles (MPs).

in sheep blood during *in vitro* VAD testing using antibodies cross-reactive with human and bovine blood. The main subtypes were CD11b^{bright}/HLA-DR^{-} and CD11b^{dim}/HLA-DR^{+}, discovered using a four-colour panel (**Figure 2**), and we suggested that these are derived from granulocytes and lymphocytes, respectively [31].

2.3.2. Platelets

The first flow cytometry assessments of platelet activation and microaggregates during *in vitro* testing in CF-LVADs was carried out by Johnson C et al. using sheep blood. Activation was assessed using CAPP2A as a lineage marker and anti-CD62P (clone Psel.KO.2.7), and was found to increase throughout the duration of the test of the PediaFlow [28]. We have used CAPP2A, BAQ125, and Annexin V to assess platelet activation in bovine blood in the CentriMag, but did not find any significant activation. However, the CentriMag has a magnetically levitated impeller, resulting in minimal heat, and also large gaps minimising blood damage, so these findings were not surprising [30] (**Figure 3**).

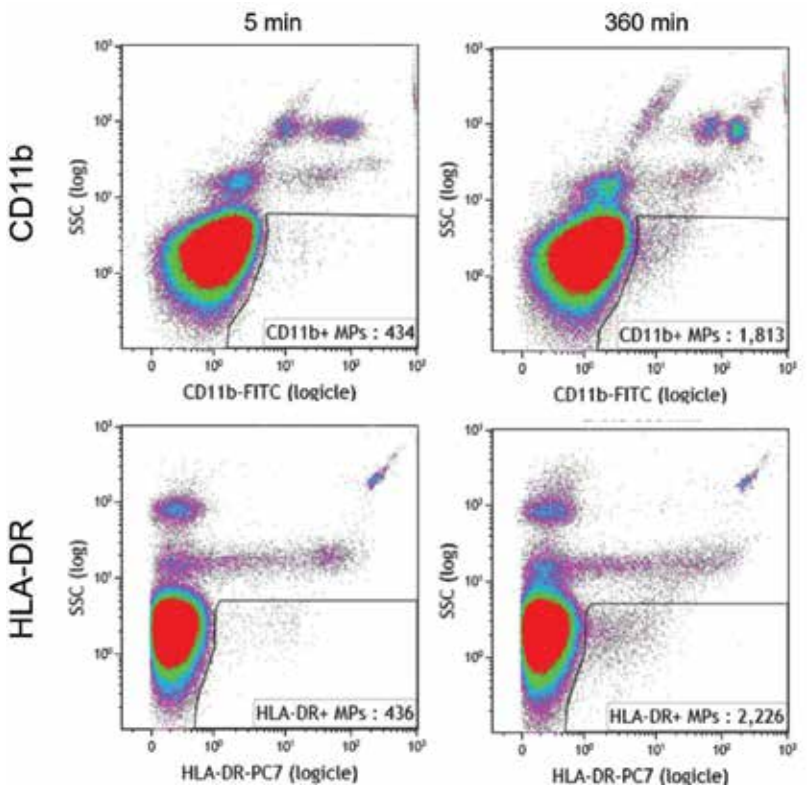

Figure 2. Flow plots showing ovine blood pumped through the CentriMag operated at a speed of 2200 rpm, flow of 5 L/min, and pressure 100 mmHg. Whole blood was collected into CPDA-1 anticoagulant primed with antibiotics/antimycotics and gentamicin. Blood was diluted with PBS to achieve a haematocrit of 30±2% according to ASTM standards and entered into the mock circulatory loop. Samples were stained with CD11b-FITC and HLA-DR-PC7. Events with a low SSC and positive for these markers were gated as CD11b or HLA-DR positive microparticles (MPs).

http://dx.doi.org/10.5772/intechopen.76437

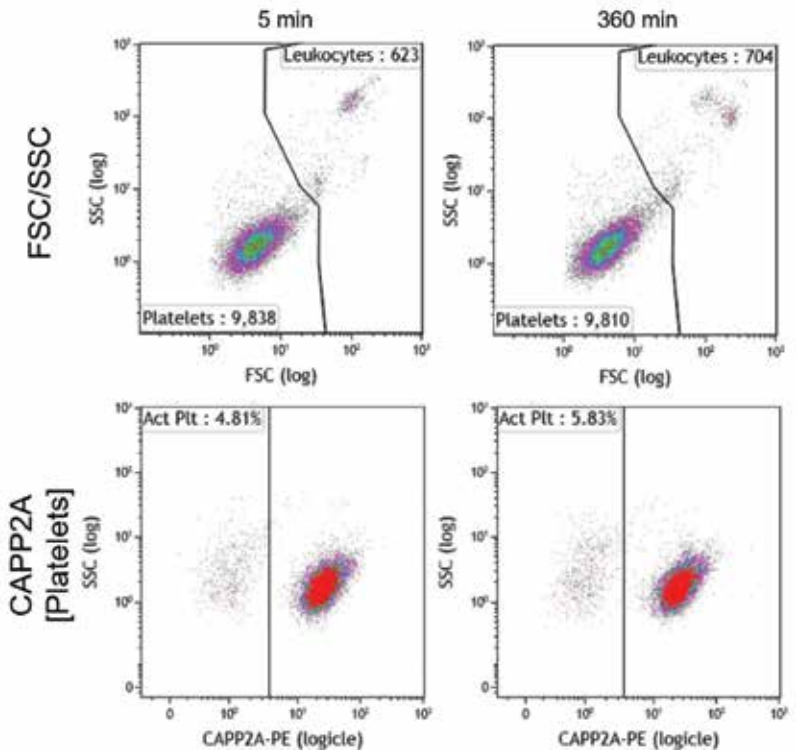

Figure 3. Flow plots showing bovine blood pumped through the CentriMag operated at a speed of 2200 rpm, flow of 5 L/min, and pressure 100 mmHg. Whole blood was collected into CPDA-1 anticoagulant primed with antibiotics/antimycotics and gentamicin. Blood was diluted with PBS to achieve a haematocrit of 30±2% according to ASTM standards and entered into the mock circulatory loop. Samples were stained with CAPP2A-PE, a marker for resting platelets. Forward and side scatter plots were used to identify platelets. CAPP2A negative platelet events were identified as activated platelets (Act Plt).

3. Future possibilities for device developers

Although flow cytometry has been used clinically to study phenotype, activation status and MPs of the main circulating cell types in patients implanted with mechanical circulatory support devices, the use of flow cytometry for pre-clinical *in vivo* and *in vitro* studies has been very limited. As can be seen in **Table 1**, there are many potential gaps that could be filled by developing assays for *in vitro* use, as well as *in vitro* assays to translate to the pre-clinical and clinical *in vivo* setting. The *in vitro* setting will always provide the worst case scenario, as the pumped blood volume is 10 times less than in the VAD-patient and the blood components are therefore experiencing an increased amount of pumping, not to mention experiencing plastic tubing instead of endothelial coated vasculature. In addition, there is no supply of oxygen or nutrients other than what is already present in the plasma, and there is no efficient removal of waste products or damage/dead cells. Cells are therefore more vulnerable *in vitro*. Therefore, if a VAD induces detectable cellular damage clinically, it will most certainly be measurable in

Cell type	Assay	In vitro		In vivo		Clinical
		Ovine	Bovine	Ovine	Bovine	
Erythrocytes	**CD235+ MPs**					✓
Leukocytes	**CD45+ MPs**	✓	✓			✓
Granulocytes	**CD11b + MPs**	✓				✓
	CD11b + expression					✓
Monocytes	**TF expression**				✓	✓
Lymphocytes	**Subset levels: CD4+, CD8+, CD4+/CD25+**					✓
	ROS, apoptosis					✓
	HLA-DR+ MPs	✓				
Platelets	**Activation**	✓	✓	✓	✓	✓
	Phosphatidylserine		✓		✓	✓
	MPs					✓
	ROS, etc.					✓
	Microaggregates			✓	✓	
GRA-PLT	**Microaggregates**				✓	✓
MON-PLT	**Microaggregates**				✓	✓
Unknown	**Phosphatidylserine MPs**					✓

Table 1. Gap analysis of assays for evaluating blood-handling devices.

an *in vitro* test. Platelet activation is so far the only assay that has been fully reverse-translated from bedside to bench, but there is no reason to believe that it should not be possible to create suitable flow cytometry assays for erythrocytes and leukocytes for all stages in the product development process. The benefits of implementing such assays for the devices in development could be identification of designs with minimal impact on blood components, and thus a reduction of the blood-damage related life-threatening complications so commonly seen in VAD-patients including bleeding, stroke, device thrombosis and infection.

3.1. Erythrocytes

The VADs in current use are designed to minimise high shears to blood for prolonged durations to avoid haemolysis. However, erythrocytes demonstrate impaired capacity to deform when exposed to shear stress well below the "haemolytic threshold" [32]. Thus, there is a need for assays that can pick up more subtle damage to erythrocytes. We propose that quantifying RBC MPs as a possible means of assessing sub-haemolytic damage should be investigated to see whether or not it can fill this need.

3.2. Leukocytes

Activated $CD15^+CD11b^+$ neutrophils, have been detected in VAD-patients and clinical data shows that the activation status might influence the patient's susceptibility to infection [5]. With additional evidence that $CD11b^+$ MPs are increased in VAD-patients, and generated during *in vitro* pumping in ovine blood, it makes sense to propose further investigations into its utility as a stratifier to identify those at the highest risk of developing infections in order to offer prophylaxis, thereby reducing infection rates.

VAD-related increases in monocytes expressing TF have been demonstrated both clinically [10, 11] and *in vivo* [21]. $CD14^+/TF^+$ MPs are elevated in primates, healthy volunteers, and patients subjected to infectious stimuli that could result in disseminated intravascular coagulation [33]. Thus, we propose that in VAD-patients with ongoing driveline infections, the presence of $CD14^+/TF^+$ monocytes/MPs potentially could identify those patients at risk for a thrombotic event in order to offer prophylaxis. Assays could also be developed for *in vitro* testing of devices to see if the combination of design, foreign material and/or shear stress in different device models results in TF-expression. However, care should be taken when assessing $CD14^+TF^+$ MPs as false positive results can be generated by the antibody preparations used [34].

The lack of pulsatility has been suggested as a factor that could be contributing to the complications related to aortic valve insufficiency, gastrointestinal bleeding, stroke, pump thrombosis, and haemolysis [35]. A link between pulsatility and blood damage has so far only been described for the blood coagulation protein von Willebrand Factor (vWF), which appears to degrade more in patients with pulsatile compared to non-pulsatile VADs [36]. As our group has shown, vWF degradation caused by shear stress in vitro can be assessed using flow cytometry a flow cytometry-based ristocetin assay [37]. However, it appears as if T cells could be another missing link needed to describe the effects of non-pulsatile [13] and pulsatile [14, 15] flow on the blood. Therefore, we propose that assays for T-cells are established for sheep and cow blood in order to study the effects of pulsatility, in order to gather more scientific evidence that could be used to interpret the clinical data.

Other leukocyte subsets of interest to develop methods for studying would be B-cells. Schuster et al. described that the T-cell apoptosis observed in patients with pulsatile VADs, was induced by a B-cell response to polyurethane, a material commonly used for the membranes in pulsatile devices [38, 39]. Continuous flow devices are typically made from metals and ceramics, and do not contain polyurethane. Hence, pulsatility studies should be made in combination with various biomaterial controls, including for example titanium alloys commonly used in VADs [40, 41].

3.3. Platelets

In vitro and *in vivo* platelet studies have so far been limited to studying activation by increased expression of platelet markers, but the expression of platelet activation surface markers has so

far failed to be linked to clinically relevant events. However, Mondal's portfolio of potential risk stratifying platelet parameters [18–20] are of importance to study *in vitro*. Hence, we propose that effort be made to translate Mondal's methods to bovine and/or sheep blood for *in vitro* studies of platelet reactive oxygen species, mitochondrial damage, and α2bβ3 expression to investigate any potential links between device design and its influence on platelet health. Since platelets are numerous in blood, very small volumes can be used to analyse them. In combination with a multidimensional approach to assess several parameters simultaneously, it would be a very attractive addition to the care pathway for patients with heart failure pre- and post-VAD implantation.

3.4. Cytokines

Cytokines have not been assessed using flow cytometry in a VAD-setting, but recent clinical data on TNFα-levels in VAD-patients might spur a change. High levels of TNF-α were associated with increased risk of bleeding complications in patients with CF-VADs (HeartMate II or HVAD) [42]. Measurement of TNF-α by flow cytometry in whole blood would offer a much more rapid method, a lower sample volume required, and could be combined with other cellular markers of interest into a multidimensional approach [43].

3.4.1. Overcoming practical hurdles

A reason for hesitating in this approach might be the limited availability of reagents for animal blood. However, progress has been made recently in this field by exploiting the cross-reactivity of some antibody clones. We identified the utility of an antibody clone targeting CD62P, clone Psel.KO.2.5, that could measure shear-induced platelet activation in human, bovine, ovine, and porcine blood [44]. Johnson et al. also made significant contributions in identifying cross-reactive platelet antibodies against bovine and ovine platelets [45]. We have used antibodies cross-reactive against bovine and human targets in developing a multicolour flow cytometry panel for sheep leukocyte MPs released during *in vitro* VAD-pumping. This panel should offer translation to both the pre-clinical *in vivo* and clinical setting [31]. To address the cost of antibodies and reduce the need for additional haematology analysers, we have also demonstrated that flow cytometry in combination with DNA dyes and counting beads could be used to assess complete leukocyte counts and viability in bovine, ovine, and human blood [46]. Although personal flow cytometers have been introduced lately, they are still not widespread and many investigators rely on the use of core facilities for flow cytometry acquisition and analysis. Where the animal lab is not in close proximity to the flow cytometry core facility there may be a need to preserve the animal blood prior to shipping for analysis. CytoChex and Streck stabilising fluid were developed to address the need to preserve CD4 antigens for HIV drug trials in remote locations for central analysis during clinical trials, but have now been shown to stabilise several human leukocyte antigens [47–49]. We are developing protocols for the use of these reagents with bovine and ovine blood to stabilise samples for several days and enable subsequent flow cytometry analysis of platelet and leukocyte parameters (in submission).

4. Conclusion

Assessment of red blood cell damage through measurement of plasma free haemoglobin is a key assay required by regulatory bodies in the development of new blood-handling devices. However, more sophisticated flow cytometry screening methods that enable evaluation of a wider array of blood cell types and blood borne proteins could be used in combination with other design tools to inform iterative design improvements. Such an approach would enable device developers to progress new designs that have minimal total blood trauma, and ultimately put safer devices on the market. The use of multiparametric flow cytometry in the design cycle and clinical use of medical devices that contact blood is in its infancy. Clearly, there are many advantages to such an approach. The key advantage is the ability to analyse the phenotype of multiple haematopoietic cell populations simultaneously in small volumes of blood. Such methodology would enable the same analysis protocols to be used at all stages of design and implementation: in vitro studies, pre-clinical studies in different animal species, and then in clinical studies once devices are implanted in humans. Multiparametric flow cytometry also enables the incorporation of functional outputs such as cell viability, apoptosis, reactive oxygen species (ROS) production and cytokine production. These are critical if the impact of device-associated biomaterials and shear stress on haematopoietic cells is to be determined; there might not be phenotypic changes but cell function might be affected dramatically. The main challenges to implementing multiparametric flow cytometry in this setting relate to the availability of reagents that are truly multi-species and enable a single methodological approach to be used across the device development life cycle. This is more challenging when it comes to cell phenotyping that typically requires antibodies to specific cell surface markers but easier to implement for functional assays related to cell viability/apoptosis and measures such as ROS. Other challenges relate to flow cytometer availability to the research and development team as that will dictate fluorochrome choice and assay design. Also, data analysis becomes demanding as the number of parameters studied simultaneously increases and machine learning approaches need to be developed alongside development of multiparameter strategies. Rapid advances in fluorochrome technology and the development of mass cytometry facilitate a multiparametric approach but there remain limitations in fluorochrome choices for reagents targeting surface markers and cytokines of cells from animal species such as cows, pigs and sheep. Demand for these reagents will drive their availability but this demand will only occur if the device development community adopt standardised approaches. Underpinning this would be a requirement from regulatory bodies for flow cytometry-based analysis of cell health and function as part of the development and evaluation of blood handling medical devices.

Conflict of interest

Ina Laura Pieper is a past employee of Calon Cardio-Technology Ltd., and a current employee and shareholder of Scandinavian Real Heart AB. Gemma Radley is an employee of Calon Cardio-Technology Ltd. Catherine A Thornton has no conflicts of interest.

Author details

Ina Laura Pieper[1,2]*, Gemma Radley[1,3] and Catherine A. Thornton[1]

*Address all correspondence to: i.l.pieper@swansea.ac.uk

1 Swansea University Medical School, Institute of Life Science, Swansea, UK

2 Scandinavian Real Heart AB, Västerås, Sweden

3 Calon Cardio-Technology Ltd, Institute of Life Science, Swansea, UK

References

[1] Krabatsch T et al. Heartmate 3 fully magnetically levitated left ventricular assist device for the treatment of advanced heart failure—1 year results from the Ce mark trial. Journal of Cardiothoracic Surgery. 2017;**12**(1):23

[2] Nascimbene A et al. Association between cell-derived microparticles and adverse events in patients with nonpulsatile left ventricular assist devices. The Journal of Heart and Lung Transplantation. 2014;**33**(5):470-477

[3] Sansone R et al. Macrovascular and microvascular function after implantation of left ventricular assist devices in end-stage heart failure: Role of microparticles. The Journal of Heart and Lung Transplantation. 2015;**34**(7):921-932

[4] Woolley JR et al. Temporal leukocyte numbers and granulocyte activation in pulsatile and rotary ventricular assist device patients. Artificial Organs. 2014;**38**(6):447-455

[5] Woolley JR et al. Temporal leukocyte numbers and granulocyte activation in pulsatile and rotary ventricular assist device patients. Artificial Organs. 2013

[6] Gasser O et al. Characterisation and properties of ectosomes released by human polymorphonuclear neutrophils. Experimental Cell Research. 2003;**285**(2):243-257

[7] Dalli J et al. Heterogeneity in neutrophil microparticles reveals distinct proteome and functional properties. Molecular & Cellular Proteomics. 2013;**12**(8):2205-2219

[8] Pluskota E et al. Expression, activation, and function of integrin αMβ2 (Mac-1) on neutrophil-derived microparticles. Blood. 2008;**112**(6):2327-2335

[9] Diehl P et al. Enhanced microparticles in ventricular assist device patients predict platelet, leukocyte and endothelial cell activation. Interactive Cardiovascular and Thoracic Surgery. 2010;**11**(2):133-137

[10] Wilhelm CR et al. Monocyte tissue factor expression and ongoing complement generation in ventricular assist device patients. The Annals of Thoracic Surgery. 1998;**65**(4):1071-1076

[11] Wilhelm CR et al. Measurement of hemostatic indexes in conjunction with transcranial Doppler sonography in patients with ventricular assist devices. Stroke. 1999;**30**(12):2554-2561

[12] Shantsila E, Lip GY. The role of monocytes in thrombotic disorders. Insights from tissue factor, monocyte-platelet aggregates and novel mechanisms. Thrombosis and Haemostasis. 2009;**102**(5):916-924

[13] Mondal NK et al. Infection, oxidative stress, and changes in circulating regulatory T cells of heart failure patients supported by continuous-flow ventricular assist devices. ASAIO Journal. 2017;**63**(2):128-133

[14] Ankersmit HJ et al. Quantitative changes in T-cell populations after left ventricular assist device implantation: Relationship to T-cell apoptosis and soluble CD95. Circulation. 1999;**100**(19 Suppl):II211-II215

[15] Ankersmit HJ et al. Activation-induced T-cell death and immune dysfunction after implantation of left-ventricular assist device. Lancet. 1999;**354**(9178):550-555

[16] Dewald O et al. Platelet activation markers in patients with heart assist device. Artificial Organs. 2005;**29**(4):292-299

[17] Matsubayashi H, Fastenau DR, McIntyre JA. Changes in platelet activation associated with left ventricular assist system placement. The Journal of Heart and Lung Transplantation. 2000;**19**(5):462-468

[18] Mondal NK et al. Intraplatelet reactive oxygen species, mitochondrial damage and platelet apoptosis augment non-surgical bleeding in heart failure patients supported by continuous-flow left ventricular assist device. Platelets. 2015;**26**(6):536-544

[19] Mondal NK et al. Oxidative stress induced modulation of platelet integrin alpha2bbeta3 expression and shedding may predict the risk of major bleeding in heart failure patients supported by continuous flow left ventricular assist devices. Thrombosis Research. 2017;**158**:140-148

[20] Mondal, Nandan K, et al. Mechanistic insight of platelet apoptosis leading to non-surgical bleeding among heart failure patients supported by continuous-flow left ventricular assist devices. Molecular and cellular biochemistry 2017;433(1-2):125-137

[21] Snyder TA et al. Leukocyte-platelet aggregates and monocyte tissue factor expression in bovines implanted with ventricular assist devices. Artificial Organs. 2007;**31**(2):126-131

[22] Carson SD, Bach R, Carson SM. Monoclonal antibodies against bovine tissue factor, which block interaction with factor VIIa. Blood. 1985;**66**(1):152-156

[23] Baker LC et al. Flow cytometric assays to detect platelet activation and aggregation in device-implanted calves. Journal of Biomedical Materials Research. 1998;**41**(2):312-321

[24] Snyder TA et al. Platelet activation, aggregation, and life span in calves implanted with axial flow ventricular assist devices. The Annals of Thoracic Surgery. 2002;**73**(6):1933-1938

[25] Snyder TA et al. Preclinical biocompatibility assessment of the EVAHEART ventricular assist device: Coating comparison and platelet activation. Journal of Biomedical Materials Research. Part A. 2007;**81**(1):85-92

[26] Johnson CA Jr et al. Biocompatibility assessment of the first generation PediaFlow pediatric ventricular assist device. Artificial Organs. 2011;**35**(1):9-21

[27] Johnson CA Jr et al. Platelet activation after implantation of the Levitronix PediVAS in the ovine model. ASAIO Journal. 2011;**57**(6):516-521

[28] Johnson CA Jr et al. Platelet activation in ovines undergoing sham surgery or implant of the second generation PediaFlow pediatric ventricular assist device. Artificial Organs. 2011;**35**(6):602-613

[29] Chan CH et al. The evaluation of leukocytes in response to the in vitro testing of ventricular assist devices. Artificial Organs. 2013;**37**(9):793-801

[30] Chan CH et al. The CentriMag centrifugal blood pump as a benchmark for in vitro testing of hemocompatibility in implantable ventricular assist devices. Artificial Organs. 2015;**39**(2):93-101

[31] Pieper IL et al. Ovine leukocyte microparticles generated by the CentriMag ventricular assist device in vitro. Artificial Organs

[32] Simmonds MJ, Meiselman HJ. Prediction of the level and duration of shear stress exposure that induces subhemolytic damage to erythrocytes. Biorheology. 2016;**53**(5-6):237-249

[33] Angelillo-Scherrer A. Leukocyte-derived microparticles in vascular homeostasis. Circulation Research. 2012;**110**(2):356-369

[34] Aass HC et al. Fluorescent particles in the antibody solution result in false TF- and CD14-positive microparticles in flow cytometric analysis. Cytometry. Part A. 2011;**79**(12):990-999

[35] Moazami N, Dembitsky WP, Adamson R. Does pulsatility matter in the era of continuous-flow blood pumps? The Journal of Heart and Lung Transplantation. 2015;**34**

[36] Crow S et al. Gastrointestinal bleeding rates in recipients of nonpulsatile and pulsatile left ventricular assist devices. The Journal of Thoracic and Cardiovascular Surgery. 2009;**137**(1):208-215

[37] Chan CH et al. The effect of shear stress on the size, structure, and function of human von Willebrand factor. Artificial Organs. 2014;**38**(9):741-750

[38] Schuster M et al. B-cell activation and allosensitization after left ventricular assist device implantation is due to T-cell activation and CD40 ligand expression. Human Immunology. 2002;**63**(3):211-220

[39] Schuster M et al. Induction of CD40 ligand expression in human T cells by biomaterials derived from left ventricular assist device surface. Transplantation Proceedings. 2001;**33**(1-2):1960-1961

[40] Walkowiak-Przybylo M et al. Adhesion, activation, and aggregation of blood platelets and biofilm formation on the surfaces of titanium alloys Ti_6Al_4V and Ti_6Al_7Nb. Journal of Biomedical Materials Research. Part A. 2012;**100(**(3):768-775

[41] Chang X, Gorbet M. The effect of shear on in vitro platelet and leukocyte material-induced activation. Journal of Biomaterials Applications. 2013;**28**(3):407-415

[42] Tabit CE et al. Tumor necrosis factor-alpha levels and non-surgical bleeding in continuous-flow left ventricular assist devices. The Journal of Heart and Lung Transplantation. 2018; **37**(1):107-115

[43] Rodriguez-Caballero A et al. A new simple whole blood flow cytometry-based method for simultaneous identification of activated cells and quantitative evaluation of cytokines released during activation. Laboratory Investigation. 2004;**84**(10):1387-1398

[44] Chan CH et al. Shear stress-induced total blood trauma in multiple species. Artificial Organs. 2017;**41**(10):934-947

[45] Johnson CA Jr et al. Flow cytometric assays for quantifying activated ovine platelets. Artificial Organs. 2008;**32**(2):136-145

[46] Pieper IL et al. Quantification methods for human and large animal leukocytes using DNA dyes by flow cytometry. Cytometry. Part A. 2016:565-574

[47] Warrino DE et al. Stabilization of white blood cells and immunologic markers for extended analysis using flow cytometry. Journal of Immunological Methods. 2005;**305**(2):107-119

[48] Schumacher A. Effect of ex vivo storage and Cyto-Chex on the expression of P-selectin glycoprotein ligand-1 (PSGL-1) on human peripheral leukocytes. Journal of Immunological Methods. 2007;**323**(1):24-30

[49] Saxton JM, Pockley AG. Effect of ex vivo storage on human peripheral blood neutrophil expression of CD11b and the stabilizing effects of Cyto-Chex. Journal of Immunological Methods. 1998;**214**(1-2):11-17

Chapter 5

Efficient Interpretation of Multiparametric Data Using Principal Component Analysis as an Example of Quality Assessment of Microalgae

Toshiyuki Takahashi

Additional information is available at the end of the chapter

http://dx.doi.org/10.5772/intechopen.71460

Abstract

Multiparametric flow cytometry (FCM) realizes high-throughput measurement, but multiparametric data make it difficult to interpret the complicated information. To present clear patterning graphs from FCM data, one must grasp the essence of the data. This study estimated the usefulness of principal component analysis (PCA), which reduces multidimensional information to arbitrary one-dimensional information. Recently, microalgae have attracted the attention of pharmaceutical, cosmetic, and food companies. Taking alga *Chlorella* as an example, this chapter presents the usefulness of PCA for the evaluation of algal quality using FCM. To evaluate the algal status effectively, *Chlorella* (control), heated algae, and metallic-treatment algae were prepared and quantified using FCM. FCM data were subjected to PCA analysis. To interpret correlativity among parameters, FCM data are generally expressed as histograms and scatter or contour plots. An operator using multiple parameters has difficulty finding high correlativity among parameters and presenting an effective graph. The PCA method produced new comprehensive axes with different inclination factors among parameters. Scatter plots using new axes showed patterns treatment dependently with different vectors. Results show that the PCA method can extract information of test objects from data and that it can contribute to effective interpretation of cell characteristics, even if data include multiparameters from FCM.

Keywords: flow cytometry, multivariable analysis, cell status, cell cycle, *Chlorella*, chlorophyll, trace metal elements, slag

1. Introduction

Flow cytometry (FCM) can provide cell optical information from microbes to model animal and plant cells. Over the last several decades, FCM with those fundamental characteristics has

served as a powerful and invaluable tool in fields such as cell biology, microbiology, protein engineering, and health care [1]. Actually, FCM has functions to conduct several procedures such as cell counting, biomarker detection, cell cycle analysis, and cell sorting. Clear patterning graphs from FCM data can elucidate correlation among several parameters. Recent FCM systems enable a user to analyze up to a dozen multiparameters including scattered light parameters in a single assay [2]. In fact, multiparametric detection realizes high-throughput measurement and cost-performance and is also time-saving of experiments in life science. For instance, ten combined experiments must be conducted when one examines five parameters of interest using several designed FCM experiments with three-color fluorophores (designated as three-color FCM). By contrast, when using a designed FCM experiment with five-color fluorophores (five-color FCM), correlation between the five parameters can be examined from only one experiment, in principle. Generally, the number of combined experiments is calculable using Pascal's triangle (**Figure 1**).

However, the number of available colors used in each experiment is restricted in conjunction with both numbers of excitation lasers and corresponding emission filters used in an instrument. **Figure 2** portrays excitation and emission spectra of representative fluorophores, as examined using online software (SpectraViewer; thermo Fisher Scientific Inc.). When only a single blue laser operating at 488 nm is used for multicolor FCM, the emission spectra of fluorophores shown in **Figure 2** resemble those in **Figure 3**. Several areas of overlapping of

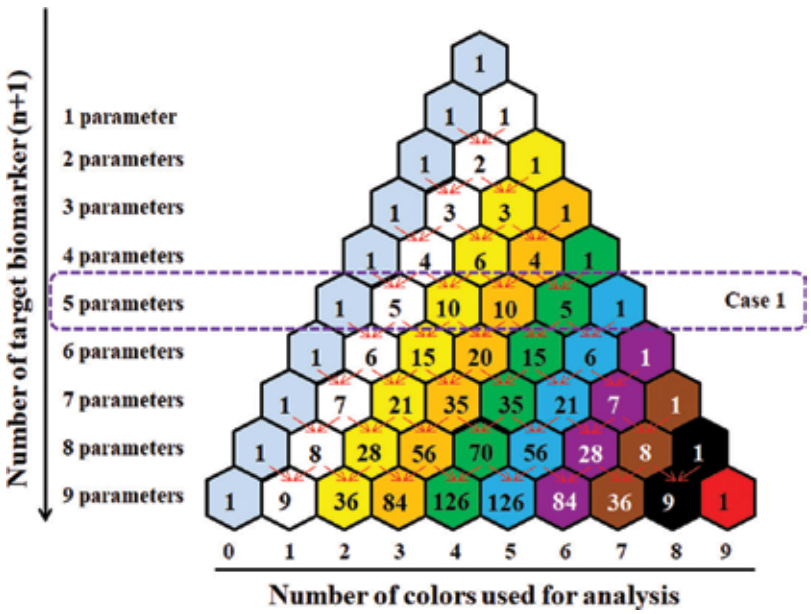

Figure 1. Correlation between the number of target parameters and that of colors used in an experiment, as shown by the Pascal's triangle. Ten combined experiments must be conducted to measure five parameters of interest using two-color FCMs for case 1 of **Figure 1**, although a system using four-color FCMs requires only five combined experiments to measure them. It is noteworthy that an experiment using just one-color FMC cannot examine any correlation between target parameters except for scattered light parameters. Multicolor FCM (more than two-color FCM) must be used to find correlation between parameters.

http://dx.doi.org/10.5772/intechopen.71460

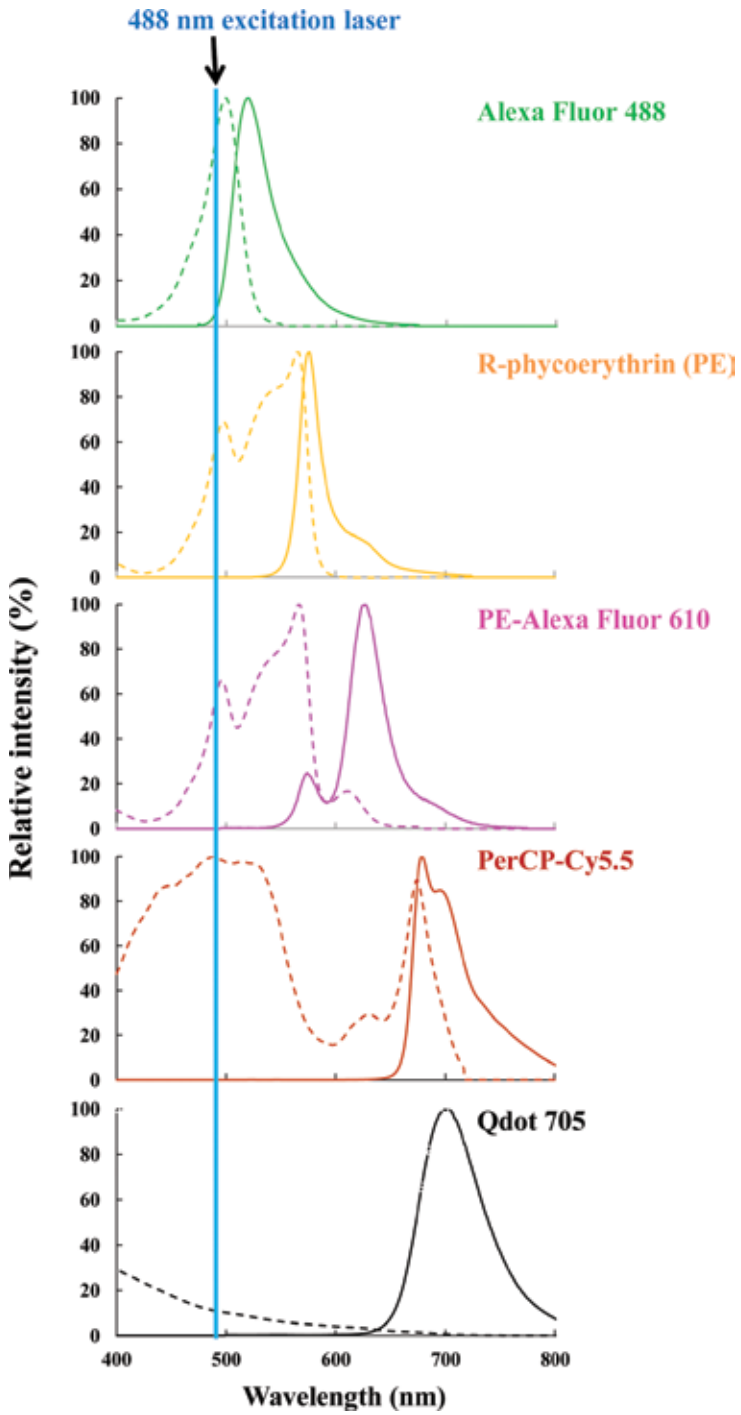

Figure 2. Fluorescence properties of representative fluorophores examined using online software (SpectraViewer; thermo Fisher Scientific Inc.). Dotted lines and solid lines respectively show the excitation spectrum and emission spectrum of each fluorophore. A vertical blue line signifying 488 nm as an example is included in each graph.

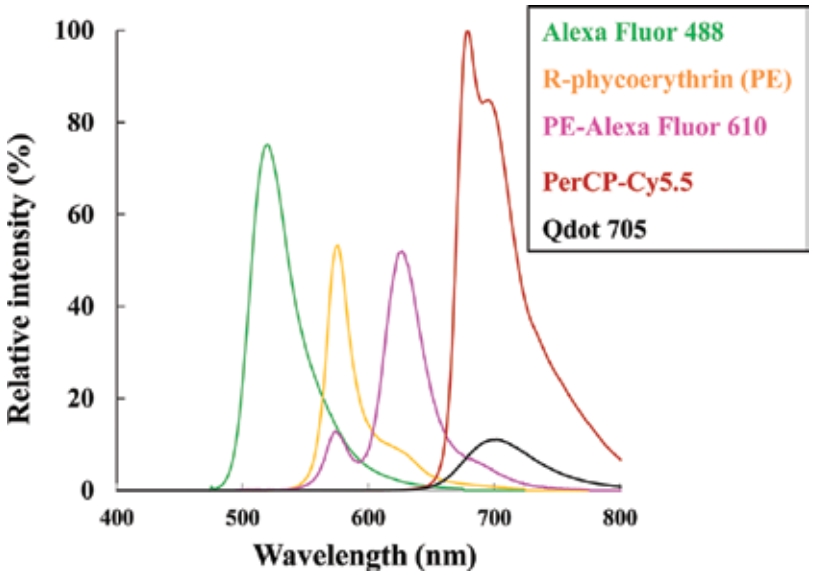

Figure 3. Fluorescence properties of representative fluorophores excited using a blue laser operating at 488 nm as an example. The graph reflects differences in the excitation intensity of each fluorophore excited using a blue laser. Here, the emission intensity of each fluorophore was calculated from each excitation spectrum in **Figure 2**.

emission spectra occur because the spectra of some fluorophores are flared at the bottom. Along with overlapping of emissions, differences of excitation efficiency might present simultaneous difficulties for multicolor FCM analysis (**Figure 3**). Using a flow cytometer detecting two colors to five colors per single laser, even when using a more high-end instrument than that described above, one must commonly discuss and interpret correlation between multiparameters based on several combined results. Just to be sure, all fluorophores excited by an arbitrary single laser does not necessarily work together because of differences in the emission efficiency of each fluorophore.

In contrast to the benefits of multiparametric FCM, multiparametric data make it difficult to get rid of extraneous data and reach an interpretation of the complicated information. Although one can make multi-dimensional graphs digitally, it is not easy to reach an accurate and clear conclusion from any multi-dimensional graph. To present clear patterning graphs from complicated FCM data, an analyst must be able to grasp the essence of the data.

To extract the essence of FCM data, this study applied principal component analysis (PCA) for multivariate analysis to the complicated FCM data and estimated the usefulness of the PCA method. Recently, some microalgae have already generated a lot of attention from pharmaceutical developers, cosmetic manufacturers, and food companies. The industrial application of algae demands the assessment of their qualities in culture. Taking green alga *Chlorella* sp. as an example and as a convenient organism for FCM, this study presents the usability of PCA method for the assessment of algal quality using FCM.

2. FCM analysis of microalgae

In addition to the numerous but unappreciated roles of phytoplankton, including microalgae, in aquatic ecosystems to support yields of fish and shellfish, several microalgae have also attracted attention from several pharmaceutical and vitamin supplement developers, along with food companies [3, 4]. Biotechnologies are sometimes classified into colors based on their respective research areas: red biotechnologies are related to medicine and medical processes. White ones are associated with industrial processes including production of chemicals [3] and biofuels [5]. Gray ones are directly related to the environment. Green ones are connected to agricultural processes including environmentally friendly solutions as alternatives to traditional processes [3, 4, 6, 7]. Blue technologies are related to marine and aquatic processes. Finally, black ones are used to develop bioterrorism. Microalgal applications have the potential to be related to most of those biotechnologies. Autotrophic algal biorefineries, for instance, can present great advantages over conventional refineries that manufacture materials using fossil fuels and over conventional microbial biorefineries that use fermentation, which requires food nutrients for microbes.

The industrial application of algae demands the selection of useful algal species, the evaluation of algal features, and the assessment of their qualities in culture [4]. The algal quality demanded is particularly important because microalgal metabolisms are strongly affected by even trace levels in the concentration of various organic and inorganic pollutants such as heavy metals [1, 8]. When assessing algal quality in culture and using those algae in industrial application, analyzing their life (cell) cycle is a crucially important technique. Cell cycle analysis using FCM is a standard procedure in versatile application of FCM. Considering the cell size of microalgae, unicellular algae such as *Chlorella* sp. are convenient model organisms for microalgal studies using FCM [9].

Algae have chlorophyll as an endogenous fluorescent biomolecule (**Figure 4A** and **B**). FCM in analogy with spectrofluorometry can pick up the chlorophyll fluorescence of algae and can evaluate some properties including chlorophyll and scattered light signals of an individual alga [9–15]. **Figure 4A–C** portrays *Chlorella*-like alga and its fluorescence properties. The wavelength of the maximal fluorescence near 680 nm is from algal chlorophyll (solid curve in **Figure 4C**). Algae are sensitive to heat treatment (dotted curve in **Figure 4C**) [11–14] because the thermal stress damages the thylakoid membrane, which is related to structural and functional changes of the photosystem (PS) II and PS I, thereby interrupting the Calvin cycle [16, 17]. Inducing heat stress in algae reduces chlorophyll fluorescence (dotted curve in **Figure 4C**) and increases yellow fluorescence derived from chlorophyll degradation [11]. Consequently, red fluorescence can indicate vigorous algae, whereas yellow fluorescence indicates stressed and dying algae [11–14]. **Figure 4D** takes a dotted graph from FCM data using a *Chlorella*-like alga (SA-1 strain) to present an example. Both the cell size detected as forward scatter signals (FSS) and chlorophyll contents of algae as red fluorescence channel are correlated strongly with the algal cell cycle [9, 10, 15, 18]. Here, algae are categorized into three populations (Stages 1–3) as described in reports of previous studies [9, 10, 15, 18]: Stage (St.) 1, "growth" stage; St. 2, "maturation" stage; and St. 3, "division and autospore liberation" stage in **Figure 4D**.

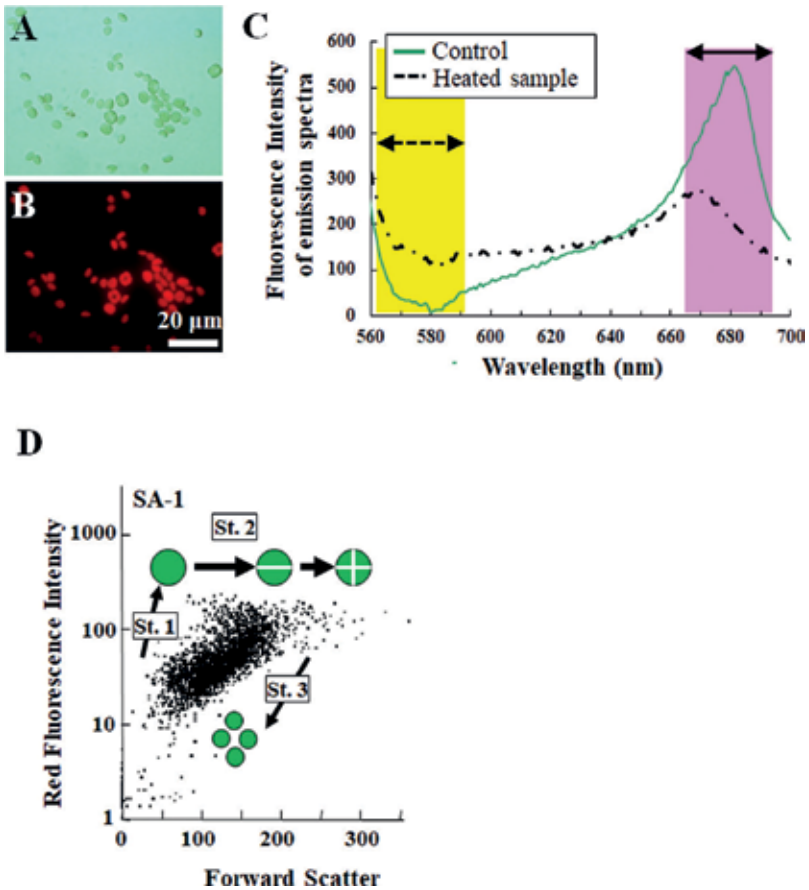

Figure 4. Fluorescence characteristics of algae and microphotographs of *Chlorella*-like alga experimentally isolated from ciliate *Paramecium bursaria*. A bright field image of *Chlorella*-like alga (A) and the corresponding fluorescence image derived from chlorophyll (B) are shown. Panel C presents fluorescence characteristics of *Chlorella*-like alga obtained using fluorescence spectroscopy. Emission spectra of algae are shown with (dotted line, heated algae) and without heat treatment (solid line, control algae). Yellow (dotted arrow) and pink (solid arrow) areas, respectively, represent detection ranges of yellow and red fluorescence channels for FCM used for this study (see *Research methods*). Panels A-D were referred and partly modified from the literature [1, 13, 15, 18].

3. Research methods

This study investigated the algal status such as viability using FCM after treatment of algae with the test condition. For this study, the author used *Parachlorella kessleri* (C-531 strain) (new nomenclature for *Chlorella kessleri*) as the model organism representing algae. The alga was obtained from the Institute of Applied Microbiology (IAM) culture collection at The University of Tokyo. Before experiments, algae were grown on CA agar plates at pH 7.2 [19] under an LD cycle (12 h light/12 h dark) at approximately 1100 lux of natural white fluorescent light and 23 ± 2°C. The algae were scratched with an inoculating needle and were suspended in fresh CA liquid medium at pH 7.2.

Chlorella (initial density of 1.0×10^4 cells/ml adjusted using hemocytometry) grown in CA medium as a control condition for 1 week under an LD cycle and algae treated with metal eluate for 1 week as a test condition were prepared, respectively, as described in earlier reports [1, 12, 14]. Moreover, algae treated with heat for 5 min at 100°C were prepared. Here, the test conditions were reference standards subjected, respectively, to metallic eluate from steelmaking by-products and heat stress. A detailed description of the metal eluate reveals that the metal eluate was made from stainless steel slag (**Table 1**) subjected to a leaching test based on JIS K0058-1: 2005 (method for chemicals in slags Part 1: Leaching test) [12, 14, 20–23]. **Table 1** presents compositions of stainless steel slag particles used for this study [12, 14, 20–22]. In brief, slag used for this study mainly contains SiO_2, CaO, Al_2O_3, MgO, MnO, and Cr_2O_3 [12, 14]. Here, all Fe and Cr compounds are described, respectively, as FeO or Cr_2O_3 because it is generally difficult to distinguish FeO and Cr_2O_3 formed from Fe and Cr in a suspended metal solution at the occasion of elemental analysis after alkali fusion of stainless steel slag [1, 12, 14].

After elution from slag at pH 6 adjusted with HCl, the solution was filtrated with a 0.45 μm pore filter to eliminate slag particles. Then the solution was used for bioassay with *Chlorella* as a test solution including trace metals. **Table 2**, which shows components of the metal eluate used for this study, includes environmental quality standards for soil pollution, marine pollution, and water pollution, along with other standards for eluent and drinking water for reference. In this study, CA medium containing eluates was first made from 25 vol% of the concentrated CA medium, which had four times that amounts of respective chemicals for making CA medium, and 75 vol% of mixture of arbitrary amounts of eluate, a definite number of algae (1.0×10^4 cells/ml), and ultrapure water. Therefore, nutrient amounts of CA medium containing eluates were the same as those of CA medium alone, but the concentrations of chemicals derived from eluate differed from those of CA medium without eluate as described in reports of earlier studies [1, 12, 14].

To characterize each algal sample using FCM, this study used a cell analyzer (Muse™; Merck Millipore Corp., Hayward, CA) with a green laser operating at 532 nm as an excitation light source, a photodiode for detection of FSS, and two fluorescence filters of a 680/30 nm band pass (BP) filter suitable for chlorophyll fluorescence (red fluorescence) and a 576/28 nm BP filter suitable for chlorophyll degradation (yellow fluorescence) (**Figure 4C**) [1, 11, 12, 14].

This study was undertaken to evaluate the correlativity between algal properties and the test condition. To evaluate the correlativity among multiple properties of algae and each stress factor, PCA of multivariate analysis was used for this study using software for multivariate analysis (Institute of Statistical Analyses, Inc.). A dimensional reduction technique, PCA, reduces multi-dimensional information to arbitrary one-dimensional information, which is a

	FeO	**SiO_2**	**CaO**	**Al_2O_3**	**MgO**	**MnO**	**Cr_2O_3**	**ZnO**	**NiO**	**CuO**
Slag A	0.74	44.1	33	5.39	7.68	4.09	3.29	0.01	0.06	0.024

Table 1. Chemical compositions of steel slag used for this study (mass%) referred from the literature [1, 12–14].

Origin of slag		Eluate of stainless steel slag	Environmental quality standards				
			Soil pollution	Marine pollution	Water pollutant	Effluent standard	Drinking water standard
Regulated substances	Total As	ND[1] (RDL[2]: 0.001)	0.01	0.1	0.01	0.1	0.01
	Total B	0.16	1		1[4]	10[4], 230[5]	1
	Total Be	ND (RDL: 0.0005)		2.5			
	Total Cd	ND (RDL: 0.0001)	0.01	0.1	0.01	0.03[6]	0.003
	Chromium (VI)	ND (RDL: 0.005)	0.05	0.5	0.05	0.5	0.05
	Total Cu	0.003	0.001	3		3	1
	Total Pb	ND (RDL: 0.0005)	0.01	0.1	0.01	0.1	0.01
	Hg	ND (RDL: 0.0001)	0.0005	0.005	0.0005	0.005	0.0005
	Total Ni	0.001	0.001	1.2			0.02
	Total Se	0.012	0.01	0.1	0.01	0.1	0.01
	Total V	ND (RDL: 0.001)		1.5			
	Total Zn	0.099		2	0.03[7], 0.02[8], 0.01[9]	2	1
	F^-	ND (RDL: 0.1)	0.8	15	0.8[4]	8[4], 15[5]	0.8
Substances out of regulation	Total Al	ND					
	Total Ca	9.3					300[10]
	Total Fe	ND				10	0.3
	Total Mg	0.9					300[10]
	Total Mn	0.028				10	0.05
	Total Si	1.8					
	Total N	0.4			0.1–1[11] 0.2–1[8]	100	0.04[12], 10[13]
	Total P	ND (RDL: 0.1)			0.005–1[11] 0.02–0.09[8]	16	

[1]Not detected.

[2]Reportable detection limit.

[3]These data from a previous study reported by Takahashi et al. [17].

[4]Standard value is not applied to coastal waters.

[5]Standard value is applied to coastal waters.

[6]The Cd value has changed from 0.1 to 0.03 mg/L since December 2014.

[7]Habitable river or lake for aquatic life.

[8]Habitable coastal water for aquatic life

[9]Habitable coastal water that requires conservation in particular for nidus and nursery ground.

[10]Total concentrations of both calcium and magnesium are limited for water hardness.

[11]Habitable lake for aquatic life.

[12]Total N contents derived from nitrite nitrogen.

[13]Total N contents derived from both nitrite nitrogen and nitrate nitrogen.

Table 2. Environmental quality standards regarding pollutions and others for effluent and drinking water, and concentrations of elements of eluate (mg/L) referred from the literature [1, 12–14].

dataset from a new axis produced by PCA [15]. According to results of the correlation matrix analysis for the data, the author calculated the contribution rate of each component, the factor loading of each parameter, and the score plot of each component. Here, each factor loading (PC1-3) generally indicates correlation factors between each parameter and each component (**Figure 5**). The statistical results obtained using PCA were interpreted to evaluate the algal status between control and test conditions.

After treatment of algae with and without eluate, the algae were quantified using hemocytometry. Here, CA medium containing several concentrations (0–70 vol%) of the metallic eluate was used for the experiment using hemocytometry. The algal proliferation ratio (average ± standard error) was expressed as a proportion of the number of algae treated with eluate to that of control without eluate [1, 12, 14].

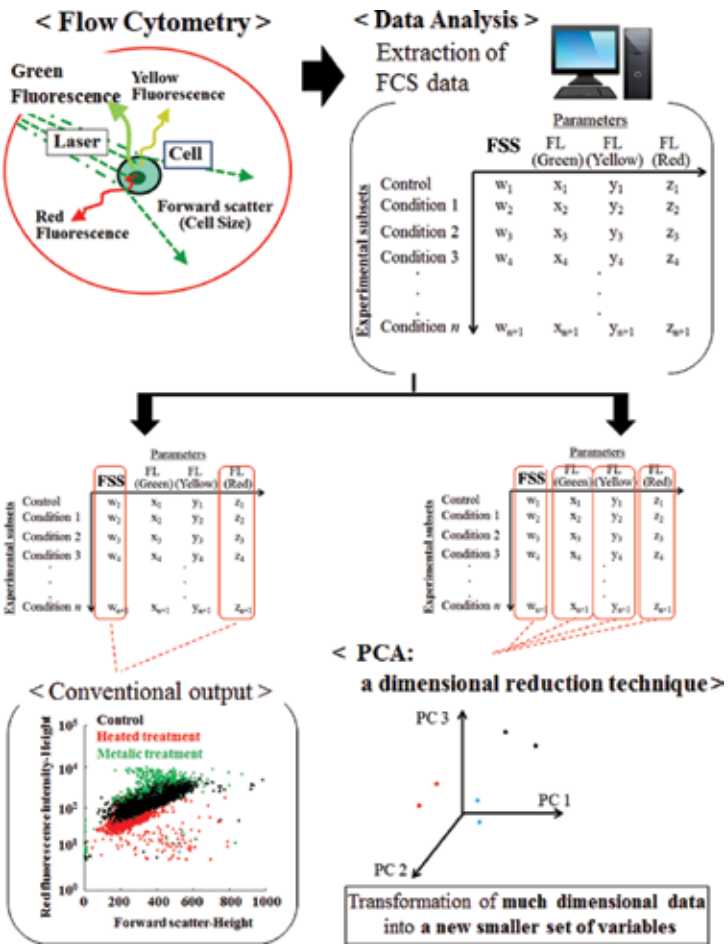

Figure 5. Outline from FCM analysis to PCA analysis of multivariate analysis. All data from FCM were extracted and subjected to PCA. Only one or two parameters are used to produce a one-dimensional (1D) histogram and 2D scatter or contour plots in conventional FCM analysis. These graphs, however, ignore some parameters of data (left below in **Figure 5**). To incorporate all information of the data, PCA transforms multi-dimensional data into a new smaller set of variables (right below in **Figure 5**).

4. Results and discussion

This study compared the effects of metallic eluate from stainless steel slag and heat treatment as an experimental stress factor on algal status, specifically that of *Chlorella* sp. [1, 12–14]. Here, CA medium containing 50 vol% of the metallic eluate was used for FCM analysis. To interpret correlativity among several parameters, FCM data are generally expressed as a 1D histogram and 2D scatter or contour plots. The more parameters an operator uses, the more difficult it becomes for the user to find high correlativity among parameters and to present an effective graph. The PCA method produced new comprehensive axes including several parameters, which have different inclination factors among parameters. The primary (PC1) and secondary (PC2) and tertiary (PC3) components, respectively, reflect 53.4, 34, and 12.6% of information for the data examined in this study (data not shown). **Figure 6A** and **B** presents the principal component loading of PC1 and PC2. Each loading shows that all parameters, including the algal size (FSS-H), red fluorescence intensity (Red-H), and yellow fluorescence (Yellow-H), are positively correlated with PC1 (**Figure 6A**). Particularly, correlation factors for both the algal size and the red fluorescence intensity were more strongly positive with PC1 than the yellow fluorescence intensity was. By contrast, the red fluorescence intensity and the yellow fluorescence intensity, respectively, show inverse and positive correlation with PC2 (**Figure 6B**). The 2D scatter plots using new axes show patterns with individually different vectors treatment dependently, as expressed by the score plot of PC1 versus PC2 (**Figure 6C**). The graph using new axes from PCA helps us to infer strong correlation between a particular parameter and the corresponding one. Consequently, the characteristics of both algal size and red fluorescence intensity are mainly reflected as the variation of algae on the positive PC1 axis (**Figure 6A** and **C**), whereas only yellow fluorescence mainly affected the variation of algae on the positive PC2 axis (**Figure 6B** and **C**). Results show that both the cell size (or red fluorescence intensity) and yellow fluorescence intensity of algae can be indicators that facilitate assessment of the variation for comparison of algae between control and heat treatment (**Figure 6C**), whereas both the cell size and red fluorescence can be indicators for comparison of algae between control and the metallic treatment (**Figure 6D**).

The results (**Figure 6**) from PCA analysis prompted us to produce plots of FSS or the red fluorescence for algae versus the yellow fluorescence intensity for algae (**Figure 7**). The 2D-dotted graph of the red versus yellow fluorescence intensity for control algae, for instance, showed 10^2–10^3 on the red channel and 10^1–10^2 on the yellow, whereas that for the heated algae showed 10^1–10^2 on the red channel and 10^1–10^3 on the yellow. By contrast to the heat treatment, the dot distribution of algae treated with metallic eluate closely resembled that of control, although that with the eluate shifted slightly upward relative to that of control algae [1, 12–14]. In analogy with the result (**Figure 6C**) from PCA analysis, the difference of algae between the control condition and metallic treatment is slight compared to the difference of algae between control and heat stress (**Figure 7**).

To conduct a precise comparison of algae of control and metallic treatments, the plot of FSS versus red fluorescence for algae was produced (**Figure 8**). Although the dot distribution

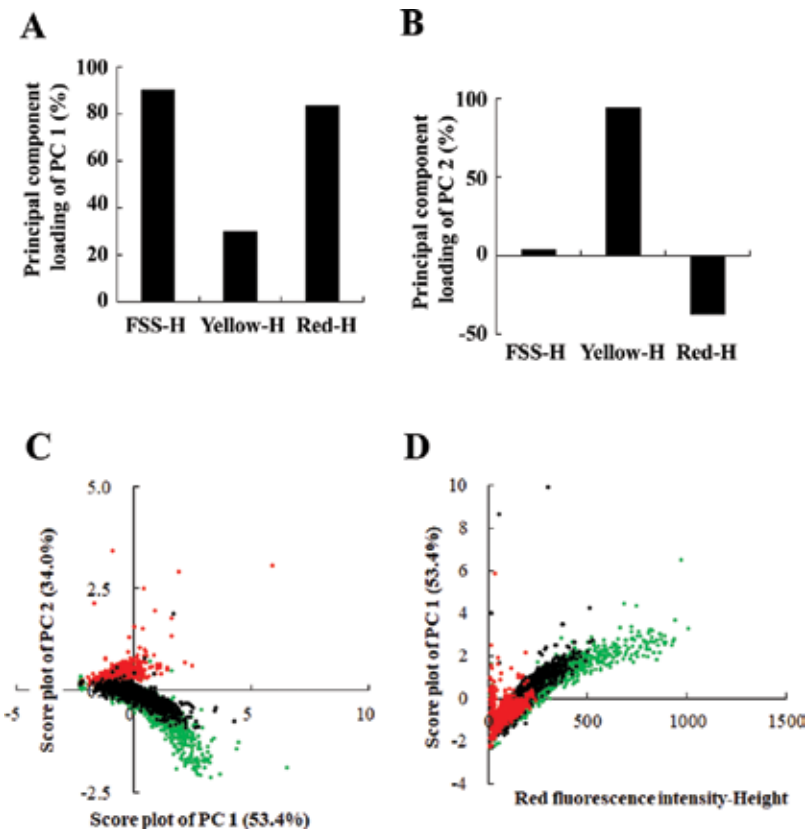

Figure 6. Condition-dependent distribution of *Chlorella* obtained using PCA method. The PCA reduces multi-dimensional information to arbitrary one-dimensional information and produces new components such as PC1–PC3. Here, factor loading plots of each parameter for PC1 (A) and PC2 (B) are shown. A score plot of PC1 vs. PC2 (C) and that of PC1 vs. red fluorescence intensity of algae (D) were produced using data from different test conditions.

of algal signals between the control and the metallic treatment was almost identical to that of the graph of the red versus the yellow fluorescence (**Figure 7**), both distributions differed on the graph of FSS versus the red fluorescence (**Figure 8**). A distinctive population (arrow in **Figure 8**) was found from algae treated only with metal eluate but not control. Drawing on the result from algal life (cell) cycle (**Figure 4D**), detection of the distinctive population in algae treated with metal eluate indicates that the algal cell cycle proceeds smoothly under the condition with metal eluate. By contrast to algae treated with metal eluate, the cell cycle of control algae seems to reach a stable stage such as a stationary phase, resulting in the near cessation of algal proliferation or extremely low proliferation activity.

In addition to estimation of algal population dynamics using FCM coupled with PCA analysis, direct quantification of algae using hemocytometry was conducted as described in earlier reports [1, 12–14]. The quantification specifically examined whether algal growth dynamics implied from the result of PCA analysis (**Figure 8**) was confirmed on algae

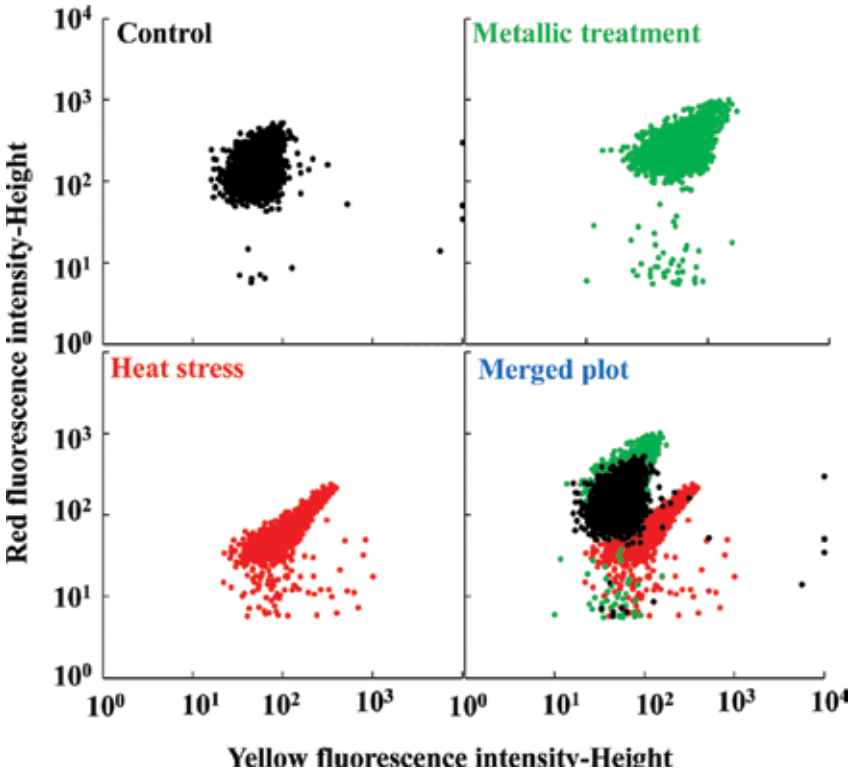

Figure 7. Distribution of *Chlorella* obtained using FCM on a graph of the red fluorescence intensity vs. the yellow fluorescence intensity, modified from the literature [1, 12–14]. The heat stress and the metallic treatment samples, respectively, derive from algae treated with heat and algae treated with a metallic solution containing concentrations of eluate of 50 vol%.

treated with metallic eluate. **Figure 9** shows the relation between the *Chlorella* proliferation ratio and the concentrations of the metallic eluate from steel slag in the test solution. As described in the explanation of research methods, all nutrient amounts derived from the CA medium, other than elements derived from slag eluate, were constant with each experiment condition. Results show that the number of algae increased according to the concentration of eluate up to 30 vol% (**Figure 9**). The algal numbers under more than 30 vol% of eluate (up to 70 vol%) were almost constant [12–14]. Reportedly, the addition of metallic eluate used for this study increases the concentration of aquatic CO_2 related to photosynthesis of algae [12–14]. The increased aquatic CO_2, which is found to be related to the presence of Ca^{2+} in eluate, might improve the rates of photosynthesis and algal proliferation [12–14].

It is noteworthy that approaches using PCA method (mainly **Figure 8**) have already exposed the effects of metallic eluate on algal growth without the proliferation test of algae treated with metallic eluate. Actually, 2–4 cells of autospore (St. 2) and algae after division (St. 3) other than algae at the growth stage (St. 1) were detected from control, whereas all types of algae at each stage (Sts. 1–3) were done from algae treated with metallic eluate (**Figure 10**).

http://dx.doi.org/10.5772/intechopen.71460

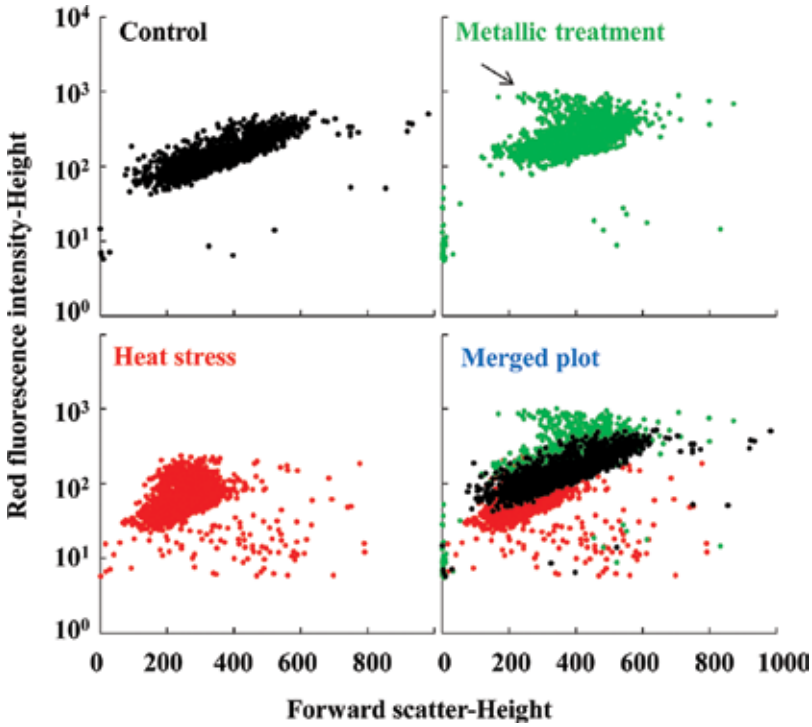

Figure 8. Distribution of *Chlorella* obtained using FCM on a graph of algal size vs. red fluorescence intensity. The heat stress and the metallic treatment samples, respectively, derive from algae treated with heat and those treated with a metallic solution containing concentrations of eluate of 50 vol%. The arrow indicates the distinctive population detected only from those treated with metallic eluate.

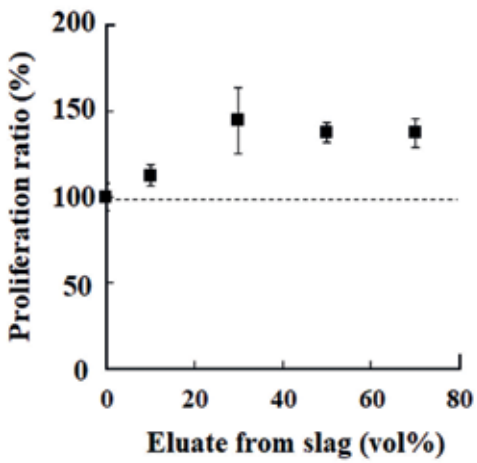

Figure 9. Effect of metallic eluate used for this study on algal growth modified from the literature [1, 12, 14]. The dotted line shows the proliferation ratio of control algae.

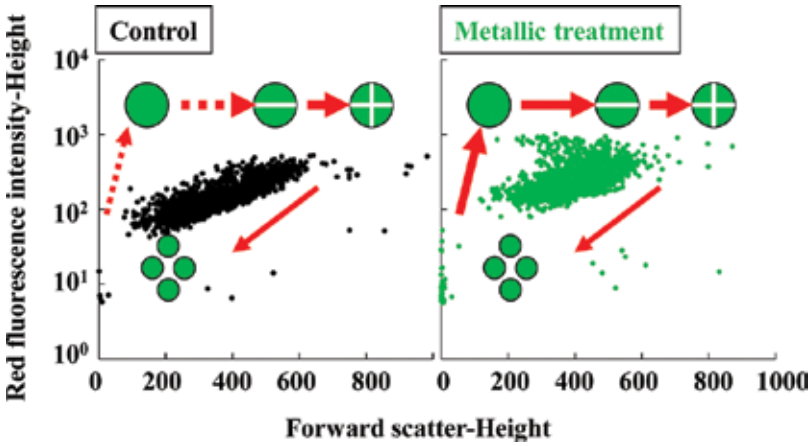

Figure 10. Effects of metallic eluate used for this study on algal growth. Here, each dotted graph in this figure is made from **Figure 8**.

Consequently, the cell cycle of algae treated with metallic eluate could continue to proceed smoothly even for algae after 7-day incubation when the control algae proliferation activity occurred at a low rate.

5. Conclusion

Multicolor FCM systems enable us to analyze up to a dozen multiparameters in a single assay and realize high-throughput measurement in life science. Countervailing the advantages of multiparametric FCM, multiparametric data make it difficult to interpret the resultant complicated information. Although multiparametric FCM is attractive relative to single or little parametric FCM in terms of cost performance and saving time of experiments, those benefits are meaningless unless the method leads to accurate and clear conclusions from multiparametric data. To elicit clear patterning graphs from FCM data and to grasp the essence of the data, this study examined the usefulness of PCA method of multivariate analysis. Comparison of control algae with several algae treated with test conditions such as heat and metallic eluate was conducted using FCM. To ascertain differences between control and test conditions about algal properties, FCM data were subjected to PCA analysis. Consequently, results from PCA analysis imply that both the red fluorescence intensity and the yellow one of algae can be an indicator for assessment of the variation for comparison of algae between control and heat treatment (**Figure 6C**), whereas both the cell size and the red fluorescence of algae can be an indicator for comparison of algae between control and metallic treatment (**Figure 6D**). It is striking that approaches coupled with PCA analysis have already exposed the effects of metallic eluate on algal growth with no proliferation test of algae. The result reveals that the low concentrations of metallic eluate used for this study induce algae to increase for a more prolonged period than in the control condition. Results show that PCA

method can extract information of test objects from data and that it can contribute to effective interpretation of cell characteristics, even if the data include several optical parameters from multiparametric FCM.

Acknowledgements

This research was mainly supported by a Grant for Young Scientists from the Iron and Steel Institute of Japan and partly by a Grant-in-Aid for Exploratory Research from Japan Society for the Promotion of Science (KAKENHI Grant Numbers 23658280 and 17 K05955).

Author details

Toshiyuki Takahashi

Address all correspondence to: mttaka@cc.miyakonojo-nct.ac.jp

Department of Chemical Science and Engineering, National Institute of Technology, Miyakonojo College, Miyakonojo, Miyazaki, Japan

References

[1] Takahashi T. Quality assessment of microalgae exposed to trace metals using flow cytometry. In: Shiomi N, Waisundara VY, editors. Superfood and Functional Food – Development of Superfood and its Role in Medicine. Croatia: InTechOpen; 2017. p. 29-45

[2] Baumgarth N, Roederer M. A practical approach to multicolor flow cytometry for immunophenotyping. Journal of Immunological Methods. 2000;**243**:77-97

[3] Spolaore P, Joannis-Cassan C, Duran E, Isambert A. Commercial applications of microalgae. Journal of Bioscience and Bioengineering. 2006;**101**:87-96. DOI: 10.1263/jbb.101.87

[4] Arashida R. Characteristics of the microalgae euglena and its applications in foods and ecological fields. The Japan Society of Photosynthesis Reserach. 2012;**22**:33-38

[5] Chisti Y. Biodeisel from microalgae. Biotechnology Advances. 2007;**25**:294-306. DOI: 10.1016/j.biotechadv.2007.02.001

[6] Mallick N. Biotechnological potential of immobilized algae for wastewater N, P and metal removal: A review. Biometals. 2002;**15**:377-390. DOI: 10.1023/A:1020238520948

[7] Hameed MSA, Ebrahim OH. Biotechnological potential uses of immobilized algae. International Journal of Agriculture and Biology. 2007;**9**:183-192

[8] Nriagu JO, Pacyna JM. Quantitative assessment of worldwide contamination of air, water and soils by trace metals. Nature. 1988;**333**:134-139. DOI: 10.1038/333134a0

[9] Gerashchenko BI, Takahashi T, Kosaka T, Hosoya H. Life cycle of unicellular algae. In: Current Protocols in Cytometry. Vol. **52**. USA: John Wiley & Sons, Inc.; 2010. p. 11.19.1-11.19.6. DOI: 10.1002/0471142956.cy1119s52

[10] Gerashchenko BI, Kosaka T, Hosoya H. Optical compartmentation of vegetating algae species as a basis for their growth-specific characterizaton. Cytometry. 2002;**48**:153-158. DOI: 10.1002/cyto.10120

[11] Takahashi T. Direct evaluation of endosymbiotic status in *Paramecium bursaria* using capillary flow cytometry. Cytometry Part A. 2014;**85**:911-914. DOI: 10.1002/cyto.a. 22562

[12] Takahashi T, Yokoyama S. Bioassay of components eluted from electric arc furnace steel slag using microalgae *Chlorella*. (in Japanese). Tetsu-to-Hagané. 2015;**101**:506-514. DOI: 10.2355/tetsutohagane.TETSU-2014-130

[13] Takahashi T. Application of phytoplankton. In: Kanematsu H, Barry DM, editors. Corrosion Control and Surface Finishing – Environmentally Friendly Approaches. Japan: Springer; 2016. p. 213-224. DOI: 10.1007/978-4-431-55957-3_19

[14] Takahashi T, Yokoyama S. Bioassay of components eluted from electric arc furnace steel slag using microalgae *Chlorella*. ISIJ International. 2016;**56**:1495-1503. DOI: 10.2355/isijinternational.ISIJINT-2015-539

[15] Takahashi T. Simultaneous evaluation of life cycle dynamics between a host paramecium and the endosymbionts of *Paramecium bursaria* using capillary flow Cytometry. Scientific Reports. 2016;**6**:31638. DOI: 10.1038/srep31638

[16] Taylor DL. The nutritional relationship of *Anemonia sulcata* (PENNANT) and its Dinofla gellate Symbiont. Journal of Cell Science. 1969;**4**:751-762

[17] Weis VM, Reynolds WS, de Boer MD, Krupp DAA. Host-symbiont specificity during onset of symbiosis between the dinoflagellates *Symbiodinium* spp. and planula larvae of the scleractinian coral *Fungia scutaria*. Coral Reefs 2001;**20**:301-308.

[18] Takahashi T. Life cycle analysis of endosymbotic algae in an endosymbiotic situation with *Paramecium bursaria* using capillary flow cytometry. Energies. 2017;**10**:1413. DOI: 10.3390/en10091413

[19] Nishihara N, Horiike S, Takahashi T, Kosaka T, Shigenaka Y, Hosoya H. Cloning and characterization of endosymbiotic algae isolated from *Paramecium bursaria*. Protoplasma. 1998;**203**:91-99. DOI: 10.1007/BF01280591

[20] Takahashi T, Ogura Y, Ogawa A, Kanematsu H, Yokoyama S. An effective and economic strategy to restore acidified freshwater ecosystems with steel industrial byproducts. Journal of Water and Environment Technology. 2012;**10**:347-362. DOI: 10.2965/jwet.2012.347

[21] Yokoyama S, Suzuki A, Nik Hisyamudin BMN, Kanematsu H, Ogawa A, Takahashi T, Izaki M, Umemoto M. Serial batch elution of electric arc furnace oxidizing slag discharged from normal steelmaking process into fresh water. ISIJ International. 2010;**50**:630-638. DOI: 10.2355/isijinternational.50.630

[22] Yokoyama S, Shimomura T, Hisyamudin MNN, Takahashi T, Izaki M. Influence of amount of oxidizing slag discharged from stainless steelmaking process of electric arc furnace on elution behavior into fresh water. Journal of Physics Conference Series. 2012;**352**:012051. DOI: 10.1088/1742-6596/352/1/012051

[23] Yokoyama S, Suzuki A, Izaki M, Umemoto M. Elution behavior of electronic arc furnace oxidizing slag into fresh water. Tetsu-to-Hagané. 2009;**95**:434-443. DOI: 10.2355/tetsutohagane.95.434

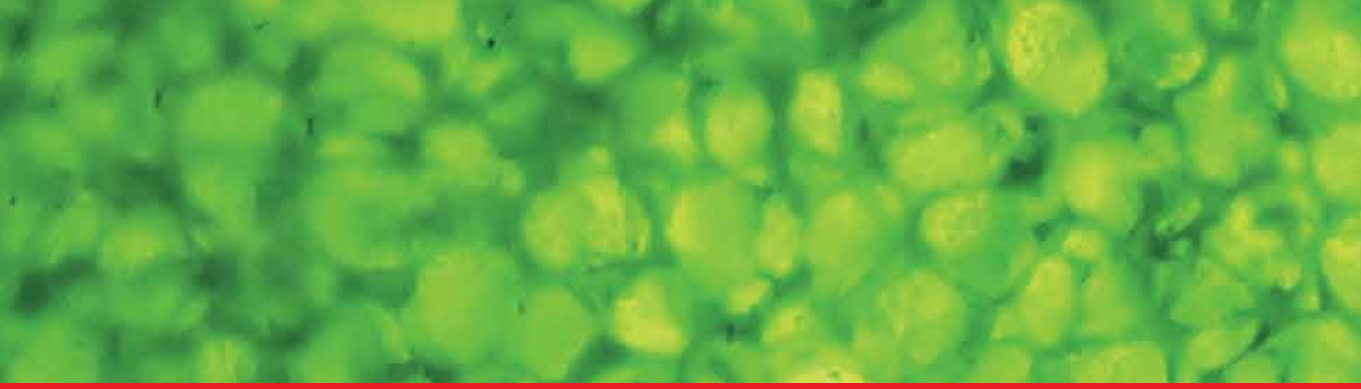

Edited by Marica Gemei

Flow cytometry's informative potential has been underestimated for many years because of a lack of adequate instruments, automation, reagents, and know-how to approach, integrate, and also substitute other techniques giving single information per assay. In the last decade, flow cytometers have become capable of performing high-throughput screening and high content analysis, evaluating tens of different samples' features in a single run up to 1536 formats on multiple cell populations. The introduction of imaging flow cytometry has filled the gap between flow cytometry and conventional high content imaging screening, putting flow cytometry at the center of many laboratories, which can now cover with a single instrument the vast majority of needs in research programs. The flow cytometry community is a multidisciplinary and diversified group with many different interests and fields of action. These characteristics have prompted the evolution of the techniques, applications, and instruments that allow the use of complex, sophisticated, and standardized and reliable flow cytometric assays in academic and industrial programs.

Published in London, UK

IntechOpen

ISBN 978-1-83881-361-1